Cats, Rotating Waves and Photons

An Excursion into Light-Matter Interaction

by

Mohammad Ayyash

A thesis
presented to the University of Waterloo
in fulfillment of the
thesis requirement for the degree of
Master of Science
in
Physics (Quantum Information)

Waterloo, Ontario, Canada, 2023

Author's Declaration

I hereby declare that I am the sole author of this thesis. This is a true copy of the thesis, including any required final revisions, as accepted by my examiners.

I understand that my thesis may be made electronically available to the public.

Abstract

This thesis hopes to achieve two modest goals. The primary goal is to formulate a practical theory for generating cat states by employing a resonant or detuned strong drive on a qubit coupled to a resonator. An incidental outcome of this approach is the ability to encode a qubit state within a resonator state using cat states. The secondary goal is to showcase the robustness of this theory in the face of practical implementation challenges, including decoherence and the existence of more than two levels. In this pursuit, we extend the theory to include a driven qutrit-resonator system. The theory is aimed at a circuit QED implementation using a transmon or charge qubit.

Acknowledgements

In these final hours before the submission deadline, as I conclude two days without sleep, it becomes challenging to express gratitude to everyone.

First and foremost, I would like to express my profound gratitude to my parents, Rana and Mutaz, without whom none of this would have been possible. Their boundless love and unwavering support have consistently served as my lifeline. Throughout my upbringing, I was encouraged to nurture curiosity, explore the world, and think critically. I am certain that nothing I do could ever truly repay them, and I remain forever grateful to have them as my parents.

Beyond my parents, I am incredibly grateful for a vast circle of family and close friends, too numerous to list individually. Out of this circle, I would like to explicitly thank both of my grandfathers, who were strong resilient figures and role models in many aspects of my life. Both of them passed away in 2020 during the pandemic, and not a day goes by where I don't miss them.

I would like to thank my supervisor, Matteo Mariantoni, for teaching me many things in science and otherwise. My initial encounter with him was in 2019 when he taught an electrodynamics course. At that time, I was an eager yet somewhat disoriented undergraduate student, grappling with numerous physics questions, many of which were quite annoying. To his credit, he patiently entertained the majority of my questions, and he occasionally admitted to not having an answer. Through my long interactions with him on the board and in cold meeting rooms, I learned what it means to truly *know* and *understand* a subject. It was the great Lev Landau who once said, "A method is more important than a result," and Matteo, you have indeed taught me a method.

I would like to thank the excellent instructors I had the privilege of learning from at the University of Waterloo. In particular, I would like to thank Achim Kempf, John Watrous, and Eduardo Martín-Martínez for teaching in a manner that made the material, not only understandable but intuitive. They taught courses that truly left me inspired.

I would like to thank my committee members, Alan Jamison and Crystal Senko, for providing me with critical feedback on my research and for reading this thesis. They helped me improve the presentation of this work.

I would like to thank Luca Dellantonio who spent a lot of time helping me and teaching me how to properly write a paper and the art of storytelling through figures.

I would like to thank all the Digital Quantum Matter Lab group members. I learned a lot through our discussions and very long group meetings. In particular, I would like

to thank Xicheng (Christopher) Xu who has worked on circuit QED closely with me. He helped ground the theory to reality.

I would like to thank my friends and colleagues at the Institute for Quantum Computing (IQC) for a providing a great environment where free inquiry is encouraged. I will not forget all the inspiring discussions sparked during cookie time[1].

Lastly, I would like thank all my Jiu Jitsu training partners at Gentle Arts Dojo and Riyadh Combat Club for giving me an outlet to relieve stress and enjoy physical activity beyond the monotony of going to the gym.

[1] I am still hoping Norbert or future IQC Directors will stop buying terrible cookies.

Dedication

إهداء

إهداء إلى من رحلوا بالأبدان وذكراهم خالدة في الأذهان،
جدي وجدي وخالتي...

Dedicated to those who have departed, but their memory is eternal.
My grandfathers and my aunt...

Table of Contents

List of Figures

List of Tables

أما النجاح فلا نجاح لأمة

ما أيدت أقوالها أفعالها

As for success, there is no success for a nation

whose slogans are not backed by actions

Chapter 1

Introduction

Light-matter interaction resides at the core of the fundamental quest for knowledge, while simultaneously driving a (potential) technological revolution. From the red light stopping you at the intersection, to the fiber optics carrying your favorite melodies across oceans, to the satellites communicating your position, the interactions of light or electromagnetic (EM) waves with matter underlie most of the functions in our daily life. The power of harnessing such interactions cannot be overstated.

These interactions, as with everything else, must adhere to the principles of quantum mechanics. Quantum mechanics is the framework tackling the small constituent objects forming everything around us. Unfortunately, we are too big for quantum mechanics. The quantum-mechanical nature of most things around us decoheres at our level. Thus, to uncover the *finer* quantum-mechanical nature of light-matter interaction, we must find a smaller scope than everyday objects.

Cavity quantum electrodynamics (QED) is the branch of physics concerned with studying light-matter interactions in a confined space. In particular, it refers to light confined in a hollow space surrounded by mirrors – a cavity, with atoms in the midst. By externally exciting the atoms, we can cause them to emit or absorb photons from the confined EM field. When done right, these phenomena occur in a coherent and detectable manner via the transmission and reflection of external signals through the cavity.

While nature gives us atoms and we can confine light in cavities, the coupling between light and matter is inherently limited in these natural settings. In pursuit of exotic phenomena, we can synthesize 'artificial atoms' and confine light on a chip. This enables us to achieve coupling strengths unimaginable in the natural world. Furthermore, this approach empowers us to harness quantum effects generated on these chips in a robust, replicable,

and scalable manner. To engineer these 'atoms on a chip,' we use the ultra-low-dissipation platform provided by superconducting circuits – the field recognized as circuit QED. In this context, linear circuits, comprising lumped elements or distributed elements, fulfill the role of cavities by confining light. Meanwhile, nonlinear or 'anharmonic' circuits assume the role of artificial atoms. This thesis is focused on developing a practical theory for generating quantum-mechanical states in a superconducting cavity or resonator using these artificial atoms. The states of concern exhibit highly nonclassical features and are known as 'Schrödinger cat states'. The theory presented aims to account for practical considerations such as interference of higher energy levels of the atoms, spurious effects of cross-talk, and decoherence effects.

The structure and main results of the thesis are now outlined. In Ch. 2, the basic tools of this thesis are introduced. A brief overview of quantum mechanics in closed and open systems is presented. Classical states within quantum theory and signatures of nonclassicality are discussed. The simplest model of an atom, whether artificial or real, is introduced as a two-level system or qubit. Its semiclassical and quantum interactions with light are explored through the semiclassical and quantum Rabi models. The various regimes of coupling strength between light and matter are succinctly explored, spanning from the seminal Jaynes-Cummings model [27] to the exotic deep-strong coupling regime. Schrödinger cat states in quantum optics are defined and their properties are discussed. Finally, an overview of the relevant elements of circuit QED are presented. An LC resonator in its lumped- and distributed-element forms is introduced. The Cooper-pair box in its charge and transmon regimes is introduced. The capacitive coupling of a Cooper-pair box and a resonator is discussed. In Ch. 3, a continuously driven qubit coupled to a resonator is extensively studied, to generate a cat state. The material presented in that chapter serves as a critical analysis and extension of an existing cavity QED proposal [58]. The strong driving regime is examined. The rotating-wave-approximation conditions that permit us to neglect counter-rotating terms are found to be affected by the drive parameters. A protocol for encoding a qubit state into a resonator via cat states is formulated based on resonant strong driving. The cat states generated by this protocol are found to be 'very fast' (experimental parameters in Ch. 3 quantify how fast; spoiler alert - between 5 and 50 nanoseconds). The size of the cats generated by this method grows *quadratically* in time. The protocol is found to be robust against qubit and resonator decoherence. In Ch. 4, the system studied is extended to be a three-level system or qutrit with selection rules conforming to those of a Cooper-pair box, a cascade-type or Ξ-type qutrit. Both qutrit transitions are considered to be coupled to the drive and resonator. The theory developed for the qubit is generalized for a weakly-anharmonic qutrit and is found (with some modifications) to generate cat states. The protocol for encoding a qubit state in a

resonator is generalized to use a qutrit for that purpose. In the strongly-anharmonic limit, it is found that the qubit treatment holds for the most part with some perturbations due to the third state interfering. Finally, a framework is developed for dealing with arbitrarily anharmonic qutrits. The conditions needed to potentially create superpositions of coherent states, including the possibility of generating a cat state are discussed. In Ch.5, a brief conclusion summarizing this work is presented with an outlook on what can be done next.

Chapter 2

Preliminaries

In this chapter, we cover the basic topics relevant to the material developed later in this thesis. This chapter should serve as a basic introduction to all the relevant models, techniques and concepts used. Throughout the chapter, we explicitly cite references when a result is directly quoted from the reference or is deemed to not be commonly known. For elementary quantum mechanics and open systems, we relied on Refs. [53, 9, 11]. For phase space methods and Gaussian states, we relied on Refs. [41, 64, 54]. For quantum optics, we relied on Refs. [22, 32, 34, 23]. For circuit QED, we relied on Refs. [4, 33, 39].

2.1 Basic Quantum Mechanics

In this section, we review the basic elements of quantum mechanics used in this thesis.

The states of a quantum system belong to a Hilbert space, $\mathcal{H}$, which we consider in two instances: a finite-dimensional (qubit) instance and an infinite-dimensional instance (harmonic oscillator). A pure state of a system is represented as a vector in the Hilbert space, $|\psi\rangle \in \mathcal{H}$. All states have a norm of 1, $|\langle\psi|\psi\rangle| = 1$. When considering experimental imperfections in state preparation and decoherence effects, a statistical description of quantum states is employed. This is represented by a density operator or matrix, $\hat{\rho}$. The matrix belongs to the space of linear operators acting on $\mathcal{H}$, denoted as $\hat{\rho} \in \mathcal{L}(\mathcal{H})$. In particular, density matrices comprise the set of positive semi-definite matrices acting on $\mathcal{H}$ with a trace of unity, $\mathrm{Tr}(\hat{\rho}) = 1$. The trace unity condition is equivalent to the norm condition. For a pure state $|\psi\rangle$, the density matrix is given by $\hat{\rho} = |\psi\rangle\langle\psi|$. If we consider a set of pure states $|\psi_1\rangle, |\psi_2\rangle, ..., |\psi_n\rangle$ with associated probabilities p_k, the density matrix

describing the statistical mixture of these states along with their associated probabilities is $\hat{\rho} = \sum_{k=1}^{n} p_k |\psi_k\rangle\langle\psi_k|$. An observable, $\hat{A}$, constitutes a Hermitian or self-adjoint operator, i.e., $\hat{A}^\dagger = \hat{A}$, acting on $\mathcal{H}$. This property guarantees that the eigenvalues – the values we observe in experiments – are indeed real. For two coupled quantum systems with Hilbert spaces $\mathcal{H}_1$ and $\mathcal{H}_2$, their joint Hilbert space is the tensor product of the two spaces, $\mathcal{H}_1 \otimes \mathcal{H}_2$. A state that can be written as the tensor product of two pure states in the original Hilbert spaces, $|\psi_1\rangle \otimes |\psi_2\rangle$, where $|\psi_1\rangle \in \mathcal{H}_1$ and $|\psi_2\rangle \in \mathcal{H}_2$, is called a product state. Otherwise, if a state cannot be expressed as a product state, it is an entangled state. In this thesis, we drop the tensor product (for states and operators), '$\otimes$', and keep it implicit.

The time-evolution of a closed quantum system is generated by the system's Hamiltonian, $\hat{H}$. The dynamics of a pure state are governed by the Schrödinger equation, which is given by

$$i\hbar \frac{d}{dt} |\psi(t)\rangle = \hat{H} |\psi(t)\rangle . \tag{2.1}$$

For a more complete description that accommodates both pure and mixed states, the evolution of a density matrix is dictated by the von Neumann equation:

$$i\hbar \frac{d}{dt}\hat{\rho} = [\hat{H}, \hat{\rho}]. \tag{2.2}$$

This perspective, where states evolve in time, is known as the Schrödinger picture. An equivalent viewpoint is the Heisenberg picture, where the states remain fixed while the operators evolve in time. For an operator $\hat{A}$, the Heisenberg equation of motion is given by

$$i\hbar \frac{d}{dt}\hat{A} = -[\hat{H}, \hat{A}] + i\hbar \frac{\partial}{\partial t}\hat{A}. \tag{2.3}$$

The time-evolution of a closed system is unitary, ensuring that the probabilities and norms of the states are preserved.

Thus far we have only considered closed system dynamics. In practice, a quantum system is never truly isolated but rather interacts with the environment. In this thesis, we are working with systems operating near the milliKelvin temperature range. As a result, we consider our system(s) to interact with a bath of harmonic oscillators at zero temperature, and we employ the typical Born and Markov approximations to arrive at a Lindblad master equation [9, 11]

$$\frac{d}{dt}\hat{\rho} = -[\hat{H}, \hat{\rho}] + \sum_k \gamma_k \mathcal{D}(\hat{L}_k)\hat{\rho}, \tag{2.4}$$

where $\mathcal{D}(\hat{O})\hat{\rho} = \hat{O}\hat{\rho}\hat{O}^\dagger - \frac{1}{2}\{\hat{O}^\dagger\hat{O}, \hat{\rho}\}$ is the dissipator for a given operator $\hat{O}$, γ_k is a rate parameter for the k^{th} Lindblad jump operator $\hat{L}_k$ describing decoherence effects.

We now define the two quantum systems of interest: the qubit and harmonic oscillator. We start with the qubit operators and eigenstates. We take the qubit free Hamiltonian to be $\hat{H} = \hbar\omega_{\text{q}}\hat{\sigma}_z/2$ where $\hat{\sigma}_z = |\text{e}\rangle\langle\text{e}| - |\text{g}\rangle\langle\text{g}|$ describes the population difference between the excited state $|\text{e}\rangle$ and the ground state $|\text{g}\rangle$ of the qubit and ω_{q} is the qubit transition frequency. Here, $|\text{g}\rangle$ and $|\text{e}\rangle$ are eigenstates of $\hat{H}$ with the property $\hat{\sigma}_z|\text{g}\rangle = -|\text{g}\rangle$ and $\hat{\sigma}_z|\text{e}\rangle = |\text{e}\rangle$. When we introduce a classical field interacting with the qubit, we will resort to using $\hat{\sigma}_+ = |\text{e}\rangle\langle\text{g}|$ and $\hat{\sigma}_- = \hat{\sigma}_+^\dagger$ as the raising and lowering operators of the qubit, and we define $\hat{\sigma}_x = \hat{\sigma}_+ + \hat{\sigma}_-$. Meanwhile, the harmonic oscillator free Hamiltonian is $\hat{H} = \hat{p}^2/2m + m\omega^2\hat{q}^2/2$. Here, $\hat{p}$ and $\hat{q}$ are the (generalized) momentum and position operators, m is the 'mass' of the oscillator and ω is the oscillator's resonance frequency. We typically rewrite this Hamiltonian as $\hat{H} = \hbar\omega(\hat{a}^\dagger\hat{a} + 1/2)$, where $\hat{a}$ and $\hat{a}^\dagger$ are the bosonic annihilation and creation operators. The usual commutation relation, $[\hat{a}, \hat{a}^\dagger] = \hat{\mathbb{I}}$, holds true. Henceforth, we drop the constant offset of $\hbar\omega/2$. The eigenstates of the harmonic oscillator are the *Fock states*, $|n\rangle$. They are eigenstates of the number operator, $\hat{a}^\dagger\hat{a}$, where $\hat{a}^\dagger\hat{a}|n\rangle = n|n\rangle$. In the case of the harmonic oscillator, the Heisenberg uncertainty principle states $\Delta q\Delta p \geq \hbar/2$, where $\Delta O = (\langle\hat{O}^2\rangle - \langle\hat{O}\rangle^2)^{1/2}$. Note that the vacuum state saturates the inequality. Next, we take a look at all the non-trivial states saturating this inequality.

The annihilation operator admits an eigenstate $|\alpha\rangle$, where $\hat{a}|\alpha\rangle = \alpha|\alpha\rangle$, $\alpha \in \mathbb{C}$. These states are related to the vacuum state through the displacement operator

$$|\alpha\rangle = \hat{D}(\alpha)|0\rangle, \tag{2.5}$$

where

$$\hat{D}(\alpha) := \exp\big(\alpha\hat{a}^\dagger - \alpha^*\hat{a}\big). \tag{2.6}$$

This state saturates the uncertainty principle and has equal variances in $\hat{q}$ and $\hat{p}$, i.e., $\Delta q = \Delta p = \sqrt{\hbar/2}$. We can rewrite a coherent state in the Fock basis as

$$|\alpha\rangle = e^{-|\alpha|^2/2}\sum_{n=0}^{\infty}\frac{\alpha^n}{\sqrt{n!}}|n\rangle. \tag{2.7}$$

The coherent states also form a basis for the Hilbert space but it is overcomplete,

$$\int d^2\alpha\,|\alpha\rangle\langle\alpha| = \pi\hat{\mathbb{I}}. \tag{2.8}$$

Here, $d^2\alpha$ is in the sense of integrating over the real and imaginary parts of α.

One can consider ways to keep the uncertainty principle inequality saturated while simultaneously altering the variances — increasing one and decreasing the other. This leads us to squeezed (vacuum) states, which result from applying the squeeze operator on the vacuum state,

$$|\zeta\rangle = \hat{S}(\zeta)\,|0\rangle\,, \tag{2.9}$$

where

$$\hat{S}(\zeta) := \exp\big((\zeta^*\hat{a}^2 - \zeta\hat{a}^{\dagger 2})/2\big) \tag{2.10}$$

and $\zeta \in \mathbb{C}$. This state has uneven variances in $\hat{q}$ and $\hat{p}$ but the product of the variances is fixed at $\hbar/2$. Squeezed states played a crucial role in interferometers used to detect gravitational waves [12]. Similar to the coherent states, squeezed states can be rewritten in the Fock basis as

$$|\zeta\rangle = \frac{1}{\sqrt{\cosh(r)}} \sum_{n=0}^{\infty} \frac{\sqrt{(2n)!}}{2^n n!} (-e^{i\phi}\tanh(r))^n\,|2n\rangle\,, \tag{2.11}$$

where $r = |\zeta|$ and $\phi = \arg(\zeta)$. Coherent and squeezed states together with the vacuum state are known as (pure) *Gaussian states*. Their probability distributions, $|\psi(q)|^2$, are Gaussian distributions. As we will discuss next, these states are widely believed to be the set of 'classical' states within quantum theory[1]. The notion of classical vs. non-classical will become more apparent when we next introduce quasiprobability distributions in phase space.

In classical mechanics, the phase space formulation is an insightful tool to investigate the dynamics of a system. Typically, the state of a system is a single point, (q, p), on a deterministic trajectory or curve. In quantum mechanics, a single point is not sufficient to describe the system, as it could be in a superposition of different states each with an associated probability. For this purpose we need a distribution over phase space. For a bosonic mode, we define the Wigner function for a given state $\hat{\rho}$ as

$$W(q,p) = \frac{1}{2\pi\hbar}\int_{-\infty}^{\infty} dx\, e^{-ipx/\hbar}\,\langle q + x/2|\,\hat{\rho}\,|q - x/2\rangle\,. \tag{2.12}$$

[1]Note that classical systems do not possess a ground state. Coherent states, in the limits of the correspondence principle, behave as one would expect a classical oscillator to. Some controversy still surrounds squeezed states, as some consider them to be non-classical, despite the demonstration that classical systems can indeed be squeezed; see Refs. [52, 14, 43].

This was E.P. Wigner's attempt to represent a quantum state using a real distribution over phase space. He wrote this while working on quantum corrections to thermodynamics equilibrium [65]. The Wigner function satisfies some properties of a probability distribution and as such it is called a quasiprobability distribution. It integrates to unity, i.e., $\int dq \int dp W(q,p) = 1$, but it can have *negative* values. This means that it cannot be thought of an actual probability distribution. Its marginals, however, are strictly real and correspond to the position and momentum distributions of the state. This leads us to an important result known as Hudson's theorem [26, 59], which asserts that any pure state with a nonnegative Wigner function must have a Gaussian function for its Wigner function. These states precisely correspond to the previously mentioned Gaussian states, and indeed, the definition is often stated as follows: Gaussian states are those states whose Wigner functions are Gaussian distributions. Because non-classicality is characterized by Wigner negativity and Wigner functions that are nonnegative are associated with Gaussian states, this underlies the statement that Gaussian states constitute the class of (pure) classical states within the framework of quantum theory.

Lastly, we re-express the Wigner function in its 'coherent-state representation' as it is the commonly used form,

$$W(\alpha,\alpha^*) = \frac{1}{4\pi^2\hbar}\int d^2\beta\, e^{\beta^*\alpha-\beta\alpha^*}\,\mathrm{Tr}\Big(\hat{D}(\beta)\hat{\rho}\Big). \tag{2.13}$$

For N modes characterized by $\hat{a}_k$ and $\hat{a}_k^\dagger$ (for $k = 1, ..., N$), we generalize the displacement operator to

$$\begin{aligned}\hat{D}(\vec{\alpha}) =& \exp\left(\sum_{k=1}^{N}\alpha_l\hat{a}_k^\dagger - \alpha_k^*\hat{a}_k\right) = \prod_{k=1}^{N}\exp\Big(\alpha_k\hat{a}_k^\dagger - \alpha_k^*\hat{a}\Big)\\ =& \prod_{k=1}^{N}\hat{D}(\alpha_k),\end{aligned} \tag{2.14}$$

where $\vec{\alpha} = (\alpha_1, \alpha_2, ..., \alpha_N)^T$. Using the N-mode displacement operator, we can write the N-mode Wigner function as

$$W(\vec{\alpha},\vec{\alpha}^*) = \frac{1}{(4\pi^2\hbar)^N}\int d^2\beta_1 ... \int d^2\beta_N\, e^{\vec{\beta}^*\cdot\vec{\alpha}-\vec{\beta}\cdot\vec{\alpha}^*}\,\mathrm{Tr}\Big(\hat{D}(\vec{\beta})\hat{\rho}\Big), \tag{2.15}$$

where $\vec{\beta} = (\beta_1, ..., \beta_N)^T$,'$\cdot$' is to be taken as the dot product between two vectors and $\hat{\rho}$ is the joint density matrix of the N modes. In this thesis, the Wigner function is used

to visualize nonclassical resonator states generated by interacting with a driven qubit in various coupling schemes.

In the next section, we discuss the basic models of light-matter interaction in the semiclassical approximation followed by a full quantum descripton. As such, we will couple the qubit and harmonic oscillator and discuss their interaction, which varies according the coupling strength regime.

2.2 Qubit-resonator system

In this section, we introduce the models of light-matter interaction relevant to this thesis. We start with the semiclassical Rabi model (SRM) that originated in the study of atoms [2] with nuclear spin interacting with magnetic fields [50]. Then taking into consideration the quantization of the EM field [15, 18], qubit-field interactions require a full quantum-mechanical description. This leads us to the simplest model entailing such a description, the quantum Rabi model (QRM). We discuss the key predictions of the semiclassical and fully quantum models. We outline the coupling strength regimes of the QRM.

Semiclassical Rabi model

To begin our discussion of light-matter interaction, we consider a one-electron atom placed in an EM field. The electron with a negative charge $-e$ and the nucleus with a positive charge e together define an electric dipole $\vec{d} = e\vec{r}$, where $\vec{r}$ is the displacement vector from the nucleus to the electron. We consider the nucleus is fixed at the origin. Typically, the electron displacement is very small compared to the wavelengths of interest. As a result, this allows us to make the long-wavelength (*dipole*) approximation where the field is spatially uniform, i.e., $\vec{E}(\vec{r}, t) \simeq \vec{E}(t)$, where this is the field near the center of the nucleus. This results in an interaction Hamiltonian known as the dipole Hamiltonian $H_{\mathrm{I}} = -\vec{d} \cdot \vec{E}$. Treating the one-electron atom quantum-mechanically, results in the dipole moment being an operator,

$$\vec{d} \mapsto \hat{d} = e\hat{\vec{r}}. \tag{2.16}$$

[2] Henceforth, we refer to the atoms in these models as qubits or qudits depending on the context.

We consider the atom in its simplest case, a two-level system or qubit. The electric dipole matrix elements are found by

$$\hat{d} = \hat{\mathbb{I}}\,\hat{d}\,\hat{\mathbb{I}} = \sum_{j,k} |j\rangle \underbrace{\langle j|\,\hat{d}\,|k\rangle}_{d_{jk}} \langle k| = \sum_{jk} d_{jk}\,|j\rangle\langle k|$$

where

$$d_{jk} = e\int d^3r\, \psi_j^*(\vec{r}) r \psi_j(\vec{r})$$

and $\psi_k(\vec{r}) = \langle \vec{r}|k\rangle$ is the k^{th} energy eigenstate position wavefunction. Typically, the atom-field interaction of interest is when a particular atomic transition is close to the field frequency. When the atomic transition and the field are near resonance, only the population of the two states involved in this transition are significantly altered by the presence of the field. In this case, a qubit serves as a good approximation of an atom. Concretely, we restrict ourseleves to the ground and first excited states, $\{|\mathrm{g}\rangle, |\mathrm{e}\rangle\}$, and, as such,

$$\hat{d} = d_{\mathrm{eg}}\,|\mathrm{e}\rangle\langle\mathrm{g}| + d_{\mathrm{ge}}^*\,|\mathrm{g}\rangle\langle\mathrm{e}|\,.$$

Considering a monochromatic field with frequency ω_{d}, the interaction Hamiltonian between the qubit and the field is

$$\hat{H}_{\mathrm{I}} = -\hat{d}\cdot\vec{E} \propto \underbrace{(\hat{\sigma}_+ + \hat{\sigma}_-)}_{\text{qubit operators}} \cos(\omega_{\mathrm{d}} t).$$

This leads us to the semiclassical Rabi model (SRM), which constitutes the simplest model of light-matter interaction, where a qubit interacts with a monochromatic classical field. The full Hamiltonian of this model reads as

$$\hat{H}_{\mathrm{R}} = \frac{\hbar\omega_{\mathrm{q}}}{2}\hat{\sigma}_z + \hbar\Omega\cos(\omega_{\mathrm{d}} t)\hat{\sigma}_x, \tag{2.17}$$

where ω_{q} is the qubit transition frequency, ω_{d} is the classical field frequency, and Ω is the classical field strength. The time-evolution for this Hamiltonian, as it stands, cannot be solved analytically.

To simplify the problem, we introduce the rotating frame. A driven system's response oscillates at the drive frequency. The amplitude of the response is at a maximum when the system is resonant with the drive. We can think of the rotating frame as a means to track the response of a system with respect to the drive frequency. This enables us to

describe the frequency of the system's response relative to the driving frequency when it is detuned from the drive. The rotating frame also allows us to resolve the system response into slow oscillating terms, quasi-resonant with the drive, and fast oscillating terms, far-detuned from the drive. This is achieved by using a unitary transformation on the system Hamiltonian.

We now transform to the rotating frame of the classical field by means of the unitary transformation $\hat{U}_\mathrm{d} = \exp\left(-i\omega_\mathrm{d} t\hat{\sigma}_z/2\right)$. The Hamiltonian in this frame reads as

$$\begin{aligned}\hat{H}_\mathrm{R}^\mathrm{Rot} &= \hat{U}_\mathrm{d}^\dagger \hat{H}_\mathrm{R} \hat{U}_\mathrm{d} + i\hbar\dot{\hat{U}}_\mathrm{d}^\dagger \hat{U}_\mathrm{d} \\ &= \frac{\hbar(\overbrace{\omega_\mathrm{q} - \omega_\mathrm{d}}^{\Delta})}{2}\hat{\sigma}_z + \frac{\hbar\Omega}{2}(\hat{\sigma}_+ + \hat{\sigma}_- + e^{+i2\omega_\mathrm{d}t}\hat{\sigma}_+ + e^{-i2\omega_\mathrm{d}t}\hat{\sigma}_-),\end{aligned} \tag{2.18}$$

where Δ is the detuning between the qubit and the classical field. When the field strength satisfies $\Omega/2 \ll 2\omega_\mathrm{d}$, the terms oscillating with $e^{\pm i2\omega_\mathrm{d}t}$ operate on a much faster and separated timescale than the other terms. When the amplitude of the prefactor (Ω) is small compared to the oscillation frequencies, the total effect on the relevant timescales averages to zero. As a result, we can perform a rotating-wave approximation (RWA) that neglects the fast-oscillating terms. It is equivalent to time-averaging these terms over the a period $T = 2\pi/(2\omega_\mathrm{d})$. Performing said RWA allows us to obtain the Hamiltonian

$$\hat{H}_\mathrm{R}^{\mathrm{Rot}\prime} = \frac{\hbar(\omega_\mathrm{q} - \omega_\mathrm{d})}{2}\hat{\sigma}_z + \frac{\hbar\Omega}{2}(\hat{\sigma}_+ + \hat{\sigma}_-) \tag{2.19}$$

Back in the original 'lab' frame, the Hamiltonian now reads as

$$\hat{H}_\mathrm{R}' = \frac{\hbar\omega_\mathrm{q}}{2}\hat{\sigma}_z + \frac{\hbar\Omega}{2}(e^{-i\omega_\mathrm{d}t}\hat{\sigma}_+ + e^{+i\omega_\mathrm{d}t}\hat{\sigma}_-). \tag{2.20}$$

Under the resonance condition $\Delta = 0$, starting in the ground state $|\psi_\mathrm{i}\rangle = |\mathrm{g}\rangle$, we time-evolve in the rotating frame under Eq. (2.19) and obtain the state at time t,

$$|\psi(t)\rangle^\mathrm{Rot} = \cos\left(\frac{\Omega t}{2}\right)|\mathrm{g}\rangle - i\sin\left(\frac{\Omega t}{2}\right)|\mathrm{e}\rangle\,. \tag{2.21}$$

Then, we find the probability of the system being in the excited state at any given time to be

$$P_{|\mathrm{e}\rangle}(t) = |\,\langle \mathrm{e}|\psi(t)\rangle\,|^2 = \sin^2\left(\frac{\Omega t}{2}\right). \tag{2.22}$$

This probability oscillates with frequency Ω, known as the *Rabi frequency*, and the oscillations are commonly referred to as *Rabi oscillations*.

When $\Delta \neq 0$, Rabi oscillations still occur but the probability never reaches unity. This results in a dressing of the qubit frequency known as the *ac-Stark shift*. As the strength of the field grows, the fast-oscillating (counter-rotating) terms become more prominent and lead to a shift in the qubit resonance frequency. This shift is known as the *Bloch-Siegert shift* and is proportional to $\Omega^2/(\omega_\mathrm{q} + \omega_\mathrm{d})$ [5, 56, 67].

In the following chapters of this thesis, we shall refer to a classical field of the form described here as a driving field.

Quantum Rabi model

In the SRM, the qubit serves as a quantized model of matter (first quantized) while the field is classical. A natural step towards a full quantum-mechanical description of light-matter interaction is the (second) quantization of the radiation field. We shall avoid discussing the procedure of second quantization and assume its final result: the modes of the radiation field behave as a set of independent quantized harmonic oscillators. The Hamiltonian of the field reads as (ignoring the constant off-set)

$$\hat{H}_\mathrm{F} = \sum_k \hbar\omega_k \hat{a}_k^\dagger \hat{a}_k, \tag{2.23}$$

where ω_k is the frequency of the k^{th} mode and $\hat{a}_k$, $\hat{a}_k^\dagger$ are the usual bosonic creation and annihilation operators of the k^{th} mode which obey the commutation relations $[\hat{a}_j, \hat{a}_k^\dagger] = \delta_{jk}$. For the scope of light-matter interactions in a confinement such as cavity QED or circuit QED, the quantized radiation field is that of a cavity (resonator).

We are typically interested in a single mode interacting with a qubit confined in the cavity (be it an atom in a cavity or a superconducting qubit coupled to a resonator circuit). Thus, moving forward when we refer to a resonator we strictly mean a particular mode of interest in the resonator. As in the the SRM, we work in the dipole approximation. In a similar argument to the two-level approximation, we usually consider the mode of interest to be close to the transition frequency of the qubit. As a result, the interaction with other modes insignifanctly affects the qubit states' populations. Thus, we also employ the single-mode approximation (discarding other modes). In this context, the interaction between a qubit and a resonator originates from the same dipole interaction for a classical

field but instead the field is quantized,

$$\hat{H}_{\mathrm{I}} = -\hat{d}\cdot\hat{\vec{E}} \propto \underbrace{(\hat{\sigma}_+ + \hat{\sigma}_-)}_{\text{qubit operators}} \overbrace{(\hat{a}^\dagger + \hat{a})}^{\text{field operators}} \ . \tag{2.24}$$

We can now describe the qubit interacting with the quantized field of the resonator in what is known as the QRM. The Hamiltonian of this model reads as

$$\hat{H}_{\mathrm{QR}} = \frac{\hbar\omega_{\mathrm{q}}}{2}\hat{\sigma}_z + \hbar\omega_{\mathrm{r}}\hat{a}^\dagger\hat{a} + \hbar g(\hat{\sigma}_+ + \hat{\sigma}_-)(\hat{a}^\dagger + \hat{a}), \tag{2.25}$$

when ω_{r} is the resonator frequency and g is the strength of the qubit-resonator interaction. This model serves as a basis for investigating truly quantum-mechanical light-matter interactions. This means that it makes predictions that cannot be recreated by any classical theory.

The eigenvalue problem for the QRM Hamiltonian, $\hat{H}\,|E_n\rangle = E_n\,|E_n\rangle$, cannot be solved analytically[3]. However, this Hamiltonian can be simplified by making some approximations. To motivate such approximations, we first transform to the interaction picture. When the Hamiltonian of a system is composed of two (or more) terms and one of them is exactly solvable, it is useful to 'eliminate' the solvable part and focus on the difficult or unsolved part. This typically is the case when we consider a problem with composite Hilbert spaces, where we completely understand how the 'bare' (or uncoupled) Hamiltonian terms behave and we seek to understand the coupling terms jointly acting on the full Hilbert space. This is done using a unitary transformation that goes into a frame where the bare Hamiltonian terms are eliminated and the interaction terms are left (in a form still accounting for the bare terms).

We now transform to the interaction picture using $\hat{U}_0 = \exp\left(-i\hat{H}_0 t/\hbar\right)$, where $\hat{H}_0 = \hbar\omega_{\mathrm{q}}\hat{\sigma}_z/2 + \hbar\omega_{\mathrm{r}}\hat{a}^\dagger\hat{a}$. Then, the interaction picture Hamiltonian is

$$\begin{aligned}\hat{H}^{(\mathrm{I})} &= \hat{U}_0^\dagger\hat{H}_{\mathrm{QR}}\hat{U}_0 + i\hbar\dot{\hat{U}}_0^\dagger\hat{U}_0 \\ &= \hbar g(\underbrace{\hat{\sigma}_+\hat{a}^\dagger e^{i(\omega_{\mathrm{q}}+\omega_{\mathrm{r}})t} + \hat{\sigma}_-\hat{a}e^{-i(\omega_{\mathrm{q}}+\omega_{\mathrm{r}})t}}_{\text{counter-rotating}} + \overbrace{\hat{\sigma}_+\hat{a}e^{i(\omega_{\mathrm{q}}-\omega_{\mathrm{r}})t} + \hat{\sigma}_-\hat{a}^\dagger e^{-i(\omega_{\mathrm{q}}-\omega_{\mathrm{r}})t}}^{\text{rotating}}),\end{aligned} \tag{2.26}$$

[3]It can be solved *semi*-analytically where the eigenvalues can be found using transcendental equations [8].

where we note two types of terms: *rotating* terms which oscillate with the detuning $\omega_{\mathrm{q}}-\omega_{\mathrm{r}}$, and *counter-rotating* terms which oscillate with the sum of the frequencies $\omega_{\mathrm{q}}+\omega_{\mathrm{r}}$. In the regime where

$$|\omega_{\mathrm{q}}-\omega_{\mathrm{r}}| \ll \omega_{\mathrm{q}}+\omega_{\mathrm{r}} \text{ and } g \ll \min(\omega_{\mathrm{q}},\omega_{\mathrm{r}}), \tag{2.27}$$

we can perform an RWA to neglect the counter-rotating terms and obtain the effective interaction Hamiltonian

$$\hat{H}^{(\mathrm{I})} \simeq \hat{H}^{(\mathrm{I})}_{\mathrm{JC}} = \hbar g(\hat{\sigma}_+\hat{a}+\hat{\sigma}_-\hat{a}^\dagger). \tag{2.28}$$

Reverting back to the Schrödinger picture, the full Hamiltonian reads as

$$\hat{H}_{\mathrm{JC}} = \frac{\hbar\omega_{\mathrm{q}}}{2}\hat{\sigma}_z + \hbar\omega_{\mathrm{r}}\hat{a}^\dagger\hat{a} + \hbar g(\hat{\sigma}_+\hat{a}+\hat{\sigma}_-\hat{a}^\dagger). \tag{2.29}$$

This is known as the Jaynes-Cummings model (JCM) and it is the most commonly used descendant of the QRM. A key feature of the JCM Hamiltonian is the fact that its eigenvalue problem is analytically solvable. This can be traced to the nature of the rotating terms, as they are *excitation-preserving* terms. To elaborate on this idea, let us consider the subspace spanned by $\{|\mathrm{e}\rangle|n\rangle, |\mathrm{g}\rangle|n+1\rangle\}$ for some fixed n. We first note that the free Hamiltonians of the qubit and resonator leave these states unchanged. Next, we consider the action of the interaction terms on these states:

$$\hat{\sigma}_+\hat{a}|\mathrm{g}\rangle|n+1\rangle = \sqrt{n+1}\,|\mathrm{e}\rangle|n\rangle,$$
$$\hat{\sigma}_-\hat{a}^\dagger|\mathrm{e}\rangle|n\rangle = \sqrt{n+1}\,|\mathrm{g}\rangle|n+1\rangle,$$

and

$$\hat{\sigma}_+\hat{a}|\mathrm{e}\rangle|n\rangle = \hat{\sigma}_-\hat{a}^\dagger|\mathrm{g}\rangle|n+1\rangle = 0.$$

Due to this, the only allowed transitions in the JCM are $|\mathrm{g}\rangle|n+1\rangle \leftrightarrow |\mathrm{e}\rangle|n\rangle$. Then, the dynamics are confined in a $2-$dimensional subspace for each n. This means that the Hamiltonian is block-diagonal. For a fixed n, the 2×2 Hamiltonian can be expressed as

$$\hat{H}^{(n)} = \begin{array}{c} \\ |\mathrm{e}\rangle|n\rangle \\ |\mathrm{g}\rangle|n+1\rangle \end{array} \begin{array}{c} \langle\mathrm{e}|\langle n| \qquad\qquad \langle\mathrm{g}|\langle n+1| \\ \begin{pmatrix} \hbar n\omega_{\mathrm{r}} + \frac{\hbar\omega_{\mathrm{q}}}{2} & \hbar g\sqrt{n+1} \\ \hbar g\sqrt{n+1} & \hbar(n+1)\omega_{\mathrm{r}} - \frac{\hbar\omega_{\mathrm{q}}}{2} \end{pmatrix} \end{array}. \tag{2.30}$$

Then, it is straightforward to find the eigenvalues and eigenstates as

$$E_{n,\pm} = \hbar\omega_{\mathrm{r}}\left(n+\frac{1}{2}\right) \pm \frac{\hbar}{2}\sqrt{(\omega_{\mathrm{q}}-\omega_{\mathrm{r}})^2+4g^2(n+1)}, \tag{2.31a}$$

$$|+n\rangle = \cos\left(\frac{\theta_n}{2}\right)|\mathrm{e}\rangle\,|n\rangle + \sin\left(\frac{\theta_n}{2}\right)|\mathrm{g}\rangle\,|n+1\rangle\,, \tag{2.31b}$$

$$|-n\rangle = \sin\left(\frac{\theta_n}{2}\right)|\mathrm{e}\rangle\,|n\rangle - \cos\left(\frac{\theta_n}{2}\right)|\mathrm{g}\rangle\,|n+1\rangle\,, \tag{2.31c}$$

where $\theta_n = \arctan\big(2g\sqrt{n+1}/(\omega_\mathrm{q}-\omega_\mathrm{r})\big)$ is the mixing angle.

Having derived the JCM eigenstates and eigenvalues, we now discuss key phenomena that can only occur when the field is quantized. The qubit-resonator system exhibits quantized Rabi oscillations dependent on the photon number, n, and the qubit-resonator detuning. The frequency at which these oscillations occur is known as the *quantum Rabi frequency*

$$\omega_\mathrm{QR}^n = \sqrt{(\omega_\mathrm{q}-\omega_\mathrm{r})^2 + 4g^2(n+1)}.$$

Increasing the photon number leads to a higher frequency; a predicition requiring a quantized description of the field. When there are initially no photons in the resonator and the qubit is excited, the swap of photons between the qubit and resonator is know as *vacuum Rabi oscillations*. In addition to vacuum Rabi oscillations, if we probe the resonator with an ac signal over varying frequencies and measuring the intraresonator photon number, we observe a splitting at zero frequency known as the *vacuum Rabi splitting* [61, 63]. These phenomena cannot be explained without a quantized field having a vacuum state and emitting and absorbing photons.

The qubit-resonator coupling strength, g, is an important parameter that radically changes the dynamics we observe. To highlight some of the different regimes dictated by g, we first introduce κ, the resonator photon loss rate or its linewidth. The photon loss rate introduces an additional constraint on experimental feasibility. To achieve the JC regime determined by Eq. (2.27), we additionally require being in the strong coupling (SC) regime, i.e., when $g \gg \kappa$. This ensures that the dynamics are discernible and not completely dominated by losses.

By increasing g to a value close to the limit of the RWA validity, we need to incorporate the counter-rotating terms perturbatively. This results in what is known as the *Bloch-Siegert shift*, where both the qubit and resonator frequencies experience a frequency shift proportional to $\omega_\mathrm{BS} = g^2/(\omega_\mathrm{q}+\omega_\mathrm{r})$, and this shift scales up with the number of photons present in the resonator. This occurs when $g/\omega_\mathrm{r} \sim 0.1$ and is known as the ultrastrong coupling (USC) regime. We can perturbatively describe this regime up to second order in

$g/(\omega_{\rm q}+\omega_{\rm r})$, by the Hamiltonian [51]

$$\hat{H}_{\rm USC} \simeq \hat{H}_{\rm JC} + \hbar\omega_{\rm BS}\left(\hat{\sigma}_z\hat{a}^\dagger\hat{a} + \frac{\hat{\sigma}_z}{2} - \frac{1}{2}\right). \tag{2.32}$$

The perturbative treatment of the counter-rotating terms breaks down as the coupling strength increases. The USC represents a hallmark of novel light-matter interactions achieved in circuit QED. Such coupling strengths between qubits and resonators are beyond our reach in cavity QED using natural atoms and light. In this regime and as g gets larger, the qubit-resonator levels become more hybridized, and the interactions with the environment and other systems require careful considerations [2]. The system can no longer be thought of as a qubit and resonator interacting and each separately interacting with other systems (e.g. external drives or environment). Instead, the qubit-resonator system's eigenstates are entangled and the system as a whole interacts with other systems.

The regimes of the QRM we have discussed thus far implicitly assume near-resonance conditions, i.e., $\omega_{\rm q} \simeq \omega_{\rm r}$. While the outlined features hold qualitatively for small detunings, it is worth briefly examining a detuned regime of the QRM with distinct features: the dispersive regime. This regime occurs when $g/(\omega_{\rm q}-\omega_{\rm r}) \ll 1$. As long as the RWA of Eq. (2.27) remains valid, the system is described, up to second order in $g/(\omega_{\rm q}-\omega_{\rm r})$, by the Hamiltonian:

$$\hat{H}_{\rm disp,\ RWA} = \frac{\hbar\omega_{\rm q}}{2}\hat{\sigma}_z + \hbar\omega_{\rm r}\hat{a}^\dagger\hat{a} + \hbar\omega_{\text{ac-S}}\left(\hat{\sigma}_z\hat{a}^\dagger\hat{a} + \frac{1}{2}\hat{\sigma}_z\right), \tag{2.33}$$

where $\omega_{\text{ac-S}} = g^2/(\omega_{\rm q}-\omega_{\rm r})$ represents the *ac-Stark shift* frequency. The dispersive regime also extends beyond the RWA of Eq. (2.27). Using only the condition $g/(\omega_{\rm q}-\omega_{\rm r}) \ll 1$, the dispersive Hamiltonian, up to second order in $g/(\omega_{\rm q}-\omega_{\rm r})$ and $g/(\omega_{\rm q}+\omega_{\rm r})$, reads as [69]

$$\hat{H}_{\rm disp} = \frac{\hbar\omega_{\rm q}}{2}\hat{\sigma}_z + \hbar\omega_{\rm r}\hat{a}^\dagger\hat{a} + \frac{\hbar}{2}\left(\omega_{\rm BS}+\omega_{\text{ac-S}}\right)\hat{\sigma}_z\left(\hat{a}^\dagger+\hat{a}\right)^2, \tag{2.34}$$

where both, Bloch-Siegert and ac-Stark shifts are present. The dispersive regime allows for a quantum-non-demolition (QND) measurement of the qubit via the resonator, i.e., the qubit state is not destroyed in the measurement process. The term $\hat{\sigma}_z\hat{a}^\dagger\hat{a}$, in the dispersive Hamiltonians, dresses the resonator frequency with a positive (negative) shift when the qubit is in the excited (ground) state.

2.3 Schrödinger cat states

In the early days of quantum theory, properties like entanglement and superposition, along with their connection to the macroscopic world, underwent intense scrutiny. Early investigations led to the formulation of paradoxes such as the Einstein-Podolsky-Rosen paradox [16] and Schrödinger's cat paradox [55]. The cat paradox revolves around a microscopic object entangled with a macroscopic one, existing in a superposition of two distinct macroscopic states. This paradox was formulated to probe issues related to quantum measurement in entangled microscopic-macroscopic systems, as well as the quantum-to-classical transition.

Beyond the cat paradox, cat states became well defined non-classical states in different fields of quantum theory. In the field of quantum optics, cat states refer to a specific occurrence where an EM field mode is in a superposition of two macroscopically distinguishable states. In this thesis, we focus on a particular case where the field is in a superposition of two coherent states with opposite phases. These states have experienced a recent resurgence in interest for two main reasons. Firstly, cat states provide a valuable resource for investigating fundamental aspects of quantum mechanics and pushing the boundaries of quantum coherence. As the size of the cat state grows, moving from mesoscopic or microscopic to macroscopic physics, it allows for the exploration of foundational questions. This growth in size, measured by the total number of photons, enables the study of the limits of quantum coherence [70]. Secondly, cat states have generated interest in the development of error correction codes for quantum computation. They can be used to encode logical qubits, making amplitude damping or photon loss errors more easily correctable [30]. In this section, we define even and odd cat states, their statistical properties and common methods used to generate them. Note that there are many bosonic codes using cat states to logically encode a qubit, but we shall avoid discussing error correction schemes as they are not directly relevant to this thesis. We are strictly interested in the generation of cat states.

We begin by defining even and odd cat states as

$$|C_+\rangle = \frac{1}{\sqrt{\mathcal{N}_+}}\left(|\alpha\rangle + |-\alpha\rangle\right), \tag{2.35a}$$

$$|C_-\rangle = \frac{1}{\sqrt{\mathcal{N}_-}}\left(|\alpha\rangle - |-\alpha\rangle\right), \tag{2.35b}$$

where α is some complex number and $\mathcal{N}_\pm = 2(1 \pm \exp(-2|\alpha|^2))$ is the normalization; when $|\alpha|$ is large, $\mathcal{N}_\pm \to 2$. The terms 'even' and 'odd' refer to the contributions of Fock states.

An even cat state comprises a superposition of even Fock states, $|2n\rangle$. Conversely, an odd cat state is composed of odd Fock states, $|2n+1\rangle$. The parity of the state holds significant importance in specific error correction schemes. The parity of a cat state residing in a resonator can be measured by using a dispersively coupled qubit, without causing the resonator state to collapse. This form of measurement has minimal back-action [20].

The parity measurement provides a means to identify and monitor instances of photon loss, as the loss of a single photon would alter the state's parity. The parity can also be visualized through the Wigner function of a cat state. Besides the two lobes in the Wigner function, the number of negative dips in the interference region signifies the parity; if it is even (odd), the the cat is even (odd). The Wigner functions of these states along with their Fock state distributions are shown in Fig. 2.1. When accounting for dissipative effects, the lobes of the cat state, $|\pm\alpha\rangle$, evolve to lobes of smaller amplitude, $|\pm\alpha e^{-\kappa t}\rangle$ [32]. The interference region, however, decays much faster than the lobes. Eventually, the state converges to a steady state of an incoherent statistical mixture of coherent states $\hat{\rho}_{\text{ss}} = (|\alpha\rangle\langle\alpha| + |-\alpha\rangle\langle-\alpha|)/2$.

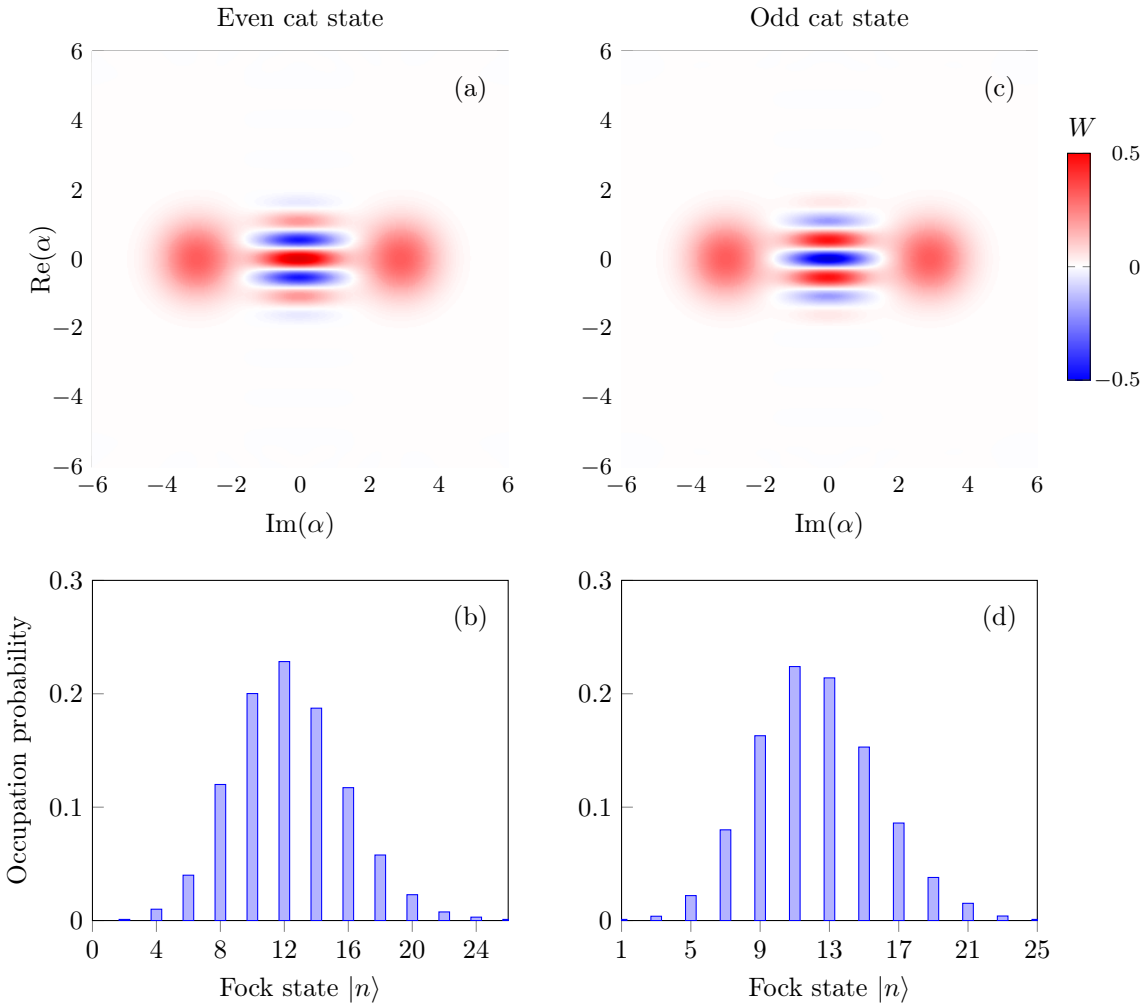

Figure 2.1: Wigner functions and Fock state distributions of even and odd cat states with $\alpha = 2$.

The cat states introduced above are also known as two-component cat states (due to the contribution of two coherent states). In general an N-component cat state can be defined as a superposition of N coherent states. In particular, N-component cat states of interest are those of equal amplitude ($|\alpha|$) distributed on a circle, i.e, a superposition of coherent states $\left|\alpha e^{i2\pi k/N}\right\rangle$ for $k = 0, 1, ..., N-1$. The recent interest in these particular cat states is due to the rotational symmetry in phase space and its relation to error correction codes [21]. In Fig. 2.2, the Wigner functions of a three-component cat state, $\propto |\alpha\rangle + \left|\alpha e^{i2\pi/3}\right\rangle + \left|\alpha e^{i4\pi/3}\right\rangle$,

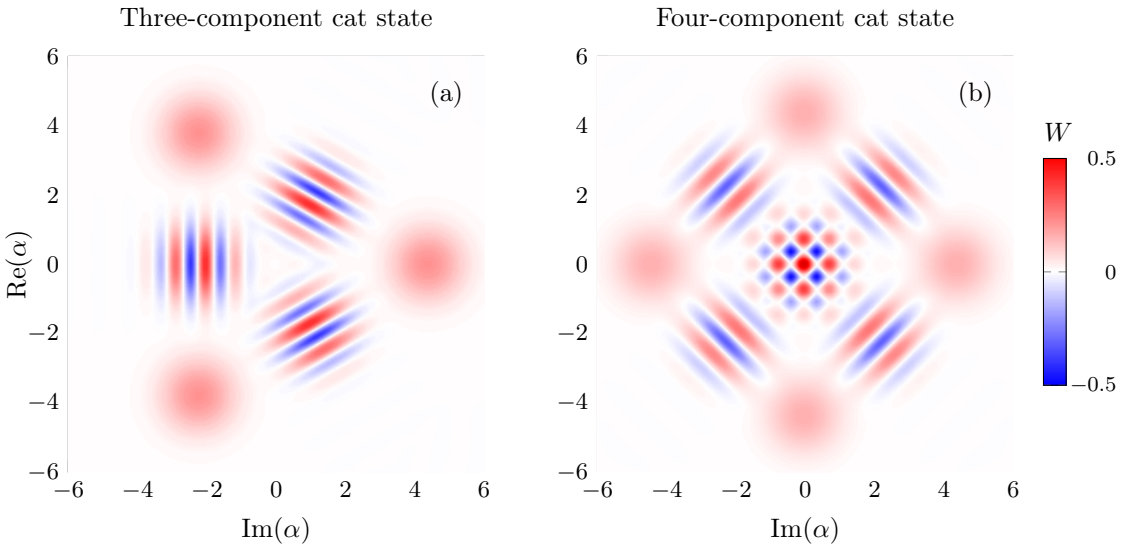

Figure 2.2: Wigner functions of three- and four-component cat states with $\alpha = 3$.

and a four-component cat state, $\propto |\alpha\rangle + \left|\alpha e^{i2\pi/4}\right\rangle + \left|\alpha e^{i4\pi/4}\right\rangle + \left|\alpha e^{i6\pi/4}\right\rangle$, are shown.

2.4 Circuit QED

The discussions on light-matter interaction presented earlier have been abstracted from an implementation scheme. This work is purely theoretical; however, its primary motivation lies in presenting a practical and experimentally-feasible theory for a circuit QED setup. The purpose of this section is to introduce the two main elements in a light-matter interaction scheme: the resonator—light and the anharmonic circuit behaving as an 'artificial atom'—matter. There exists a plethora of superconducting circuits with anharmonic spectra that can effectively serve as a qubit (or qudit). We will be concerned with an anharmonic circuit known as the Cooper-pair box. As for the resonator, we are mainly concerned with a lumped-element resonator and we also briefly discuss two-dimensional distributed-element resonators.

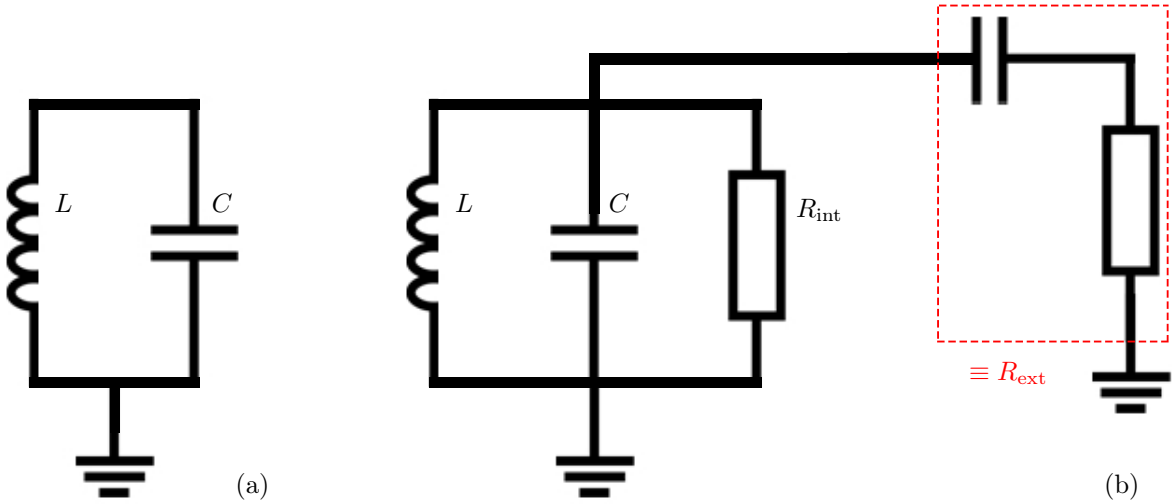

Figure 2.3: Lumped-element LC resonator circuit diagram.

LC resonator

The simplest quantum mechanical circuit is the LC resonator. The LC resonator is defined by an inductance L and a capacitance C. This gives it a frequency of $\omega_{\text{r}} = 1/\sqrt{LC}$. Here, we are interested in a circuit whose spatial dimensions are much smaller than the wavelengths of its harmonics. In such a case, we can simply treat it as a lumped-element circuit. Typically, for a resonator with $\omega_{\text{r}} = 2\pi \times 5\,\text{GHz}$, the associated wavelength is $\sim 6\,\text{cm}$ while its spatial dimensions are on the order of $\sim 100\,\mu\text{m}$. Thus, it is justified to reduce it to a lumped-element circuit.

The classical Hamiltonian of an LC resonator is

$$H_{LC} = \frac{Q^2}{2C} + \frac{\Phi^2}{2L} = \frac{Q^2}{2C} + \frac{1}{2}C\omega_{\text{r}}^2\Phi^2, \tag{2.36}$$

where Q is the charge stored in the capacitor and Φ is the flux passing through the inductor. In dealing with circuits we usually deal with currents, I, and voltages, V, so it is useful to remember that they are related to the charge and flux through these relations:

$$Q(t) = \int_{-\infty}^{t} d\tau I(\tau) \text{ and } \Phi(t) = \int_{-\infty}^{t} d\tau V(\tau).$$

This Hamiltonian exactly coincides with that of a mechanical harmonic oscillator, with the charge, Q, playing the role of the momentum and the flux, Φ, playing the role of the position. In this analogy, the inductive energy is the potential energy and the capacitive or charging energy is the kinetic energy. Since Φ is the 'position', the capacitive energy is $CV^2/2 = C\dot{\Phi}^2/2$. Thus, due to this form we can think of it as the kinetic energy. As such, the LC resonator plays the role of a quantum harmonic oscillator or a quantized field mode. For that purpose, we proceed with canonical quantization – promoting the classical functions Q and Φ to the operators $\hat{Q}$ and $\hat{\Phi}$ satisfying the canonical commutation relation

$$[\hat{\Phi}, \hat{Q}] = i\hbar.$$

We can then define these operators in term of the creation and annihilation operators as

$$\hat{\Phi} = \Phi_0(\hat{a}^\dagger + \hat{a}), \tag{2.37a}$$

$$\hat{Q} = iQ_0(\hat{a}^\dagger - \hat{a}), \tag{2.37b}$$

where $\Phi_0 = \sqrt{\hbar/2\omega_r C}$ and $Q_0 = \sqrt{\hbar\omega_r C/2}$ are the zero-point fluctuation flux and charge values. Using these definitions, we can arrive at the usual quantum harmonic oscillator Hamiltonian introduced in Sec. 2.1. When is such a quantum-mechanical description of an LC resonator appropriate? The energy, $\hbar\omega_r$, needs to be much larger than the thermal energy $k_B T$, i.e., $\hbar\omega_r \gg k_B T$. Then, for the desired GHz microwave frequency operation range, the quantum regime can be achieved around $\sim 10\,\mathrm{mK}$. For this frequency range, the inductance and capacitance of an LC resonator need to be on the order of $\sim 0.1\,\mathrm{nH}$ and $\sim 10\,\mathrm{fF}$, respectively. With all these conditions, one can cool down a microwave resonator and prepare it in its ground state, $|0\rangle$, with minimal thermal photons. Henceforth, we generally assume the quantized nature of the described circuits and proceed assuming they are already canonically quantized.

The LC resonator is also characterized by its photon loss rate, κ. This parameter is related to its quality factor by $\kappa = \omega_r/Q_r$. This loss rate is due to internal and external losses. Internal losses can be attributed to dielectric and conductor losses. External loss can be attributed to coupling and external radiation. The total loss can be quantified by a total resistance, $R_{\mathrm{tot}} = (R_{\mathrm{int}}^{-1} + R_{\mathrm{ext}}^{-1})^{-1}$ (see Fig. 2.3). This resistance can then be related to the photon loss rate by $\kappa = 1/R_{\mathrm{tot}}C$.

While we introduced the simplest linear superconducting circuit in a lumped-element format, a resonator can also be two- and three-dimensional. A two-dimensional example is a coplanar waveguide transmission line (TL) resonator with a set of discretized equally-spaced field modes depending the boundary conditions (e.g. $\lambda/2$ or $\lambda/4$). The TL is a

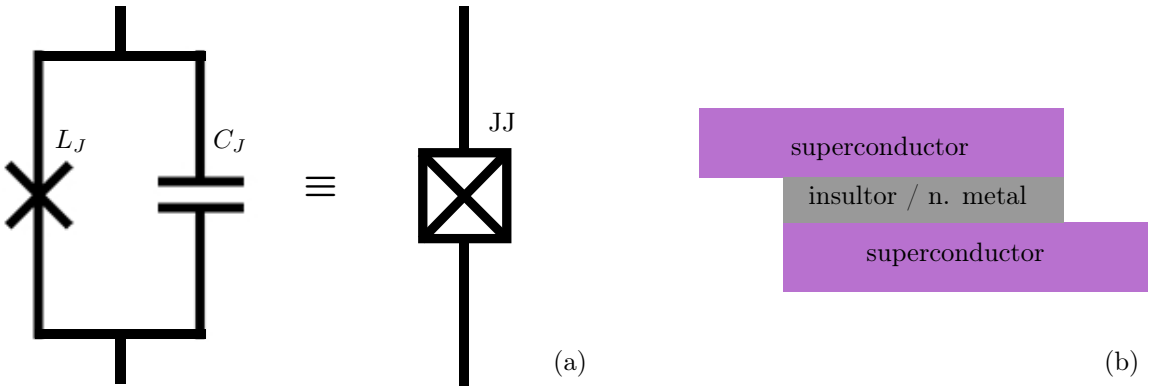

Figure 2.4: Lumped-element circuit diagram and schematic of a Josephson Junction.

distributed circuit and, as such, it is chracterized by an inductance per unit length $\widetilde{l}$, a capacitance per unit length $\widetilde{c}$ and a length d. Then, the fundamental mode frequency, $\omega_{\mathrm{r}0}$, depends on d, $\widetilde{l}$, $\widetilde{c}$ and the boundary conditions; $\omega_{\mathrm{r}0} \propto 1/d(\widetilde{l}\widetilde{c})^{1/2}$. A typical distributed-element resonator length is around $\sim 1\,\mathrm{cm}$. For a TL with fundamental mode frequency $\omega_{\mathrm{r}0}$ and photon loss rate $\kappa_0 = \omega_{\mathrm{r}0}/Q_{\mathrm{r}}$, the higher modes' frequencies are multiples (depending on the boundary condition) of the fundamental mode and the photon loss rate also increases for higher modes as $\kappa_m \propto \omega_{\mathrm{r}m}$, where for the m^{th} mode, κ_m is the photon loss rate and $\omega_{\mathrm{r}m}$ is the mode frequency. In the context of the work done in this thesis, we simply care about a single mode.

Cooper-pair box: charge and transmon qubits

For the purpose of creating artificial atoms, we would like to address the individual transitions between states. This is not possible in a resonator as it is harmonic and the energy levels are equally spaced. We need to introduce some source of nonlinearity (or anharmonicity).

All superconducting circuits used as artifical atoms incorporate a nonlinear element and in most of them it happens to be a Josephson junction (JJ) (possibly multiple). A JJ is composed of two superconducting slates separated by an insulating layer (or normal metal) as shown in Fig. 2.4(b). It is based on the Josephson effect, that predicted the tunnelling of Cooper pairs between superconducting slates across a non-superconducting

barrier. The JJ can be represented by a nonlinear Jospheson element (thought of as a nonlinear inductor) L_J and an intrinsic junction capacitance C_J (see Fig. 2.4(a)). The JJ is characterized by two constitutive relations:

$$I = I_c \sin(\varphi) \tag{2.38}$$

and

$$\frac{d}{dt}\varphi = \frac{2\pi}{\Phi_0} V, \tag{2.39}$$

where I is the current flowing into the JJ, V is the voltage across the junction, φ is the superconducting phase across the junction, I_c is the critical current (above which quasiparticle currents form) and Φ_0 is the flux quantum. The phase is related to the flux through $\varphi = 2\pi\Phi/\Phi_0$. The precise form of Eq. (2.38) prescribes the nonlinear element we seek for our artifical atoms. The energy associated with the JJ can be found using Joule's power law, $dE/dt = IV$. Using the constitutive relations and then integrating, we find

$$\frac{dE_J}{dt} = I_c \sin(\varphi)\frac{\Phi_0}{2\pi}\frac{d\varphi}{dt} \rightarrow \int_0^t I_c \sin(\varphi)\frac{\Phi_0}{2\pi}\frac{d\varphi}{dt}dt$$

$$\rightarrow \int_{\varphi_0}^{\varphi} \frac{\Phi_0 I_c}{2\pi}\sin(\varphi')d\varphi'.$$

Then, setting $\varphi_0 = 0$ yields

$$E_J = E_{J0}(1 - \cos(\varphi)), \tag{2.40}$$

where $E_{J0} = \Phi_0 I_c/2\pi$ and we usually drop the constant offset of E_{J0}. Henceforth, we simply denote E_{J0} by E_J. The Josephson inductance, L_J, can be easily derived from the constitutive relations as

$$L_J(\varphi) = \frac{L_J}{\cos(\varphi)} = \frac{\Phi_0}{2\pi I_c \cos(\varphi)}. \tag{2.41}$$

Typically, the JJ has an associated plasma frequency that is far too high, beyond the microwave regime we are interested in (it can reach $\sim$ THz). To remedy this problem, we usually shunt the JJ with a capacitor with much larger capacitance, C_S, than the intrinsic junction capacitance, C_J. The total capacitance is $C_\Sigma = C_S + C_J$. This device described is known as the Cooper-pair box (CPB). The Hamiltonian of the CPB reads as

$$\hat{H}_{\text{CPB}} = \frac{(\hat{Q} - Q_g)^2}{2C_\Sigma} - E_J \cos\left(\frac{2\pi}{\Phi_0}\hat{\Phi}\right) = 4E_C(\hat{n} - n_g)^2 - E_J\cos(\hat{\varphi}), \tag{2.42}$$

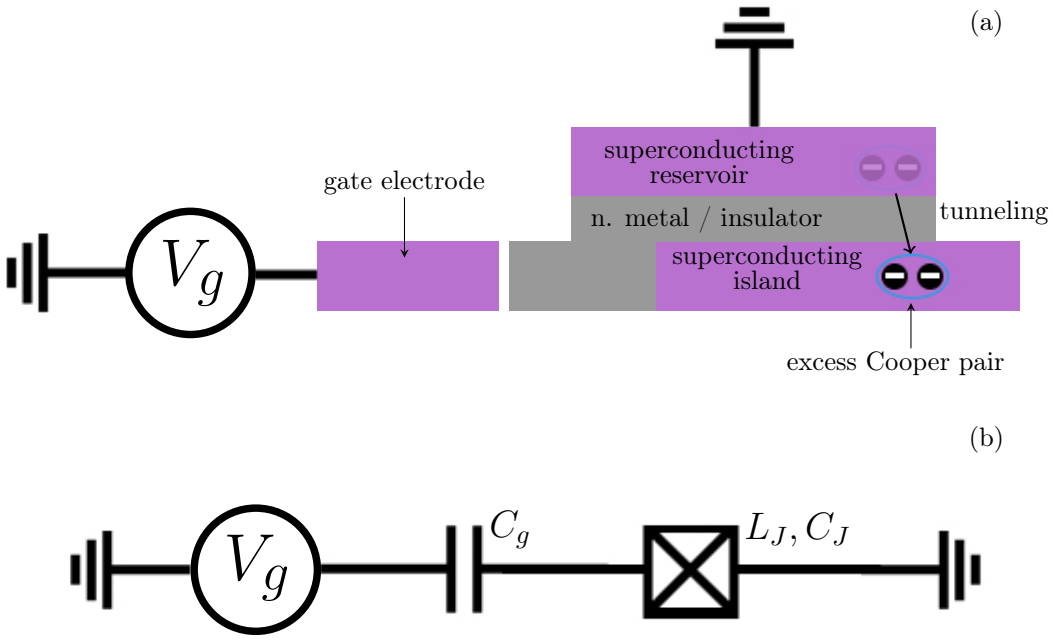

Figure 2.5: Physical schematic of the Cooper-pair box and its circuit diagram. The gate voltage source, V_g, can be used to pump excitations into the system via the gate electrode.

where $\hat{Q}$ and $\hat{\Phi}$ are the charge and flux operators of CPB and Q_g is an offset gate charge. The Hamiltonian is then rewritten in terms of the charge number and phase oerators, $\hat{n} = \hat{Q}/2e$ and $\hat{\varphi} = 2\pi\hat{\Phi}/\Phi_0$. Here, $E_C = e^2/2C_\Sigma$ is the charging energy and $n_g = Q_g/2e$ is the offset charge number. The presence of the cosine term in the Hamiltonian ensures the anharmonicity of the spectra. This means individual transitions can then be addressed by a drive.

The physical picture of the CPB can be summarized as follows. The relevant physical degree of freedom for this circuit is the *charge*. In particular, the excess number of Cooper pairs present on the superconducting island (see Fig. 2.5) is our quantum variables in which we can encode our qubit. When a Cooper pair tunnels from the reservoir to the superconducting island, the total charge on each slab differs and there is a net electric field across the junction that is the field of a *physical dipole*. When operating at the sweet spot in the charge regime, $E_J/E_C \leq 1$, the first two energy levels are well isolated from higher

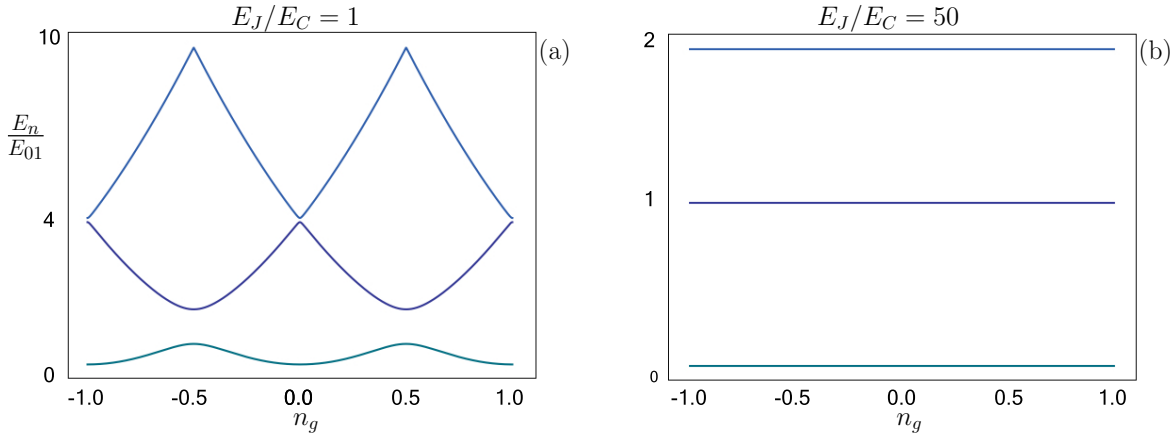

Figure 2.6: Cooper-pair box spectrum vs. offset charge in the charge ($E_J/E_C = 1$) and transmon ($E_J/E_C = 50$) regimes. The first three levels are shown ($n = 0, 1, 2$) and are rescaled by E_{01}, where $E_{nm} = E_n - E_m$.

levels, and this allows us to treat the circuit as an effective qubit. Next, we rewrite the CPB Hamiltonian in the charge basis

$$\hat{H}_{\mathrm{CPB}} = 4E_C \sum_{n_Q} \left[(n_Q - n_g)^2 \left| n_Q \right\rangle\!\left\langle n_Q \right| - \frac{E_J}{2} (\left| n_Q \right\rangle\!\left\langle n_Q + 1 \right| + \left| n_Q + 1 \right\rangle\!\left\langle n_Q \right|) \right]. \tag{2.43}$$

Then, we can choose to truncate at two levels, $n_Q = 0$ and $n_Q = 1$, for an effective qubit. The Hamiltonian is then simplified to

$$\hat{\tilde{H}}_{\mathrm{CPB}} = 4E_C \left[(-n_g)^2 \left| \tilde{0} \right\rangle\!\left\langle \tilde{0} \right| + (1 - n_g)^2 \left| \tilde{1} \right\rangle\!\left\langle \tilde{1} \right| - \frac{E_J}{2} (\left| \tilde{0} \right\rangle\!\left\langle \tilde{1} \right| + \left| \tilde{1} \right\rangle\!\left\langle \tilde{0} \right|) \right]. \tag{2.44}$$

To represent this Hamiltonian using Pauli matrices, we offset it and rewrite the Hamiltonian as

$$\hat{\tilde{H}}_{\mathrm{CPB}} = -\frac{4E_C(1 - 2n_g)}{2} \hat{\tilde{\sigma}}_z - \frac{E_J}{2} \hat{\tilde{\sigma}}_x, \tag{2.45}$$

where $\hat{\tilde{\sigma}}_z = \left| \tilde{0} \right\rangle\!\left\langle \tilde{0} \right| - \left| \tilde{1} \right\rangle\!\left\langle \tilde{1} \right|$ and $\hat{\tilde{\sigma}}_x = \left| \tilde{0} \right\rangle\!\left\langle \tilde{1} \right| + \left| \tilde{1} \right\rangle\!\left\langle \tilde{0} \right|$. This is Hamiltonian is known as the physical basis Hamiltonian. We can now diagonalize it to obtain the energy representation

$$\hat{H}_{\mathrm{qubit}} = \frac{\hbar \omega_{\mathrm{q}}}{2} \hat{\sigma}_z, \tag{2.46}$$

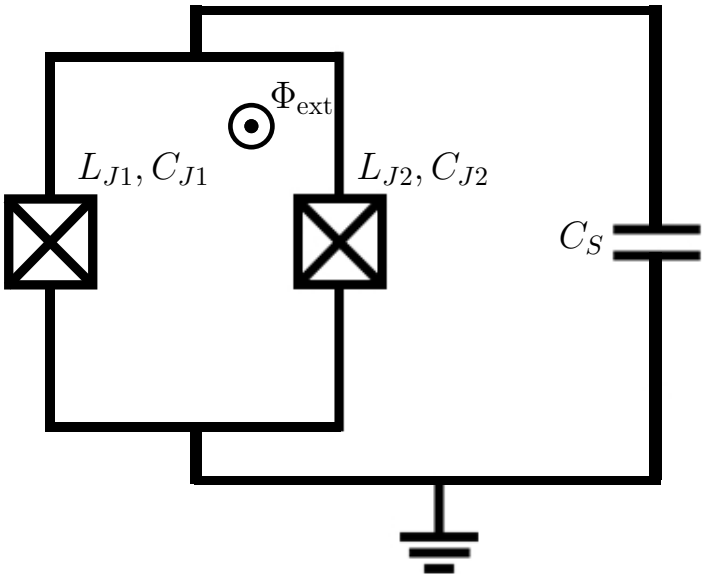

Figure 2.7: Flux-tunable Cooper-pair box circuit diagram.

where $\hbar\omega_{\text{q}} = \sqrt{E_J^2 + (4E_C(1-2n_g))^2}$ and $\hat{\sigma}_z$ is written in the energy eigenbasis.

In practice, we would like to tune E_J *in situ* as it determines the effective qubit frequency. For this purpose, we typically place two JJs in parallel to form a superconducting quantum interference device (SQUID) that can be threaded by external flux. The SQUID then behaves as an effective tunable JJ. Figure 2.7 shows a circuit diagram of a SQUID in parallel with a shunting capacitance. The introduction of a flux-tunable junction induces dephasing due to flux noise, whereas fixed-frequency qubits experience no pure dephasing (γ_ϕ, the pure dephasing rate, is zero). Thus, any model assuming a tunable qubit must account for such dephasing noise.

If we consider the distant (at the sweep spot) third level, we would have a strongly anharmonic qutrit. This is quite relevant for the work presented in this thesis. To the extent of accounting for higher levels, we now move onto discussing the extraction of selection rules. Unlike atomic physics, there is no general theory determining the selection rules between states, rather each anharmonic circuit implementation has its own selection rules that can be extracted from its Hamiltonian. We now elaborate how to extract the CPB selection rules in general, and we discuss the relevant nearest-neighbor (n^{th} state to $(n+1)^{\text{st}}$ state) allowed selection rules. We rewrite the CPB Hamiltonian in the phase (φ)

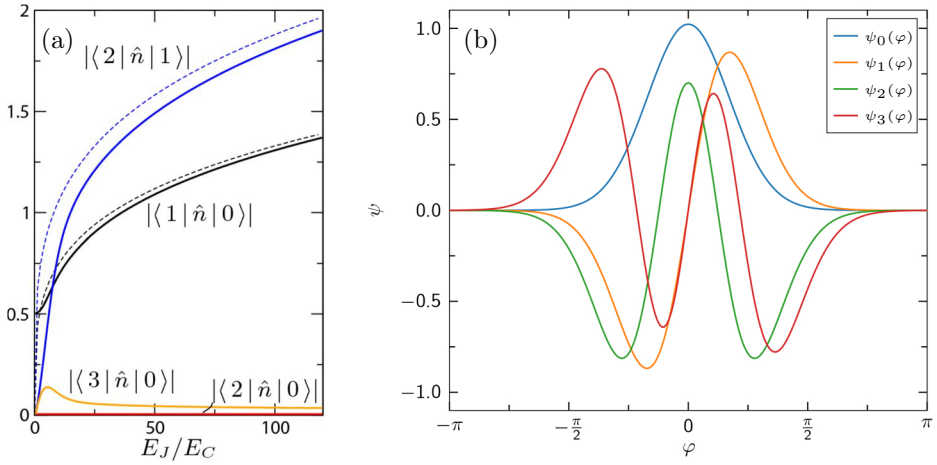

Figure 2.8: Some of the CPB transition matrix elements and phase wavefunctions. (a) The solid lines represent exact solutions obtained through Eq. (2.49), and the dashed lines represent asymptotic solutions obtained through Eq. (2.50). Figure taken from Ref. [33]. (b) First four phase wavefunctions. Figure taken from Ref. [10].

basis using the fact that $\hat{n}_Q = -i\partial/\partial\hat{\varphi}$,

$$\hat{H}_{\text{CPB}} = 4E_C\left(-i\frac{\partial}{\partial\hat{\varphi}} - n_g\right)^2 - E_J\cos(\hat{\varphi}). \tag{2.47}$$

We denote the CPB energy eigenstates as $\{|E_k\rangle\}$. Then, we represent said states using the phase representation wavefunction, $\psi_k(\varphi) = \langle\varphi|E_k\rangle$. The phase basis is restricted to $\varphi \in [-\pi, \pi)$. With this representation, we may now state an eigenvalue problem in terms of the CPB Hamiltonian

$$\left[4E_C\left(-i\frac{\partial}{\partial\varphi} - n_g\right)^2 - E_J\cos(\varphi)\right]\psi_k(\varphi) = E_k\psi_k(\varphi). \tag{2.48}$$

The statement of this eigenvalue problem exactly matches the Mathieu equation and can be solve analytically using Mathieu functions [13]. Since we use a capacitvely coupled external drive to excite the CPB, we seek to find the possible transitions the charge or number of cooper pairs operator can induce, i.e, energy eigenstate transition matrix elements $\langle E_j|\,\hat{n}_Q\,|E_k\rangle$. We now rewrite these transition matrix elements using the phase

representation

$$\begin{aligned}\langle E_j|\,\hat{n}_Q\,|E_k\rangle &= \int d\varphi \int d\varphi'\ \langle E_j|\varphi\rangle\,\langle\varphi|\,\hat{n}_Q\,|\varphi'\rangle\,\langle\varphi'|E_k\rangle \\ &= -i\int d\varphi\,\psi_j^*(\varphi)\frac{\partial}{\partial\varphi}\psi_k(\varphi).\end{aligned} \tag{2.49}$$

This is the general procedure for obtaining CPB selection rules. In Fig. 2.8 some of the first few transition matrix elements are shown where it is clear that the two-photon transition matrix element, $\langle E_2|\,\hat{n}_Q\,|E_0\rangle$, is forbidden and the three-photon transition matrix element, $\langle E_3|\,\hat{n}_Q\,|E_0\rangle$, is strongly suppressed and approaches zero at higher E_J/E_C ratios. For nearest-neighbor transitions, we can asymptotically express the matrix elements as [33]

$$\langle E_{n+1}|\,\hat{n}_Q\,|E_n\rangle \simeq \sqrt{\frac{n+1}{2}}\left(\frac{E_J}{8E_C}\right)^{1/4}, \tag{2.50}$$

where we can see the harmonic scaling of these transitions, i.e., $\propto\sqrt{n+1}$. For our work, we incorporate the third level into our considerations, approximating the CPB as a three-level system or qutrit. Based on the outlined selection rules, we have a cascade Ξ-type qutrit, allowing only nearest neighbor transitions.

The charge qubit suffers from sensitivity to charge noise. This can be interpreted from Fig. 2.6(a) where slight transaltions in the value of n_g change the eigenvalue (hence changing ω_{q}). This is referred to as charge dispersion. We now explore a different regime of the CPB known as the *transmon* regime. This regime is characterized by $E_J/E_C \gg 1$ where there is an exponential decrease in the charge dispersion while maintaining anharmonicity. This is shown in Fig. 2.6(b) where the energy eigenvalues form flat bands for varying n_g. In this regime, the qubit frequency is $\omega_{\mathrm{q}} \simeq \sqrt{8E_JE_C} - E_C$ and the third state is much closer to the second state than in the charge regime. The transmon is commonly referred to as a 'weakly anharmonic oscillator' for this reason. We rewrite the phase and number of Cooper pair operators in terms of the creation and annihilation operators, following a similar prescription as in Eq. (2.37),

$$\hat{\varphi} = \varphi_0(\hat{a}^\dagger + \hat{a})$$

and

$$\hat{n}_Q = in_{Q0}(\hat{a}^\dagger - \hat{a}),$$

where $\varphi_0 = (2E_C/E_J)^{1/4}$ and $n_{Q0} = (E_J/2E_C)^{1/4}/2$. Then, we can expand the cosine term

to fourth order and obtain the following Hamiltonian

$$\begin{aligned}\hat{H}_{\mathrm{CPB}} &\simeq \sqrt{8E_C E_J}\hat{a}^\dagger\hat{a} - \frac{E_C}{12}(\hat{a}^\dagger + \hat{a})^4 \\ &\overset{\mathrm{RWA}}{\simeq} \underbrace{\left(\sqrt{8E_C E_J} - E_C\right)}_{\hbar\omega_{\mathrm{q}}}\hat{a}^\dagger\hat{a} - \frac{E_C}{2}\hat{a}^{\dagger 2}\hat{a}^2. \end{aligned} \tag{2.51}$$

This Hamiltonian exhibits the form of a weakly anharmonic oscillator where there is a quartic perturbation. The coefficient of the anharmonic term is E_C, so it can be thought of as a quantifier of anharmonicity. In the transmon regime, $E_{12} := E_1 - E_2$ separation is less than the E_{01} separation. We define $\xi = E_{12} - E_{01}$ as the anharmonicity parameter between the first and second transition. Indeed, E_C is related to the anharmonicity via $E_C = -\xi$. In the charge regime, ξ is positive (operating at the sweet spot, it is negative at other n_g values), whereas in the transmon regime, it is negative. The aforementioned selection rules of the charge regime apply here. This means that if the third level is included, the transmon can also be modeled as a Ξ-type qutrit.

Coupling a qubit and a resonator

So far, we separately introduced the main players of a typical circuit QED setup, a linear circuit – our quantized field (mode) and an anharmonic circuit – our artificial atom. We now couple these two components.

We consider a capacitve coupling between a transmon and a lumped-element resonator. Then, the full circuit QED 'qubit-resonator' Hamiltonian reads as

$$\hat{H}_{\mathrm{cQED}} = \frac{\hat{Q}_{\mathrm{t}}^2}{2\widetilde{C_\Sigma}} - E_J\cos\left(\frac{2\pi}{\Phi_0}\hat{\Phi}_{\mathrm{t}}\right) + \frac{\hat{Q}_{\mathrm{r}}^2}{2\widetilde{C_{\mathrm{r}}}} + \frac{\hat{\Phi}_{\mathrm{r}}^2}{2L_{\mathrm{r}}} + \frac{C_g}{\bar{C}^2}\hat{Q}_{\mathrm{t}}\hat{Q}_{\mathrm{r}}{}^{4}, \tag{2.52}$$

where the subscript 't' refers to the transmon operators and 'r' refers to the resonator operators. Here, $\widetilde{C_\Sigma}$ is the renormalized transmon capacitance, $\widetilde{C_{\mathrm{r}}}$ is the renormalized resonator capacitance, C_g is the coupling capacitance and $\bar{C}$ is the cross-capacitance between all elements (due to the inversion of the capacitance matrix). When the transmon is truncated to a qubit, this Hamiltonian effectively acts as a variant of the QRM. Using the transmon approximation in Eq. (2.51) and the creation and annihilation definitions of the

[4]The offset charge, Q_g, was dropped since we can ignore it in the transmon regime.

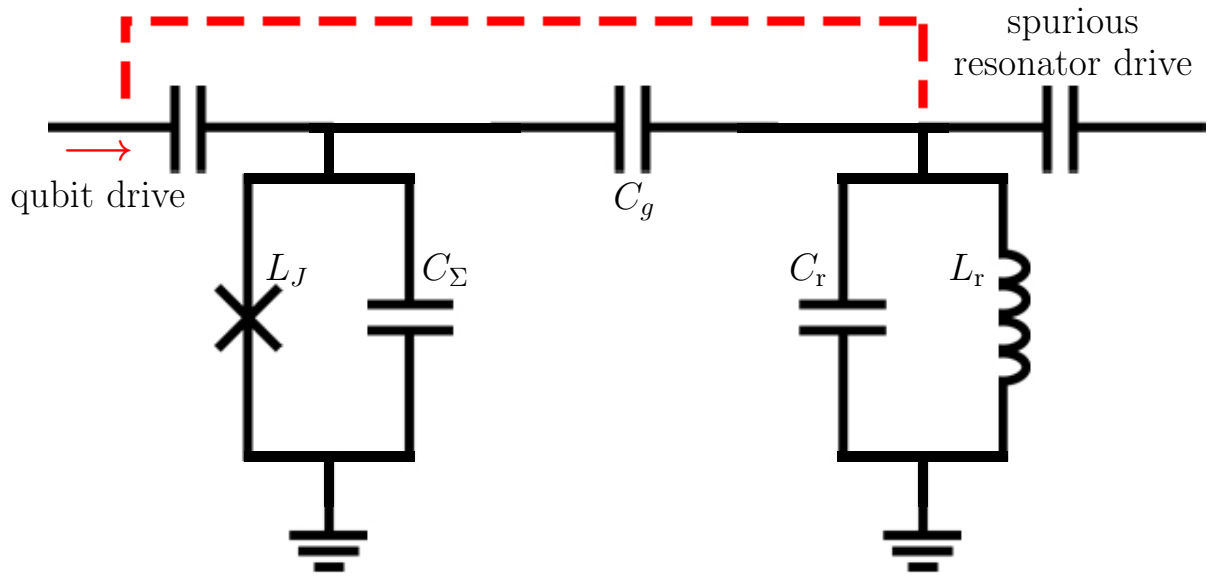

Figure 2.9: Lumped-element circuit diagram of qubit-resonator system highlighting cross-talk effects.

operators ($\hat{b}$, $\hat{b}^\dagger$ for the transmon and $\hat{a}$, $\hat{a}^\dagger$ for the resonator), the circuit QED Hamiltonian can be rewritten as

$$\hat{H}_\mathrm{cQED} \simeq \hbar\omega_\mathrm{q}\hat{b}^\dagger\hat{b} - \frac{E_C}{2}\hat{b}^{\dagger 2}\hat{b}^2 + \hbar\omega_\mathrm{r}\hat{a}^\dagger\hat{a} - \hbar g(\hat{b}^\dagger - \hat{b})(\hat{a}^\dagger - \hat{a}) \tag{2.53a}$$

$$\left(\substack{\text{Two-level}\\\text{approximation}} \rightarrow\right) \simeq \frac{\hbar\omega_\mathrm{q}}{2}\hat{\sigma}_z + \hbar\omega_\mathrm{r}\hat{a}^\dagger\hat{a} - \hbar g(\hat{\sigma}_+ - \hat{\sigma}_-)(\hat{a}^\dagger - \hat{a}), \tag{2.53b}$$

where $g = C_g Q_{0,\mathrm{t}} Q_{0,\mathrm{r}}/\hbar\bar{C}^2$; $Q_{0,\mathrm{t}}$ is the transmon zero-point charge and $Q_{0,\mathrm{r}}$ is the resonator zero-point charge. This final form of the Hamiltonian illuminates the clear connection to the QRM.

In addition to the coupling, we usually drive the qubit (or resonator) to pump some excitations into the system, perform gates, readout the qubit or resonator, etc. A capacitive network such as this always leads to cross-talk between different nodes – even when the parasitic capacitances are minimized[5]. Typically, this leads to spurious couplings – a fraction of the coupling between the originally coupled nodes. Figure 2.9 displays a circuit diagram of a coupled qubit-resonator system and points out the cross-talk between the

[5]When inverting a capacitance matrix, an entry of zero in the original capacitance matrix can yield nonzero entries in the inverse matrix.

qubit drive and resonator. For low power driving, on either subsystem, the effects are negligible. However, for strong driving driving, like the cases considered in this thesis, the effects can significantly with the desired outcome. In particular, a spurious drive applied to the resonator populates it with a coherent state, resulting in a displacement of whatever state previously existed.

To end this section, Table 2.1 lists typical circuit QED parameters relevant for a qubit-resonator system. While the work presented in this thesis is theoretical, its motivation is to propose a practical theory based on experimentally feasible parameter regimes to obtain a cat state using a qubit or qutrit. In the next chapter, we show that our proposal can be implemented with worse-than-average parameters and still outperform some methods for the purpose of generating a cat state.

Parameters	Value(s)
$\omega_{\rm r}/2\pi$	$\sim 4-10$ GHz
$\omega_{\rm q}/2\pi$	$\sim 4-10$ GHz
$g/2\pi$	$\sim 20-200$ MHz
$\tau_g = 2\pi/g$	$\sim 5-50$ ns
κ $(T_{1\rm r}^{-1})$	< 100 kHz $(> 10\mu{\rm s}^{-1})$
γ_1 (T_1^{-1})	< 50 kHz $(> 20\mu{\rm s}^{-1})$
γ_ϕ[6]	< 100 kHz

Table 2.1: Typical circuit QED experimental parameters observed in our group.

2.5 Outline of the analytic calculations

In the previous sections, we covered the basic elements of quantum mechanics used in this thesis, the relevant light-matter interaction models and the underlying physics of a circuit QED implementation. In this last preliminary section, we hope to succinctly outline the reoccurring theme of analytic calculations performed in this thesis.

The starting point—in both the qubit and qutrit chapters— is a driven QRM model in which the qubit is driven, i.e., the SRM and QRM considered both at once. We proceed in several steps unravelling different layers of complexity. First, we resort to a rotating frame (driving frame) to simplify the time-dependence in the Hamiltonian. In the rotating frame, we derive the requisite rotating-wave approximation (RWA) conditions for eliminating

[6] $\gamma_\phi = T_2^{-1} - (2T_1)^{-1}$.

(∗) Transform to driving frame $\hat{H}^{\mathrm{d}} = \hat{U}_{\mathrm{d}}^{\dagger}\hat{H}\hat{U}_{\mathrm{d}} + i\hbar\dot{\hat{U}}_{\mathrm{d}}^{\dagger}\hat{U}_{\mathrm{d}}$

$\longrightarrow$ Derive RWA conditions to drop counter-rotating terms

$\longrightarrow$ Simplified Hamiltonian

(∗) Find dressed states and transform to interaction picture $\hat{H}^{(\mathrm{I})}$

$\longrightarrow$ Derive strong driving RWA conditions

$\longrightarrow$ Effective Hamiltonian

$\longrightarrow$ Analytic results

Figure 2.10: Outline of the analytic calculations.

counter- or fast-rotating driving *and* interaction terms. Then, we perform said RWA and arrive at a simplified Hamiltonian. After which, we find the qubit or qutrit dressed states and transform to the interaction picture. In the interaction picture, we seek to distinguish interaction terms arising on different timescales. In particular, we seek to eliminate interaction terms modulated by the driving strength (Ω or Ω_1 and Ω_2, defined later). To eliminate these terms, conditions for a *strong driving* RWA are formulated. Once this strong driving RWA is performed, an effective Hamiltonian is arrived at. The effective Hamiltonian is then used to analytically obtain the time-evolved state for a particular initial state. Lastly, the analytical results are verified with numerical simulations performed without any of the approximations used to derive the analytical result. These numerical simulations also account for decoherence as is outlined in App. A. Figure 2.10 displays a summary of the steps used in obtaining analytical results.

Chapter 3

Driven Qubit-Resonator System

The qubit-resonator system embodied by the QRM is a fundamental tool for many quantum-mechanical foundational investigations and practical technological applications. In this chapter, we add a periodic drive to the qubit. This approach allows us to explore a different aspect of the qubit-resonator interaction and gain further insights into its behavior. By adding a drive to the qubit, we arrive at the driven QRM. The drive dresses the qubit frequency and, as a result, it affects its interaction with the resonator. We carefully explore the exact conditions required to perform an RWA, as is usually done to obtain the JCM, and demonstrate how the driving parameters play a crucial role in determining the regimes of validity for an RWA.

The material presented in this chapter serves as a critical analysis and generalization of the cavity QED study conducted in the work of Ref. [58]. The structure of the chapter is as follows. In Sec. 3.1, we begin by stating the system Hamiltonian and establishing the necessary conditions for implementing an RWA within the framework of qubit-drive resonant conditions. Then, we delve into the RWA Hamiltonian and explore how a second, distinct RWA can be imposed under strong driving conditions. Furthermore, we explore the application of this approach in generating a cat state. In Sec. 3.2, we expand the theory to cover arbitrary detuning scenarios. We discover that it remains feasible to generate a cat state, similar to the resonant case, albeit with a reduced number of photons. We verify the robustness of our predictions by numerically solving a master equation that accounts for qubit relaxation, dephasing, and resonator relaxation. The qubit-resonator dynamics and the Wigner functions of the resonator state following a projective measurement on the qubit are displayed for the different regimes. In Sec. 3.3, we discuss a practical consideration of cross-talk between the qubit drive and the resonator leading to a spurious resonator drive. We resolve the issue by adding a drive on the resonator with a properly selected

amplitude and phase for perfect cancellation. In Sec. 3.4, we show how the theory generalizes to a driven qubit coupled simultaneously to many resonators. We demonstrate how to synthesize multipartite entangled Bell-like cat states. Finally, we compare our proposal to two commonly used methods for generating cat states in Sec. 3.6.

3.1 Resonant strong driving of the qubit

We start by considering the Hamiltonian associated with the driven QRM that reads as

$$\hat{H} = \frac{\hbar\omega_{\mathrm{q}}}{2}\hat{\sigma}_z + \hbar\omega_{\mathrm{r}}\hat{a}^\dagger\hat{a} + \hbar g(\hat{\sigma}_+ + \hat{\sigma}_-)(\hat{a}^\dagger + \hat{a}) + \hbar\Omega\cos(\omega_{\mathrm{d}}t)(\hat{\sigma}_+ + \hat{\sigma}_-), \tag{3.1}$$

The Hamiltonian of Eq.(3.1) can be written in the frame of the driving field by means of the unitary transformation $\hat{U} = \exp\left[-i\omega_{\mathrm{d}}t(\hat{\sigma}_z/2 + \hat{a}^\dagger\hat{a})\right]$,

$$\begin{aligned}\hat{H}^{\mathrm{d}} &= \hat{U}^\dagger\hat{H}\hat{U} + i\hbar\dot{\hat{U}}^\dagger\hat{U} \\ &= \frac{\hbar\Delta}{2}\hat{\sigma}_z + \hbar\delta\hat{a}^\dagger\hat{a} \\ &+ \hbar g\left(\hat{\sigma}_+\hat{a} + \hat{\sigma}_-\hat{a}^\dagger + e^{+i2\omega_{\mathrm{d}}t}\hat{\sigma}_+\hat{a}^\dagger + e^{-i2\omega_{\mathrm{d}}t}\hat{\sigma}_-\hat{a}\right) \\ &+ \frac{\hbar\Omega}{2}\left(\hat{\sigma}_+ + \hat{\sigma}_- + e^{+i2\omega_{\mathrm{d}}t}\hat{\sigma}_+ + e^{-2i\omega_{\mathrm{d}}t}\hat{\sigma}_-\right),\end{aligned} \tag{3.2}$$

where $\Delta = \omega_{\mathrm{q}} - \omega_{\mathrm{d}}$, $\delta = \omega_{\mathrm{r}} - \omega_{\mathrm{d}}$, and we use the exponential definition of $\cos(x) = (e^{ix} + e^{-ix})/2$.

The Hamiltonian of Eq. (3.2) can be simplified by imposing a set of RWA conditions that read as

$$\omega_{\mathrm{q}} - \omega_{\mathrm{r}} \ll \omega_{\mathrm{q}} + \omega_{\mathrm{r}} \text{ and } g \ll \min(\omega_{\mathrm{q}}, \omega_{\mathrm{r}}), \tag{3.3a}$$

$$g \ll 2\omega_{\mathrm{d}}, \text{ and} \tag{3.3b}$$

$$\Omega \ll 4\omega_{\mathrm{d}}. \tag{3.3c}$$

The conditions in Eq. (3.3a) are those used to derive the JCM from the QRM. The other two conditions allow us to account for the presence of the driving field. The condition in Eq. (3.3b) is necessary to eliminate the counter-rotating interaction terms $g(e^{+i2\omega_{\mathrm{d}}t}\hat{\sigma}_+\hat{a}^\dagger + e^{-i2\omega_{\mathrm{d}}t}\hat{\sigma}_-\hat{a})$, whereas the condition in Eq. (3.3c) is required to drop the counter-rotating

driving terms $\Omega(e^{+i2\omega_{\rm d}t}\hat{\sigma}_+ + e^{-i2\omega_{\rm d}t}\hat{\sigma}_-)/2$. Under all these RWA conditions, the Hamiltonian can be simplified to read as

$$\hat{H}^{\rm d}_{\rm RWA} = \frac{\hbar\Delta}{2}\hat{\sigma}_z + \hbar\delta\hat{a}^\dagger\hat{a} + \hbar g(\hat{\sigma}_+\hat{a} + \hat{\sigma}_-\hat{a}^\dagger) + \frac{\hbar\Omega}{2}(\hat{\sigma}_+ + \hat{\sigma}_-). \tag{3.4}$$

This Hamiltonian, which is free of any time-dependent terms, serves as the basis for the work presented in this section.

We start by considering the Hamiltonian of Eq.(3.4) under the resonant condition $\Delta = 0$. To simplify the notation, we define $\hat{H}^{\rm d}_0 = \hbar\Omega(\hat{\sigma}_+ + \hat{\sigma}_-)/2 + \hbar\delta\hat{a}^\dagger\hat{a}$ and $\hat{H}^{\rm d}_{\rm I} = \hbar g\left(\hat{\sigma}_+\hat{a} + \hat{\sigma}_-\hat{a}^\dagger\right)$. We then apply the unitary transformation $\hat{U}_0 = \exp\left(-i\hat{H}_0 t/\hbar\right)$, which allows us to obtain the interaction picture Hamiltonian

$$\begin{aligned}\hat{H}^{\rm (I)}_{\rm RWA} = \hat{U}_0^\dagger\hat{H}_{\rm I}\hat{U}_0 =& \frac{\hbar g}{2}\Big(|+\rangle\langle+| - |-\rangle\langle-| + e^{i\Omega t}|+\rangle\langle-| - e^{-i\Omega t}|-\rangle\langle+| \Big)\hat{a}e^{-i\delta t} \\ &+ \text{H.c.};\end{aligned} \tag{3.5}$$

$|\pm\rangle$ are the dressed basis qubit eigenstates, with the property that $\hat{\sigma}_x|\pm\rangle = \pm|\pm\rangle$.

The Hamiltonian of Eq. (3.21) reveals two distinct interactions taking place at different timescales. In one of them, two terms are modulated by the driving field and exhibit oscillations with functional dependence $e^{\pm i\Omega t}$. These terms can be neglected by imposing the *strong driving condition*,

$$\Omega \gg |\delta|, g. \tag{3.6}$$

This condition, however, must be considered at the same time as the condition of Eq.(3.3c); therefore, the complete condition reads as

$$g, |\delta| \ll \Omega \ll 4\omega_{\rm d}. \tag{3.7}$$

This means that Ω is characterized by a lower bound as well as an upper bound, that is, it cannot be arbitrarily large[1]. This assumption makes it possible to obtain the effective Hamiltonian

$$\hat{H}^{\rm (I)}_{\rm eff} = \frac{\hbar g}{2}\left(|+\rangle\langle+| - |-\rangle\langle-|\right)\left(\hat{a}^\dagger e^{+i\delta t} + \hat{a}e^{-i\delta t}\right). \tag{3.8}$$

[1]The work in Ref. [58] starts with the RWA form of the drive already imposed. The condition in Eq. (3.7) is the correction needed to make the theory of Ref. [58] work for a driven qubit-resonator in circuit QED.

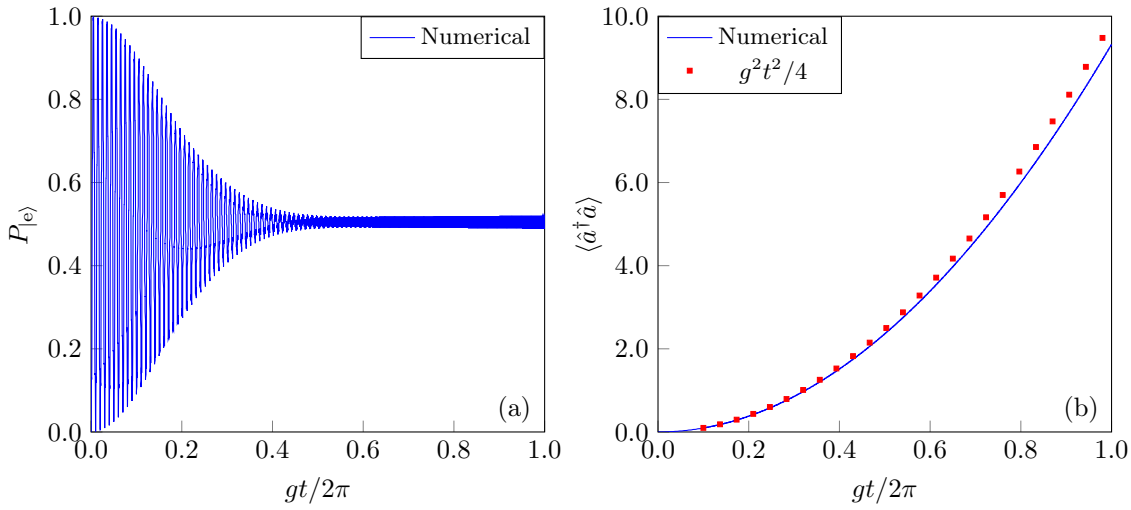

Figure 3.1: Characterization of cat states under resonance conditions. The parameters used for the simulations are: $\Omega = 2\pi \times 2\,\mathrm{GHz}$. $\Delta = \delta = 0$. $\omega_\mathrm{q} = 2\pi \times 5\,\mathrm{GHz}$. $g = 2\pi \times 20\,\mathrm{MHz}$. $\gamma_1 = \kappa = 500\,\mathrm{kHz}$. $\gamma_\phi = 1\,\mathrm{MHz}$. (a),(b) $P_{|\mathrm{e}\rangle}$ and $\langle \hat{a}^\dagger \hat{a} \rangle$ vs. normalized time $gt/2\pi$.

The dynamics associated with this Hamiltonian result in a conditional displacement of the resonator state based on the qubit state. Specifically, if the qubit is in state $|+\rangle$, the resonator state is displaced in a certain direction. Conversely, if the qubit state is in $|-\rangle$, the resonator state is displaced in the opposite direction. Thus, if we choose the initial state to be $|\psi_\mathrm{i}\rangle = |\mathrm{g}\rangle\,|0\rangle = (|+\rangle + |-\rangle)\,|0\rangle\,/\sqrt{2}$, the time evolution of the system leads, in the interaction picture, to the state

$$\begin{aligned} |\psi(t)\rangle^{(\mathrm{I})} &= \frac{1}{\sqrt{2}}(|+\rangle\,|\alpha\rangle + |-\rangle\,|-\alpha\rangle) \\ &= \frac{1}{2}\,|\mathrm{g}\rangle\,(|\alpha\rangle + |-\alpha\rangle) + \frac{1}{2}\,|\mathrm{e}\rangle\,(|\alpha\rangle - |-\alpha\rangle), \end{aligned} \tag{3.9}$$

where $\alpha = -g(e^{i\delta t} - 1)/2\delta$; when $\delta \to 0$, then $\alpha = -igt/2$.

If the qubit is measured to be in $|\mathrm{g}\rangle$, the resonator is left in a state that is proportional to the superposition of two coherent states, $\langle \mathrm{g}|\psi(t)\rangle^{(\mathrm{I})} \propto |\alpha\rangle + |-\alpha\rangle$; an *even cat state*. On the other hand, if the qubit is measured in $|\mathrm{e}\rangle$, the resonator is in the state $\langle \mathrm{e}|\psi(t)\rangle^{(\mathrm{I})} \propto |\alpha\rangle - |-\alpha\rangle$; an *odd cat state*.

Figure 3.1 displays the results of numerical simulations of the complete system Hamiltonian of Eq. (3.1), without any approximations. These simulations are performed in

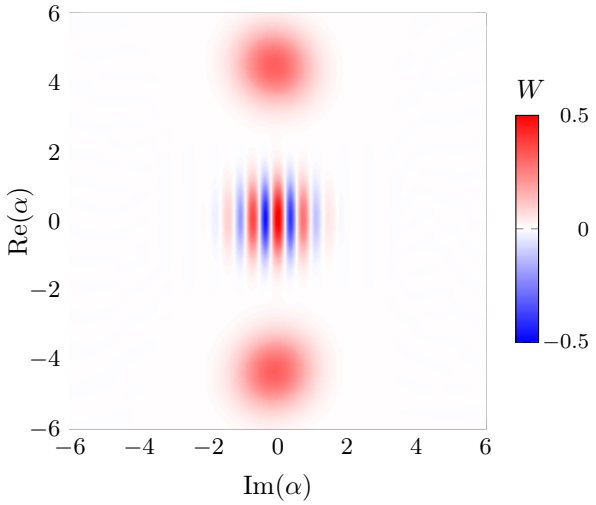

Figure 3.2: Wigner function of a resonant cat state. Heatmap of the Wigner function W of the resonator state after measuring the qubit in $|\mathrm{e}\rangle$ at $gt/2\pi = 1$. The result is obtained from the same simulation of Fig 3.1. This choice of time corresponds to an ideal cat state, accounting for the driving and interaction Bloch-Siegert shifts.

presence of both qubit and resonator decoherence by means of a Lindblad master equation, as explained in App. A. Figure 3.1 (a) shows the probability of the qubit to be in the excited state, $P_{|\mathrm{e}\rangle}$. This probability shows that as the cat state grows, the qubit population converges to an equal superposition of $|\mathrm{g}\rangle$ and $|\mathrm{e}\rangle$. Figure 3.1 (a) indicates that the photon number $n = \langle \hat{a}^\dagger \hat{a} \rangle$ grows quadratically in time. Interestingly, this behaviour persists even in presence of decoherence. The numerical results closely follow the analytical prediction $|\alpha|^2 = g^2 t^2/4$.

In order to visualize the cat states, we elect to represent them in phase space by means of the Wigner function introduced in Sec. 2.1. Here, we use the density matrix of the resonator after performing a projective measurement on the qubit state. Figure 3.2 shows W after measuring the qubit for $gt/2\pi = 1$.

The numerical simulations based on the Hamiltonian of Eq. (3.1) do not employ the approximations of Eqs. (3.3) and (3.7). This exact Hamiltonian can be rewritten in the rotating frame and interaction picture as

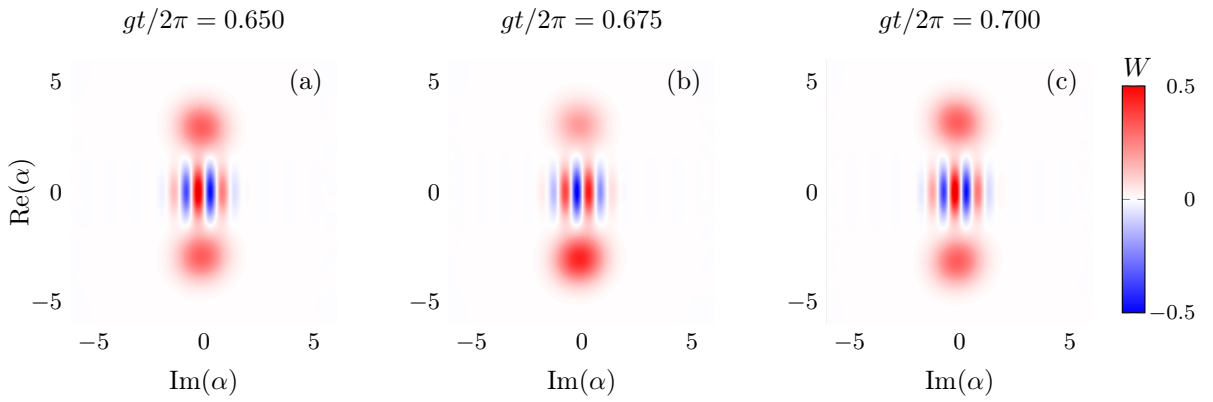

Figure 3.3: Oscillating cat state lobes due to the Bloch-Siegert shift.

$$\hat{H}^{(\mathrm{I})} = \frac{\hbar}{2}\Big(|+\rangle\langle +| - |-\rangle\langle -| + e^{i\Omega t}|+\rangle\langle -| - e^{-i\Omega t}|-\rangle\langle +| \Big) \times \left(\underbrace{\frac{\Omega}{2} e^{i2\omega_{\mathrm{d}} t}}_{\text{driving Bloch-Siegert shift}} + \overbrace{g\hat{a}^{\dagger} e^{i(2\omega_{\mathrm{d}}+\delta)t}}^{\text{interaction Bloch-Siegert shift}} + g\hat{a}e^{-i\delta t} \right) + \text{H.c.}, \tag{3.10}$$

which includes the counter-rotating driving and interaction terms. These terms lead to the driving and interaction Bloch-Siegert shifts, respectively. These two effects combined together result in the oscillation of the amplitude and weight coefficients of the cat states' lobes [47]. Except for the oscillations due to the Bloch-Siegert shifts, the numerical and analytical solutions very closely resemble each other. It is worth noting that these oscillations can be tracked deterministically, therefore allowing us to measure an ideal cat state. Figure 3.3 shows different snapshots in the time-evolution of a cat state Wigner function with the amplitudes of the lobes oscillating in time due to the Bloch-Siegert shift.

As a side note, it is worth noting that a cat state can be achieved even in absence of any strong drive, i.e., the condition $\Omega \gg g, |\delta|$ no longer holds. An example of such state is shown in Fig. 3.4. This cat state is manifestly *deformed*. To understand the origin of the deformation, we group together all the terms dropped to obtain the Hamiltonian of

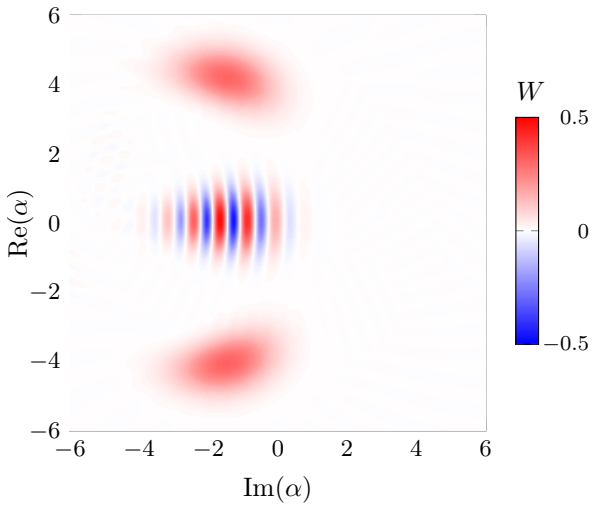

Figure 3.4: Wigner function of a deformed cat state. Heatmap of the Wigner function W of the resonator state after measuring the qubit in $|\mathrm{e}\rangle$ at $gt/2\pi = 1$. The cat state exhibits squeezing of the lobes and interference region and a displacement on the imaginary axis. The parameters used for the simulations are: $\Omega = 2\pi \times 200\,\mathrm{MHz}$. $\Delta = \delta = 0$. $\omega_\mathrm{q} = 2\pi \times 5\,\mathrm{GHz}$. $g = 2\pi \times 20\,\mathrm{MHz}$. $\gamma_1 = \kappa = 500\,\mathrm{kHz}$. $\gamma_\phi = 1\,\mathrm{MHz}$.

Eq. (3.21) in what we define the deformation Hamiltonian:

$$\begin{aligned}\hat{H}^{(\mathrm{I})}_{\mathrm{def}} &= \hat{H}^{(\mathrm{I})}_{\mathrm{RWA}} - \hat{H}^{(\mathrm{I})}_{\mathrm{eff}} \\ &= \frac{\hbar g}{2}\left(e^{i\Omega t}\,|+\rangle\langle -| - e^{-i\Omega t}\,|-\rangle\langle +|\right)\hat{a}e^{-i\delta t} + \mathrm{H.c.} \\ &= \frac{i\hbar g}{2}\left[\hat{\sigma}_y\cos(\Omega t) + \hat{\sigma}_z\sin(\Omega t)\right]\left(e^{+i\delta t}\hat{a}^\dagger - e^{-i\delta t}\hat{a}\right). \end{aligned} \tag{3.11}$$

The dynamics described by the deformation Hamiltonian also exhibit a conditional displacement, similar to Eq. (3.8). However, in this case, the displacement is modulated by the classical drive and is conditioned on two different qubit operators, $\hat{\sigma}_z$ and $\hat{\sigma}_y$. Furthermore, the deformation Hamiltonian introduces a displacement in a different direction in phase space (specifically, on the real axis) compared to the displacement generated by Eq. (3.8). In the presence of a weak drive, the contributions from $\hat{H}^{(\mathrm{I})}_{\mathrm{def}}$ become nonnegligible. When measuring in the bare basis of the qubit, $\{|\mathrm{g}\rangle, |\mathrm{e}\rangle\}$ [as required to obtain the cat state given by Eq. (3.9)], we observe a cat state that exhibits properties resembling squeezing.

3.2 Detuned regime

Thus far, our analysis has been confined to the resonance condition where $\Delta = 0$. However, to achieve scalability, it is essential to explore the generation of cat states without relying solely on qubit-drive resonance. One possible application of our theory is the generation of cat states in multiple driven qubit-resonator systems. In pursuit of this goal, we extend the theory to the qubit-drive detuned regime, where $\Delta \neq 0$.

We consider the Hamiltonian of Eq. (3.10) when $\Delta \neq 0$. In this case,

$$\begin{aligned}\hat{H}_{\text{det}}^{(\text{I})} =& \frac{\hbar}{2\varepsilon(\Delta+\varepsilon)} \\ &\times \Big[(\Delta+\varepsilon)\Omega \left|\widetilde{+}\right\rangle\!\left\langle\widetilde{+}\right| + (\Delta+\varepsilon)^2 e^{i\varepsilon t} \left|\widetilde{+}\right\rangle\!\left\langle\widetilde{-}\right| \\ &- \Omega^2 e^{-i\varepsilon t} \left|\widetilde{-}\right\rangle\!\left\langle\widetilde{+}\right| - (\Delta+\varepsilon)\Omega \left|\widetilde{-}\right\rangle\!\left\langle\widetilde{-}\right| \Big] \\ &\times \left(\frac{\Omega}{2} e^{i2\omega_{\text{d}} t} + g\hat{a} e^{-i\delta t} + g\hat{a}^\dagger e^{i(2\omega_{\text{d}}+\delta)t}\right) + \text{H.c.};\end{aligned} \tag{3.12}$$

$\varepsilon = \sqrt{\Omega^2 + \Delta^2}$ and the detuned qubit orthonormal basis is defined as $\left|\widetilde{+}\right\rangle = \sin(\theta/2)\left|\text{g}\right\rangle + \cos(\theta/2)\left|\text{e}\right\rangle$ and $\left|\widetilde{-}\right\rangle = \cos(\theta/2)\left|\text{g}\right\rangle - \sin(\theta/2)\left|\text{e}\right\rangle$, where the mixing angle $\theta = \arctan(\Omega/\Delta)$. Note that, if we set $\Delta = 0$, we recover the results of Sec. 3.1. If $\Omega \gg \Delta$, then $\left|\widetilde{+}\right\rangle \simeq \left|+\right\rangle$ and $\left|\widetilde{-}\right\rangle \simeq \left|-\right\rangle$; on the other hand, if $\Delta \gg \Omega$, we have $\left|\widetilde{+}\right\rangle \simeq \left|\text{e}\right\rangle$ and $\left|\widetilde{-}\right\rangle \simeq \left|\text{g}\right\rangle$.

We now follow a similar procedure as in Sec. 3.1 but in presence of detuning. Assuming all the conditions of Eq. (3.3) to hold true and additionally imposing the *strong driving-detuning* condition

$$g, |\delta| \ll \varepsilon \ll 4\omega_{\text{d}}, \tag{3.13}$$

we perform an RWA obtaining the effective Hamiltonian

$$\hat{H}_{\text{det, eff}}^{(\text{I})} = \frac{\hbar g\Omega}{2\varepsilon}\left(\left|\widetilde{+}\right\rangle\!\left\langle\widetilde{+}\right| - \left|\widetilde{-}\right\rangle\!\left\langle\widetilde{-}\right|\right)\left(\hat{a}^\dagger e^{+i\delta t} + \hat{a} e^{-i\delta t}\right). \tag{3.14}$$

This Hamiltonian generalizes that of Eq. (3.8) and, thus, it generates a resonator displacement conditioned on $\left|\widetilde{\pm}\right\rangle$. When initializing the system in state $\left|\psi_{\text{i}}\right\rangle = \left|\text{g}\right\rangle\left|0\right\rangle = \left(\sin(\theta/2)\left|\widetilde{+}\right\rangle + \cos(\theta/2)\left|\widetilde{-}\right\rangle\right)\left|0\right\rangle$, we obtain the time-evolved state

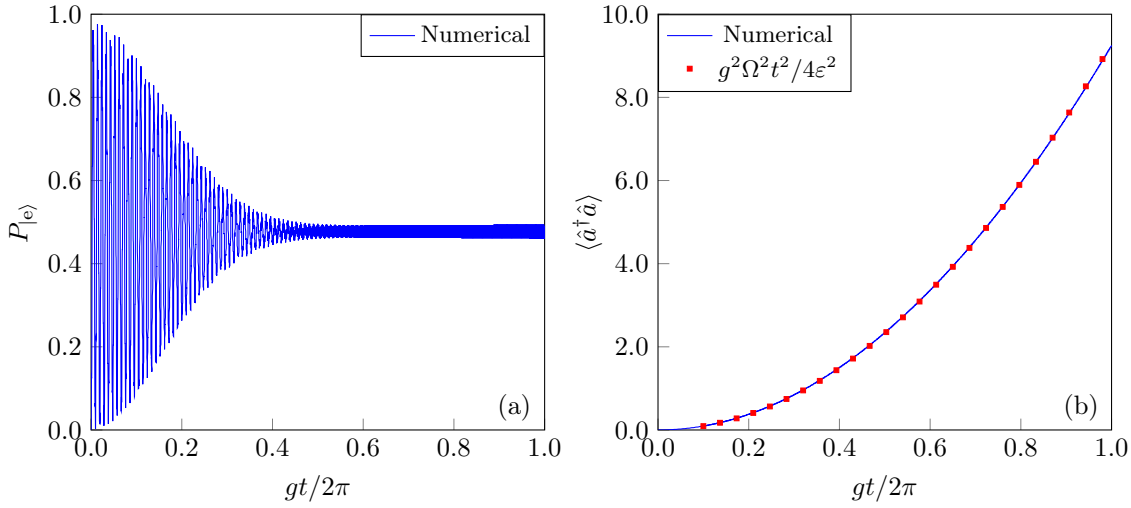

Figure 3.5: Characterization of cat states under detuned conditions. The parameters used for these simulations are identical to those used in Fig. 3.1, except for $\Delta = 2\pi \times 500\,\mathrm{MHz}$. (a),(b) $P_{|e\rangle}$ and $\langle\hat{a}^\dagger\hat{a}\rangle$ vs. normalized time $gt/2\pi$.

$$
\begin{aligned}
|\psi(t)\rangle^{(\mathrm{I})} &= \left(\sin\left(\frac{\theta}{2}\right)|\widetilde{+}\rangle\,|\widetilde{\alpha}\rangle + \sin\left(\frac{\theta}{2}\right)|\widetilde{-}\rangle\,|-\widetilde{\alpha}\rangle\right) \\
&= \Bigg[|\mathrm{g}\rangle\left(\frac{1}{2}\sin(\theta)\,|\widetilde{\alpha}\rangle + \sin^2\left(\frac{\theta}{2}\right)|-\widetilde{\alpha}\rangle\right) \\
&\quad + |\mathrm{e}\rangle\left(\frac{1}{2}\sin(\theta)\,|\widetilde{\alpha}\rangle - \cos^2\left(\frac{\theta}{2}\right)|-\widetilde{\alpha}\rangle\right)\Bigg],
\end{aligned}
\tag{3.15}
$$

where $\widetilde{\alpha} = -g\Omega(e^{i\delta t}-1)/2\varepsilon\delta$; when $\delta \to 0$, then $\widetilde{\alpha} = -ig\Omega t/2\varepsilon$. The state described by Eq. (3.15) exhibits a superposition of coherent states with opposite phases, featuring distinct weight coefficients. This results in what we refer to as an *asymmetrically weighted cat state*. Remarkably, cat states can be generated even when $\Delta \neq 0$, without necessarily requiring the system to be in the strong dispersive regime or resonant qubit-drive regime. However, it is essential to note that cat states produced in the detuned regime possess smaller amplitudes compared to those generated resonantly, even when subjected to time-evolution duration. This amplitude difference arises because $|\widetilde{\alpha}| < |\alpha|$.

Under detuning conditions, the Bloch-Siegert shift's oscillations in the lobes of the cat, can be harnessed to create an ideal cat state. This happens when the distinct weight coefficients become identical at specific times, resulting in the formation of the ideal cat

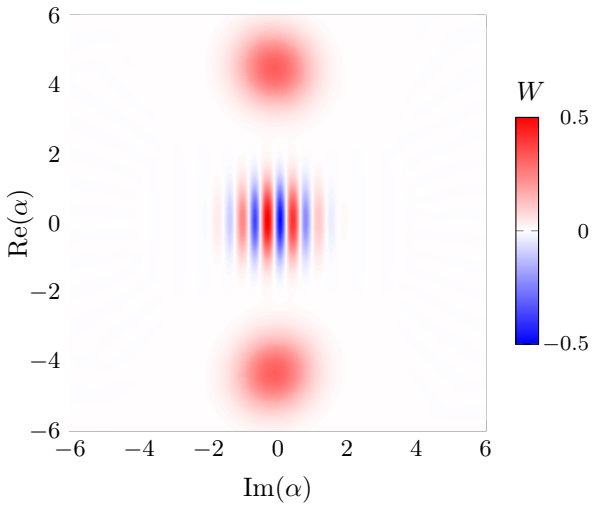

Figure 3.6: Wigner function of a detuned cat state. Heatmap of the Wigner function W of the resonator state after measuring the qubit in $|\mathrm{e}\rangle$ at $gt/2\pi = 1$. The result is obtained from the same simulation of Fig 3.5. By selecting this specific time, an ideal cat state is achieved, characterized by equal weight coefficients. This outcome is attained by leveraging the oscillations resulting from the Bloch-Siegert shift.

state.

Figure 3.5 displays the results of numerical simulations similar to those in Fig. 3.1 but under detuned conditions. The photon number behaves similarly to the resonant case, $|\widetilde{\alpha}|^2 = g^2\Omega^2 t^2/4\varepsilon^2$, growing quadratically in time. This analytical result is validated by the numerical simulations. Finally, Fig. 3.6 shows a cat state generating under detuning conditions that is nearly identical to that generated under resonance conditions.

The strong driving in the case of $\delta = 0$ – under both resonant and detuned qubit driving – mediates a cross-resonance effect as the drive is resonant with the resonator. This also explains the rapid population of the resonator with photons even if the coupling strength between the resonator and qubit is much weaker than the drive. This can be seen as quantum analogy of two weakly coupled pendulua with one of them cross-resonantly strongly driven.

Thus far, we derived analytics that account for $\delta \neq 0$, but most of our discussion has been centered around the case where $\delta = 0$. A typical microwave source in a circuit QED experiment has a frequency resolution of 0.01Hz, and a state-of-the-art resonator linewidth is around 10kHz. Thus, the only limiting factor is the intrinsic quality factor of

the resonator. Formally, the parameter δt satisfies $\delta t \ll 1$ for a detuning on the order of $\sim$kHz and for a timescale of $\sim$100ns. Then, performing a Taylor expansion of α and $\widetilde{\alpha}$ near $\delta = 0$, to first order, yields

$$\alpha = \frac{-g((1+i\delta t)-1)}{2\delta} + O(\delta^2 t^2) = \frac{-igt}{2} + O(\delta^2 t^2)$$

and

$$\widetilde{\alpha} = \frac{-g\Omega((1+i\delta t)-1)}{2\varepsilon\delta} + O(\delta^2 t^2) = \frac{-ig\Omega t}{2\varepsilon} + O(\delta^2 t^2),$$

where the results of $\delta = 0$ are recovered. Therefore, we can completely ignore the case of $\delta \neq 0$ on the timescales of interest.

3.3 Cancellation of spurious resonator driving

The presentation of our theory until now did not rely on any particular implementation considerations. In some implementations, applying a drive to the qubit results in an unintentional spurious driving of the resonator. In this section we consider this practical issue and a resolution using a drive on the resonator.

The presence of the spurious driving leads to a new system Hamiltonian that read as

$$\begin{aligned}\hat{H}' =& \frac{\hbar\omega_{\mathrm{q}}}{2}\hat{\sigma}_z + \hbar\omega_{\mathrm{r}}\hat{a}^\dagger\hat{a} + \hbar g(\hat{\sigma}_+ + \hat{\sigma}_-)(\hat{a}^\dagger + \hat{a}) + \hbar\Omega\cos(\omega_{\mathrm{d}}t)(\hat{\sigma}_+ + \hat{\sigma}_-) \\ &+ \hbar\Omega'\cos(\omega_{\mathrm{d}}t)(\hat{a}^\dagger + \hat{a}),\end{aligned} \tag{3.16}$$

where Ω' is the spurious driving strength. Typically, Ω' is merely a fraction of Ω. To address this, we add a cancellation drive on the resonator with which the Hamiltonian becomes

$$\begin{aligned}\hat{H}'' =& \frac{\hbar\omega_{\mathrm{q}}}{2}\hat{\sigma}_z + \hbar\omega_{\mathrm{r}}\hat{a}^\dagger\hat{a} + \hbar g(\hat{\sigma}_+ + \hat{\sigma}_-)(\hat{a}^\dagger + \hat{a}) + \hbar\Omega\cos(\omega_{\mathrm{d}}t)(\hat{\sigma}_+ + \hat{\sigma}_-) \\ &+ \hbar\left(\Omega'\cos(\omega_{\mathrm{d}}t) + \Omega''\cos(\omega_{\mathrm{d}}t + \phi)\right)(\hat{a}^\dagger + \hat{a});\end{aligned} \tag{3.17}$$

Ω'' is strength of the cancellation drive and ϕ is its phase. In a first run of an experiment realizing this system, we can characterize Ω' by the size of the coherent state displacing the resonator state. As such, we set the cancellation drive parameters to $\Omega'' = \Omega'$ and $\phi = \pi$. Since $\cos(x + \pi) = -\cos(x)$, we achieve a total cancellation of the spurious driving. Note that for simplicity we assumed the spurious driving remains in phase with the original

drive. Even if the driving phase changes due to the complex electrical network wiring up the experiment, this phase can be easily characterized by performing an initial run of the experiment and measuring the resonator state then characterizing the coherent state offsetting the resonator state. Characterizing the offset coherent state's amplitude and phase gives us the spurious drive's amplitude and phase.

In implementations like circuit QED, it is possible to place the cancellation drive on the resonator physically far enough that it does not affect the qubit. However, for completeness, we consider the qubit to be affected by a spurious driving due to the cancellation field. Under the same conditions for perfect cancellation, $\Omega'' = \Omega'$ and $\phi = \pi$, this effect at the Hamiltonian level looks like

$$\hat{H}''' = \frac{\hbar\omega_{\mathrm{q}}}{2}\hat{\sigma}_z + \hbar\omega_{\mathrm{r}}\hat{a}^\dagger\hat{a} + \hbar g(\hat{\sigma}_+ + \hat{\sigma}_-)(\hat{a}^\dagger + \hat{a}) + \hbar(\Omega - \Omega''')\cos(\omega_{\mathrm{d}}t)(\hat{\sigma}_+ + \hat{\sigma}_-), \tag{3.18}$$

where Ω''' is the strength of the spurious drive on the qubit. Since Ω' is usually a fraction of Ω, then Ω''' will be a fraction of Ω'' $(= \Omega')$. Thus, we may simply define $\Omega_{\mathrm{eff}} = \Omega - \Omega'''$ as the effective qubit driving strength and proceed with the conditions derived in the previous sections using Ω_{eff} in place of Ω.

3.4 Multiple resonators

In the previous sections, we fleshed out the theory and practical considerations for a single driven qubit-resonator system. We now show that, straightforwardly, when you follow these considerations for a driven qubit coupled simultaneously to N resonators, you can entangle N cat states in N different resonators.

The full Hamiltonian in the laboratory frame is

$$\hat{H} = \frac{\hbar\omega_{\mathrm{q}}}{2}\hat{\sigma}_z + \hbar\Omega\cos(\omega_{\mathrm{d}}t)(\hat{\sigma}_+ + \hat{\sigma}_-) + \sum_{k=1}^{N}\left(\hbar\omega_{\mathrm{r}k}\hat{a}_k^\dagger\hat{a}_k + \hbar g_k(\hat{\sigma}_+ + \hat{\sigma}_-)(\hat{a}_k^\dagger + \hat{a}_k)\right), \tag{3.19}$$

where k is the index of the resonators (1 to N). Following the same procedure for the single resonator case in the driving frame and using the RWA conditions of Eq. (3.3) for all resonators, we obtain the Hamiltonian

$$\hat{H}^{\mathrm{d}}_{\mathrm{RWA}} = \frac{\hbar\Delta}{2}\hat{\sigma}_z + \frac{\hbar\Omega}{2}(\hat{\sigma}_+ + \hat{\sigma}_-) + \sum_{k=1}^{N}\hbar\delta_k\hat{a}_k^\dagger\hat{a}_k + \hbar g_k(\hat{\sigma}_+\hat{a}_k + \hat{\sigma}_-\hat{a}_k^\dagger), \tag{3.20}$$

where $\delta_k = \omega_{rk} - \omega_d$. Working under the qubit-drive resonance condition $\Delta = 0$, we define $\hat{H}_0^d = \hbar\Omega(\hat{\sigma}_+ + \hat{\sigma}_-)/2 + \sum_{k=1}^N \hbar\delta_k \hat{a}_k^\dagger \hat{a}_k$ and $\hat{H}_I^d = \sum_{k=1}^N \hbar g_k \left(\hat{\sigma}_+ \hat{a}_k + \hat{\sigma}_- \hat{a}_k^\dagger\right)$. We then apply the unitary transformation $\hat{U}_0 = \exp\left(-i\hat{H}_0 t/\hbar\right)$, which allows us to obtain the interaction picture Hamiltonian

$$\hat{H}_{RWA}^{(I)} = \hat{U}_0^\dagger \hat{H}_I \hat{U}_0 = \sum_{k=1}^N \frac{\hbar g_k}{2} \Big(|+\rangle\langle +| - |-\rangle\langle -| + e^{i\Omega t} |+\rangle\langle -| - e^{-i\Omega t} |-\rangle\langle +| \Big) \hat{a}_k e^{-i\delta_k t} + \text{H.c.}. \tag{3.21}$$

To obtain the cat-state generating Hamiltonian, we work in the strong driving regime of Eq. (3.7) for all resonators. This allows us to obtain the effective Hamiltonian

$$\hat{H}_{eff}^{(I)} = \sum_{k=1}^N \frac{\hbar g_k}{2} \left(|+\rangle\langle +| - |-\rangle\langle -|\right) \left(\hat{a}_k^\dagger e^{+i\delta_k t} + \hat{a}_k e^{-i\delta_k t}\right). \tag{3.22}$$

This Hamiltonian generalizes that of Eq. (3.8) to N resonators. Following the same recipe for the single resonator case, we choose the initial state to be $|\psi_i\rangle = |g\rangle |0\rangle_1 ... |0\rangle_N = (|+\rangle + |-\rangle) |0\rangle_1 ... |0\rangle_N /\sqrt{2}$, where $|\rangle_k$ specifies the state of the k^{th} resonator. The time-evolution of this initial state yields

$$\begin{aligned} |\psi(t)\rangle^{(I)} =& \frac{1}{\sqrt{2}} (|+\rangle |\alpha_1\rangle_1 ... |\alpha_N\rangle_N + |-\rangle |-\alpha_1\rangle_1 ... |-\alpha_N\rangle_N) \\ =& \frac{1}{2} |g\rangle (|\alpha_1\rangle_1 ... |\alpha_N\rangle_N + |-\alpha_1\rangle_1 ... |-\alpha_N\rangle_N) \\ &+ \frac{1}{2} |e\rangle (|\alpha_1\rangle_1 ... |\alpha_N\rangle_N - |-\alpha_1\rangle_1 ... |-\alpha_N\rangle_N), \end{aligned} \tag{3.23}$$

where $\alpha_k = -g_k(e^{i\delta_k t} - 1)/2\delta_k$; when $\delta_k \to 0$, then $\alpha_k = -ig_k t/2$. Measuring the qubit in $|g\rangle$ leaves the resonator in a Bell-like even superposition of entangled cat states, $\langle g|\psi(t)\rangle^{(I)} \propto |\alpha_1\rangle_1 ... |\alpha_N\rangle_N + |-\alpha_1\rangle_1 ... |-\alpha_N\rangle_N$. If the qubit is found in $|e\rangle$, the resonator state is a Bell-like odd superposition of entangled cat states, $\langle e|\psi(t)\rangle^{(I)} \propto |\alpha_1\rangle_1 ... |\alpha_N\rangle_N - |-\alpha_1\rangle_1 ... |-\alpha_N\rangle_N$[2]. Such entangled cat states are valuable resources for generating Bell states in bosonic encodings [30], and also they can be used to violate of Bell's inequality [1].

[2]In fact for some encodings where the logical qubit states are $|\bar{0}\rangle \simeq |\alpha\rangle$ and $|\bar{1}\rangle \simeq |-\alpha\rangle$, the states described here are the N-partite GHZ state, $(|\bar{0}\rangle_1 ... |\bar{0}\rangle_N \pm |\bar{1}\rangle_1 ... |\bar{1}\rangle_N)/\sqrt{2}$. This works even if the cat size in each resonator is different, as long as $|\alpha|$ is large enough such that $\langle\alpha|-\alpha\rangle \approx 0$.

Similar to the spurious coupling between the drive and the resonator, there will be a small spurious coupling among the different resonators. This results in an additional interaction term

$$\hat{H}_{\mathrm{rr}} = \hbar \sum_{j=1}^{N} \sum_{k>j}^{N} g_{jk} (\hat{a}_k^\dagger + \hat{a}_k)(\hat{a}_j^\dagger + \hat{a}_j). \tag{3.24}$$

When the resonators are near resonance, the interaction is approximately a beamsplitter type $\propto (\hat{a}_k^\dagger \hat{a}_j + \hat{a}_k \hat{a}_j^\dagger)$. This certainly interferes with the protocol presented. While tackling this problem is outside the scope of this work, we mention that a simple workaround is to use a tunable coupler between each pair of resonators and set the tunable (typically flux-tunable) coupling strength, $g_{jk}^{\mathrm{tunable}}(\Phi) = -g_{jk}$. This is fairly easy to implement for the case of two resonators, but as you scale up, you run into various problems such as cross-talk and the difficulty of achieving all-to-all connectivity.

3.5 Other methods

In this section, we compare our method to the two most commonly used methods for generating cat states (in circuit QED). First, we introduce each method and then we compare it to our work.

qcMAP

We start with the 'qcMAP' method in Ref. [37], where the system of interest is also a qubit-resonator system. However, it is operated in the dispersive regime where $g \gg \omega_{\mathrm{q}} - \omega_{\mathrm{r}} \neq 0$ (see Eq. (2.33) and Eq. (2.34)). Since the qubit and resonator now dress one another's frequency via the term in the Hamiltonian $\hat{\sigma}_z \hat{a}^\dagger \hat{a}$, an external qubit drive can be conditioned on the resonator state and an external resonator drive can be conditioned on the qubit state. In particular, we can perform qubit-conditional displacements (QCD) on the resonator state and resonator-conditional rotations (RCR) on the qubit state. The QCD operation is denoted by $\hat{D}^{|\mathrm{g/e}\rangle}(\beta)$ and it displaces the resonator state by β if the qubit state matches its superscript, i.e,

$$\hat{D}^{|\mathrm{g}\rangle}(\beta) \, |\mathrm{g}\rangle \, |0\rangle = |\mathrm{g}\rangle \, |\beta\rangle$$

and

$$\hat{D}^{|\mathrm{g}\rangle}(\beta) \, |\mathrm{e}\rangle \, |0\rangle = |\mathrm{e}\rangle \, |0\rangle$$

(similarly for $\hat{D}^{|\mathrm{e}\rangle}(\beta)$). The RCR operation is denoted by $\hat{X}_\theta^{|n\rangle}$ and it applies an x-axis rotation to the qubit state if the resonator state matches its superscript, i.e.,

$$\hat{X}_\theta^{|n\rangle} |\psi_\mathrm{q}\rangle |n\rangle = e^{-i\hat{\sigma}_x\theta/2} |\psi_\mathrm{q}\rangle |n\rangle$$

and

$$\hat{X}_\theta^{|n\rangle} |\psi_\mathrm{q}\rangle |m\rangle = |\psi_\mathrm{q}\rangle |m\rangle$$

where $|\psi_\mathrm{q}\rangle$ is the qubit state. The main goal of this method is to encode an arbitrary qubit state into a resonator cat state via the map:

$$c_\mathrm{g} |\mathrm{g}\rangle + c_\mathrm{e} |\mathrm{e}\rangle \longmapsto c_\mathrm{g} |\alpha\rangle + c_\mathrm{e} |-\alpha\rangle .$$

To achieve this, the system is first initialized in the state $|\psi_\mathrm{i}\rangle = (c_\mathrm{g} |\mathrm{g}\rangle + c_\mathrm{e} |\mathrm{e}\rangle) |0\rangle$. Then, the following operations are applied in succession to obtain the final state:

$$\begin{aligned} |\psi_\mathrm{f}\rangle =& \hat{D}(-\alpha)\hat{X}_\pi^{|0\rangle}\hat{D}^{|\mathrm{g}\rangle}(2\alpha) |\psi_\mathrm{i}\rangle \\ =& \hat{D}(-\alpha)\hat{X}_\pi^{|0\rangle}(c_\mathrm{g} |\mathrm{g}\rangle |2\alpha\rangle + c_\mathrm{e} |\mathrm{e}\rangle |0\rangle) \\ =& \hat{D}(-\alpha) |\mathrm{g}\rangle (c_\mathrm{g} |2\alpha\rangle + c_\mathrm{e} |0\rangle) \\ =& |\mathrm{g}\rangle (c_\mathrm{g} |\alpha\rangle + c_\mathrm{e} |-\alpha\rangle). \end{aligned} \tag{3.25}$$

Measuring the qubit state determinstically yields the desired outcome, $\propto c_\mathrm{g} |\alpha\rangle + c_\mathrm{e} |-\alpha\rangle$. In summary, the qcMAP is exactly the sequence of operations $\hat{D}(-\alpha)\hat{X}_\pi^{|0\rangle}\hat{D}^{|\mathrm{g}\rangle}(2\alpha)$ which allows us to map the qubit state to a resonator state where c_g and c_e are encoded in different lobes of a cat state. By employing the introduced operations (QCD and RCR), it is possible to synthesize more general resonator states, such as three- and four-component cat states (introduced in Sec. 2.3). However, the quality of these states diminishes significantly beyond two lobes. The approximate gate time to obtain the desired resonator state is $T_\mathrm{gate} \simeq (15 + 2|\alpha|^2\pi)/(2|\alpha|^2\chi_\mathrm{qr})$ where $\chi_\mathrm{qr} = g^2/|\omega_\mathrm{q} - \omega_\mathrm{r}|$[3]. This gate time does not account for decoherence effects. Lastly, we rewrite the cat size as a function of time,

$$|\alpha_\mathrm{qcMAP}(t)|^2 \simeq 15/2(\chi_\mathrm{qr}t - \pi). \tag{3.26}$$

Two-photon driven Kerr-nonlinear resonator

We move on to the two-photon driven Kerr-nonlinear resonator (KNR) methods [42, 35]. This method relies on a Josephson junction (or SQUID) either embedded in the middle of

[3]It might look like there is a singularity when $\omega_\mathrm{q} = \omega_\mathrm{r}$ but operating in the dispersive regime means the qubit and resonator are detuned, and, thus, the denominator can never be zero.

$$\begin{aligned}
\hat{H}_{\mathrm{KNR}} &\xrightarrow{\text{adiabatic two-photon drive}} \hat{H}_{\mathrm{2pKNR}} \\
|0\rangle &\xrightarrow{\text{even parity preserved}} \propto |\alpha\rangle + |-\alpha\rangle \\
|1\rangle &\xrightarrow{\text{odd parity preserved}} \propto |\alpha\rangle - |-\alpha\rangle
\end{aligned}$$

Figure 3.7: Adiabatic preparation of cat states using a two-photon driven KNR. When the KNR is initialized in $|0\rangle$ (in $|1\rangle$), adiabatically ramping a resonant two-photon drive yields an even cat state (an odd cat state).

a transmission line or shunting its end. The Jospheson junction is threaded with flux to parametrically excite the transmission line. Typically, the flux threading the junction is tuned to induce a two-photon drive in the Hamiltonian. The Hamiltonian of a two-photon driven KNR in the lab frame reads as

$$\hat{H}_{\mathrm{2pKNR}} = \hbar\omega_{\mathrm{r}}\hat{a}^\dagger\hat{a} \quad \overbrace{-\hbar\eta\hat{a}^{\dagger 2}\hat{a}^2}^{\text{Kerr-nonlinear term}} \quad + \overbrace{\hbar(\Omega_{\mathrm{p}}e^{-i\omega_{\mathrm{p}}t/2}\hat{a}^\dagger + \Omega_{\mathrm{p}}^* e^{i\omega_{\mathrm{p}}t/2}\hat{a}^2)}^{\text{two-photon drive}} \tag{3.27}$$

Setting the parametric drive on a two-photon resonance with the resonator ($\omega_{\mathrm{p}} = 2\omega_{\mathrm{r}}$) and transforming to the rotating frame of the resonator using $\hat{U}_{\mathrm{r}} = \exp\left[-i\omega_{\mathrm{r}}t\hat{a}^\dagger\hat{a}\right]$, we obtain the rotating frame Hamiltonian

$$\begin{aligned}
\hat{H}^{\mathrm{r}}_{\mathrm{2pKNR}} &= \hat{U}_{\mathrm{r}}^\dagger \hat{H}_{\mathrm{2pKNR}} \hat{U}_{\mathrm{r}} + i\hbar\dot{\hat{U}}_{\mathrm{r}}^\dagger \hat{U}_{\mathrm{r}} \\
&= -\hbar\eta\hat{a}^{\dagger 2}\hat{a}^2 + \hbar(\Omega_{\mathrm{p}}\hat{a}^{\dagger 2} + \Omega_{\mathrm{p}}^*\hat{a}^2) && \text{(3.28a)} \\
&= -\hbar\eta\left(\hat{a}^{\dagger 2} - \frac{\Omega_{\mathrm{p}}^*}{\eta}\right)\left(\hat{a}^2 - \frac{\Omega_{\mathrm{p}}}{\eta}\right) + \hbar\frac{|\Omega_{\mathrm{p}}|^2}{\eta}, && \text{(3.28b)}
\end{aligned}$$

where η is the strength of the Kerr nonlinearity and Ω_{p} is the amplitude of the two-photon drive. The second form of the Hamiltonian reveals two degenerate coherent state eigenstates, $|\pm\alpha\rangle$ with $\alpha = \sqrt{\Omega_{\mathrm{p}}/\eta}$. The advantage of such degenerate eigenstates is that their even and odd superpositions (cat states), $\propto |\alpha\rangle \pm |-\alpha\rangle$, are also eigenstates. Next, we describe how to deterministically prepare cat states by leveraging the degenerate eigenstates of the two-photon driven KNR.

The degenerate eigenstates of the undriven KNR ($\hat{H}_{\mathrm{KNR}} = \hbar\omega_{\mathrm{r}}\hat{a}^\dagger\hat{a} - \hbar\eta\hat{a}^{\dagger 2}\hat{a}^2$) are the vacuum state, $|0\rangle$ and the first excited Fock state, $|1\rangle$. Since the cat states are instantaneous eigenstates of the two-photon driven KNR, the strategy is to *adiabatically* evolve $|0\rangle$ to

$\propto |\alpha\rangle + |-\alpha\rangle$ and $|1\rangle$ to $\propto |\alpha\rangle - |-\alpha\rangle$. This is enabled by the slow adiabatic ramping of the two-photon driving amplitude, $\Omega_{\rm p}$. The parity is preserved by the two-photon drive, and as such, $|0\rangle$ goes to the even cat and $|1\rangle$ goes to the odd cat. The adiabatic initialization yields cat states with $|\alpha(t)|^2 = |\Omega_{\rm p}(t)/\eta|$. To satisfy the adiabatic conditions, the drive envelope $\Omega_{\rm p}(t) = \Omega_{\rm p0}(1 - \exp((2\pi t)^4/\eta^4))$ is selected with the constant $\Omega_{\rm p0} = 4\eta$. This generates a cat state of $|\alpha|^2 \sim 4$ in a period of $\eta t/2\pi = 6.5$. To put these parameters in an experimental perspective, the Kerr nonlinearity strength, η, is typically a small fraction of the resonator frequency (a few 10s of MHz when the resonator frequency is around a few GHz [6]). As an example, taking $\eta \sim 2\pi \times 40\,\text{MHz}$, a cat of roughly 4 photons is generated in $\sim 160\,\text{ns}$.

The adiabatic scheme introduced above can be accelerated using so-called 'shortcuts to adiabaticity'. This involves the idea of a 'transitionless' or counter-diabatic drive [3]. Given a time-dependent Hamiltonian $\hat{H}(t)$ with instantaneous eigenstates $\{|k(t)\rangle\}$ and instantaneous energies $\{E_k(t)\}$, the adiabatic approximation says that the states driven by $\hat{H}(t)$ are

$$|\psi_k(t)\rangle = \exp\left[-\frac{i}{\hbar}\int_0^t d\tau\, E_k(\tau) - \int_0^t d\tau\, \langle k(\tau)|\frac{d}{d\tau}|k(\tau)\rangle\right]|k(t)\rangle\,, \tag{3.29}$$

with a (usually small) probability of a transition to other states depending on the driving parameter. The idea of counter-diabatic driving is to add a driving Hamiltonian $\hat{H}_{\rm cd}(t)$ to $\hat{H}(t)$ such that the adiabatic approximation state of Eq.(3.29) is an instantaneous eigenstate of this new Hamiltonian, i.e.,

$$(\hat{H}(t) + \hat{H}_{\rm cd}(t))\,|\psi_n(t)\rangle = \tilde{E}_n(t)\,|\psi_n(t)\rangle$$

for some $\tilde{E}_n(t)$. This means you can evolve to an instantaneous eigenstate of the original Hamiltonian in accelerated manner by introducing a specific drive without exciting unwanted transitions that occur with some probability in an adiabatic evolution.

For the Hamiltonian in Eq. (3.28), an approximate counter-diabatic driving Hamiltonian (that drives $\hat{H}_{\rm 2pKNR}$ instantaneous eigenstates $\propto |\alpha\rangle \pm |-\alpha\rangle$) is

$$\hat{H}_{\rm cd} \simeq i\hbar\frac{\dot{\alpha}(t)}{\sqrt{2(1-\exp(-2|\alpha(t)|^2))}(1+2\alpha(t))}(\hat{a}^{\dagger 2} - \hat{a}^2). \tag{3.30}$$

The presence of this counter-diabatic drive significantly reduces the time needed to generate cat states. For the same size cat as the adiabatic preparation, the counter-diabatic drive prepares the same cat in a period of $\eta t/2\pi = 1.37$, a speed up of ~ 4.74 times. Using the same example of $\eta \sim 2\pi \times 40\,\text{MHz}$, a 4-photon cat can be generated in $\sim 32\,\text{ns}$. All time estimates here account for worse-than-average single-photon resonator loss, $\kappa = \eta/(250 \times 2\pi)$, which for our example is $\sim 160\,\text{kHz}$ (see Table 2.1 for comparison).

3.6 Comparison with other methods

We now compare our method to the qcMAP method. First, we note that our proposal allows for a determinstic encoding of a qubit state into a resonator cat state. If we prepare an intial state $|\psi_{\rm i}\rangle = (c_{\rm g}\,|+\rangle + c_{\rm e}\,|-\rangle)\,|0\rangle$, then time-evolve it as described in Sec. 3.1, we obtain a final state

$$|\psi_{\rm f}\rangle = \frac{1}{2}\,|{\rm g}\rangle\,(c_{\rm g}\,|\alpha\rangle + c_{\rm e}\,|-\alpha\rangle) + \frac{1}{2}\,|{\rm e}\rangle\,(c_{\rm e}\,|\alpha\rangle - c_{\rm g}\,|-\alpha\rangle).$$

Measuring the qubit in its bare basis yields a resonator state $\propto c_{\rm g}\,|\alpha\rangle \pm c_{\rm e}\,|-\alpha\rangle$ ($\pm$ depends on the qubit state). Thus, our method can also deterministically encode a qubit state into a resonator, but there is a probabilistic phase (parity) which can be accounted for. Since, in the resonant case, our method yields $|\alpha(t)|^2 = g^2t^2/4$. Even if we include resonator decay defined by κ, the size of the cat becomes $|\alpha(t)|^2 \simeq g^2t^2e^{-\kappa t}/4$, where as the qcMAP's cat size is $|\alpha_{\rm qcMAP}(t)|^2 \simeq 15/2(\chi_{\rm qr}t - \pi)$. This means for similar parameters[4], our proposal outperforms the qcMAP by generating the same size cats in a much shorter time. In summary, the qcMAP method offers greater flexibility in achieving a wider array of resonator states. However, when it comes to generating two-component cat states, our method proves superior. Moreover, similar to the qcMAP, our method allows for encoding a qubit state into a resonator state with a probabilistic parity dependent on the qubit measurement outcome.

While the qcMAP relies on a qubit-resonator system with qubit and resonator drives, the driven two-photon KNR setup is fundamentally different from our proposal. Our method relies on the qubit-resonator interaction alongside the qubit drive as the source of nonlinearity needed to generate cat states. In contrast, with this method, where a two-photon process and a Kerr-type term are leveraged as the source of nonlinearity and counter-diabatic driving is used to accelerate adiabatic state preparation. While our method is limited by g, its functional dependence on it is quadratic and, thus, a modest value of g in the strong coupling regime will suffice. It is easier to get higher values of g (upto a 100-200 MHz for $\omega_{\rm q}, \omega_{\rm r} \sim 5$ GHz) but this is not the case for η (which even when increased makes detrimental higher order effects more significant). For the same time-evolution periods use to generate cat states presented in Ref. [49], we can obtain the same size (and even much larger) using modest values of g.

In the broader context of cat-state generating schemes, we argue that our proposal allows for a more rapid generation of cat states compared to other methods. While it does

[4]The qcMAP operates in the dispersive regime, so either $\omega_{\rm r}$ or $\omega_{\rm q}$ has to be different than our resonant case.

rely on a driven qubit and that opens it to qubit decoherence channels, the timescale for generating a cat of a size on the order of tens of photons is a small fraction of the qubit's T_1 and T_2 (encoded as γ_1 and γ_ϕ in our simulations). The simulations we performed were using significantly worse-than-average decoherent parameters (compared with Table 2.1), despite our method performs very well for generating cat states.

With the use of a tunable qubit, our protocol can be executed until the cat's lobes reach the desired size; then, the qubit can be measured and decoupled from the resonator (by detuning it very far from the resonator). For the purpose of encoding a qubit state into a two-lobed cat, our method deterministically performs the encoding up to a parity. This parity holds significant importance for bosonic quantum error correction. Once the qubit is measured, we know the parity of the cat state, and it could be tracked. This approach works well for encoding one qubit state. However, when it comes to encoding multiple qubits in different resonators, an issue arises due to differing parities. Differing parities make it difficult to properly track photon loss events. A possible solution, leveraging the speed of our method, is to repeat the cat state generation scheme until the desired parity is achieved.

We believe that a rapid resonant method (or qubit-detuned but resonator-resonant), as proposed here, presents a valuable tool for all purposes of generating a cat state.

Chapter 4

Generalization to a Qutrit

In most implementation schemes, the device is rarely truly a two-level system. In practice, most systems are in fact infinite-dimensional. Depending on how anharmonic a system is, nearby transitions could be a significant player in the dynamics of the system. In this chapter, we are interested in extending the work presented on a driven qubit-resonator system to account for this practicality.

Recall the discussions in Sec. 2.4 on the anharmonicty of a CPB in the charge and transmon regimes. We extend our considerations to a driven (cascade) Ξ-type qutrit (imposed by the CPB selection rules) interacting with a resonator. We consider both transitions to be affected by the drive and resonator. The structure of this chapter is as follows. In Sec. 4.1, we state the system Hamiltonian and derive the necessary RWA conditions for a weakly-anharmonic qutrit. We show that the cat-state-generating protocol of the previous chapter can be successfully generalized to a weakly-anharmonic qutrit with some modifications. In Sec. 4.2, we consider the qutrit to be strongly anharmonic. We show that in this scenario the qubit considerations hold true with some perturbations due to leakage and interference of the third state. In Sec. 4.3, we extend our theory to an arbitrarily-anharmonic qutrit for arbitrary parameters. Throughout the chapter, we corroborate our analytical results with numerical simulations performed with realistic experimental circuit QED parameters. Additionally, make connections to the charge and transmon regimes of the CPB.

4.1 Extension to a weakly-anharmonic qutrit

We start by generalizing the driven QRM to include a qutrit with two allowed transitions instead of a qubit. The Hamiltonian for this system reads

$$\hat{H} = \hat{H}_0 + \hat{H}_\mathrm{I} + \hat{H}_\mathrm{d}, \tag{4.1a}$$

where

$$\hat{H}_0 = \frac{\hbar\omega_\mathrm{eg}}{2}\left(|\mathrm{e}\rangle\langle\mathrm{e}| - |\mathrm{g}\rangle\langle\mathrm{g}|\right) + \frac{\hbar\widetilde{\omega}_\mathrm{f}}{2}|\mathrm{f}\rangle\langle\mathrm{f}| + \hbar\omega_\mathrm{r}\hat{a}^\dagger\hat{a}, \tag{4.1b}$$

$$\hat{H}_\mathrm{d} = \hbar\cos(\omega_\mathrm{d}t)\Big[\Omega_1(\hat{\sigma}_{1+} + \hat{\sigma}_{1-}) + \Omega_2(\hat{\sigma}_{2+} + \hat{\sigma}_{2-})\Big], \tag{4.1c}$$

and

$$\hat{H}_\mathrm{I} = \hbar\Big[g_1(\hat{\sigma}_{1+} + \hat{\sigma}_{1-}) + g_2(\hat{\sigma}_{2+} + \hat{\sigma}_{2-})\Big]\left(\hat{a}^\dagger + \hat{a}\right). \tag{4.1d}$$

Here, we define $\widetilde{\omega}_\mathrm{f} = 2\omega_\mathrm{fe} + \omega_\mathrm{eg}$, $\hat{\sigma}_{1+} := |\mathrm{e}\rangle\langle\mathrm{g}|$ ($\hat{\sigma}_{1-} = \hat{\sigma}_{1+}^\dagger$) as the raising (lowering) operator for the $|\mathrm{g}\rangle \leftrightarrow |\mathrm{e}\rangle$ (first) transition with frequency ω_eg and $\hat{\sigma}_{2+} := |\mathrm{f}\rangle\langle\mathrm{e}|$ ($\hat{\sigma}_{2-} = \hat{\sigma}_{2+}^\dagger$) as the raising (lowering) operator for the $|\mathrm{e}\rangle \leftrightarrow |\mathrm{f}\rangle$ (second) transition with frequency ω_fe. Also, Ω_1 (g_1) is the coupling strength between the drive (resonator) and the first transition, and Ω_2 (g_2) is the coupling strength between the drive (resonator) and the second transition.

We can rewrite the Hamiltonian of Eq.(4.1) in a rotating frame by means of the unitary transformation $\hat{U} = \exp\left[-it\left(\omega_\mathrm{d}\left(|\mathrm{e}\rangle\langle\mathrm{e}| - |\mathrm{g}\rangle\langle\mathrm{g}|\right) + \widetilde{\omega}_\mathrm{f}|\mathrm{f}\rangle\langle\mathrm{f}| + 2\omega_\mathrm{d}\hat{a}^\dagger\hat{a}\right)/2\right]$,

$$\begin{aligned}
\hat{H}^\mathrm{d} =& \frac{\hbar\Delta_1}{2}\left(|\mathrm{e}\rangle\langle\mathrm{e}| - |\mathrm{g}\rangle\langle\mathrm{g}|\right) + \hbar\delta\hat{a}^\dagger\hat{a} \\
&+ \frac{\hbar\Omega_1}{2}\left(\hat{\sigma}_{1+} + \hat{\sigma}_{1-} + e^{i2\omega_\mathrm{d}t}\hat{\sigma}_{1+} + e^{-i2\omega_\mathrm{d}t}\hat{\sigma}_{1-}\right) \\
&+ \frac{\hbar\Omega_2}{2}\left(e^{i\widetilde{\chi}t/2}\hat{\sigma}_{2+} + e^{-i\widetilde{\chi}t/2}\hat{\sigma}_{2-} + e^{i(\widetilde{\omega}_\mathrm{f}+\omega_\mathrm{d})t/2}\hat{\sigma}_{2+} + e^{-i(\widetilde{\omega}_\mathrm{f}+\omega_\mathrm{d})t/2}\hat{\sigma}_{2-}\right) \\
&+ \hbar\Big[g_1\left(e^{i\omega_\mathrm{d}t}\hat{\sigma}_{1+} + e^{-i\omega_\mathrm{d}t}\hat{\sigma}_{1-}\right) \\
&+ g_2\left(e^{+i(\widetilde{\omega}_\mathrm{f}-\omega_\mathrm{d})t/2}\hat{\sigma}_{2+} + e^{-i(\widetilde{\omega}_\mathrm{f}-\omega_\mathrm{d})t/2}\hat{\sigma}_{2-}\right)\Big] \times \left(e^{i\omega_\mathrm{d}t}\hat{a}^\dagger + e^{-i\omega_\mathrm{d}t}\hat{a}\right),
\end{aligned} \tag{4.2}$$

where $\Delta_1 = \omega_{\rm eg} - \omega_{\rm d}$, $\delta = \omega_{\rm r} - \omega_{\rm d}$ and $\tilde{\chi} = \widetilde{\omega}_{\rm f} - 3\omega_{\rm d}$. Henceforth, we set $\Delta_1 = 0$ so that the drive is on resonance with the first transition. Typically, $\xi = \omega_{\rm fe} - \omega_{\rm eg}$ is the anharmonicity parameter between the first and second transition. Depending on the energy level spacing of a given circuit, ξ can be negative or positive. When $\Delta_1 = 0$, the parameter $\widetilde{\chi}$ becomes proportional to the anharmonicity ξ; $\widetilde{\chi} = \widetilde{\omega}_{\rm f} - 3\omega_{\rm eg} = 2\omega_{\rm fe} - 2\omega_{\rm eg} = 2\xi$.

For a circuit QED implementation like the transmon, the first and second transition frequencies are usually close and ξ is negative. Additionally, the transition matrix elements of a transmon between the $n^{\rm th}$ and $(n+1)^{\rm st}$ state are proportional to $\sqrt{n+1}$, as discussed in Sec. 2.4. Then, it is justified to assume the coupling strengths of higher transitions scale harmonically. Thus, to simplify the analytical calculations, we assume a perfectly harmonic qutrit where $\widetilde{\chi} = 0$ (identical transition frequencies), $g_2 = \sqrt{2}g_1$ and $\Omega_2 = \sqrt{2}\Omega_1$ (harmonic scaling of coupling strengths). This will serve as a toy model to derive analytic results, after which numerical simulations, including realistic anharmonicity values, will be used to validate the results.

Assuming a perfectly harmonic qutrit, we can simplify the Hamiltonian of Eq. (4.2) by imposing a set of RWA conditions that read as

$$\omega_{\rm eg} - \omega_{\rm r} \ll \omega_{\rm eg} + \omega_{\rm r} \text{ and } \sqrt{2}g_1 \ll \min(\omega_{\rm eg}, \omega_{\rm r}), \tag{4.3a}$$

$$\sqrt{2}g_1 \ll 2\omega_{\rm d}, \text{ and} \tag{4.3b}$$

$$\sqrt{2}\Omega_1 \ll 4\omega_{\rm d}. \tag{4.3c}$$

The intuition behind the conditions is the same as the qubit case in Sec. 3.1. The conditions of Eq. (4.3a) are the usual conditions needed to arrive at a qutrit JCM Hamiltonian. The condition in Eq. (4.3b) is necessary to eliminate the counter-rotating interaction terms, whereas the condition in Eq. (4.3c) is required to drop the counter-rotating driving terms. Under all these RWA conditions, the Hamiltonian can be simplified to read as

$$\begin{aligned}\hat{H}^{\rm d}_{\rm RWA} =& \frac{\hbar\Omega_1}{2}\left(\hat{\sigma}_{1+} + \hat{\sigma}_{1-} + \sqrt{2}\hat{\sigma}_{2+} + \sqrt{2}\hat{\sigma}_{2-}\right) + \hbar\delta\hat{a}^\dagger\hat{a} \\ &+ \hbar g_1\left(\hat{\sigma}_{1+} + \sqrt{2}\hat{\sigma}_{2+}\right)\hat{a} + \hbar g_1\left(\hat{\sigma}_{1-} + \sqrt{2}\hat{\sigma}_{2-}\right)\hat{a}^\dagger.\end{aligned} \tag{4.4}$$

We now diagonalize the qutrit part of the free Hamiltonian, $\hbar\Omega_1(\hat{\sigma}_{1+} + \hat{\sigma}_{1-} + \sqrt{2}\hat{\sigma}_{2+} + \sqrt{2}\hat{\sigma}_{2-})/2$, to find the eigenvalues and eigenstates:

$$\lambda_0 = 0,\ |v_0\rangle = \frac{1}{\sqrt{3}}\left(-\sqrt{2}\,|{\rm g}\rangle + |{\rm f}\rangle\right), \text{ and} \tag{4.5a}$$

$$\lambda_\pm = \pm\frac{\hbar\Omega_1\sqrt{3}}{2},\ |v_\pm\rangle = \frac{1}{\sqrt{3}}\left(\frac{1}{\sqrt{2}}|\mathrm{g}\rangle \pm \sqrt{\frac{3}{2}}|\mathrm{e}\rangle + |\mathrm{f}\rangle\right). \tag{4.5b}$$

The zero eigenvalue state, $|v_0\rangle$, is commonly referred to as a *dark state* in quantum optics [57]. A dark state refers to a specific quantum state of a system that does not exhibit any radiative transitions or absorption. In other words, it is a state that remains unaffected by the presence of EM radiation. In this system, this means the state does not get populated by the classical drive nor does it exchange photons with the resonator. This can also be seen as a mathematical feature of the zero eigenvalue, which makes its time-evolution stationary and corresponds to its initial population.

Now that we found the dressed qutrit states, we follow the same procedure as in the qubit case by proceeding to the interaction picture. For that purpose, we define $\hat{H}_0^{\mathrm{d}} = \hbar\Omega_1\left(\hat{\sigma}_{1+} + \hat{\sigma}_{1-}\sqrt{2}\hat{\sigma}_{2+} + \sqrt{2}\hat{\sigma}_{2-}\right)/2 + \hbar\delta\hat{a}^\dagger\hat{a}$ and $\hat{H}_{\mathrm{I}}^{\mathrm{d}} = \hbar g_1(\hat{\sigma}_{1+} + \sqrt{2}\hat{\sigma}_{2+})\hat{a} + \hbar g_1(\hat{\sigma}_{1-} + \sqrt{2}\hat{\sigma}_{2-})\hat{a}^\dagger$. Then, the interaction picture Hamiltonian reads as

$$\begin{aligned}\hat{H}^{(\mathrm{I})} =& \hbar g_1\Bigg[\frac{\sqrt{3}}{2}(|v_+\rangle\langle v_+| - |v_-\rangle\langle v_-|) - \frac{\sqrt{3}}{6}|v_+\rangle\langle v_-|\, e^{i\Omega_1\sqrt{3}t} + \frac{\sqrt{3}}{6}|v_-\rangle\langle v_+|\, e^{-i\Omega_1\sqrt{3}t} \\ &- \sqrt{4}|v_+\rangle\langle v_0|\, e^{i\Omega_1\sqrt{3}t/2} + \sqrt{4}|v_-\rangle\langle v_0|\, e^{-i\Omega_1\sqrt{3}t/2} \\ &+ \frac{1}{\sqrt{3}}|v_0\rangle\langle v_+|\, e^{-i\Omega_1\sqrt{3}t/2} - \frac{1}{\sqrt{3}}|v_0\rangle\langle v_-|\, e^{i\Omega_1\sqrt{3}t/2}\Bigg]\hat{a}e^{-i\delta t} + \mathrm{H.c.}.\end{aligned} \tag{4.6}$$

Similar to the qubit case, the Hamiltonian of Eq. (4.6) comprises two distinct interactions: a time-independent (diagonal) interaction and a time-dependent-drive-modulated (off-diagonal) interaction. We now impose the strong driving condition, $g_1, |\delta| \ll \Omega_1$, which when combined with the driving RWA condition of Eq. (4.3c) becomes

$$g_1,\ |\delta| \ll \Omega_1 \ll 4\omega_{\mathrm{d}}/\sqrt{2}^{1}. \tag{4.7}$$

This allows us to neglect the drive-modulated terms and obtain the effective Hamiltonian

$$\hat{H}_{\mathrm{eff}}^{(\mathrm{I})} = \hbar g_1\frac{\sqrt{3}}{2}\left(|v_+\rangle\langle v_+| - |v_-\rangle\langle v_-|\right)\left(\hat{a}^\dagger e^{i\delta t} + \hat{a}e^{-i\delta t}\right). \tag{4.8}$$

This Hamiltonian generalizes that of Eq. (3.8) for our qutrit case. Interestingly, it generates displacement in the resonator conditioned on two of the three qutrit dressed basis states,

[1] Note that the qutrit bound is tighter than the qubit bound in Eq. (3.7).

$|v_+\rangle$ and $|v_-\rangle$. This means that for any initial product state between the qutrit and the resonator, $|\psi_\mathrm{i}\rangle = (c_0 |v_0\rangle + c_+ |v_+\rangle + c_- |v_-\rangle) |\psi_\mathrm{r}\rangle$, the term involving the dark state remains unchanged in the time-evolved state, $|\psi(t)\rangle = \hat{U}(t,0)[(c_+ |v_+\rangle + c_- |v_-\rangle) |\psi_\mathrm{r}\rangle] + c_0 |v_0\rangle |\psi_\mathrm{r}\rangle$, where $\hat{U}(t,0)$ is the time-evolution operator. This is not exclusive to product states – even if the initial state is entangled and has a term involving $|v_0\rangle$, the term remains unchanged in the time-evolved state.

We now analyze the dynamics stemming from the qubit recipe for generating a cat state, where the initial state is $|\psi_i\rangle = |\mathrm{g}\rangle |0\rangle$. We rewrite the qutrit state using the dressed basis $\{|v_0\rangle, |v_+\rangle, |v_-\rangle\}$, and we find that $|\psi_i\rangle = |\mathrm{g}\rangle |0\rangle = (c_{\mathrm{g}0} |v_0\rangle + c_{\mathrm{g}+} |v_+\rangle + c_{\mathrm{g}-} |v_-\rangle) |0\rangle$, where $c_{\mathrm{g}0} = -\sqrt{2/3}$ and $c_{\mathrm{g}\pm} = 1/\sqrt{6}$. Then, the interaction picture time-evolved state is

$$\begin{aligned} |\psi(t)\rangle^{(\mathrm{I})} &= c_{\mathrm{g}0} |v_0\rangle |0\rangle + c_{\mathrm{g}+} |v_+\rangle |\alpha\rangle + c_{\mathrm{g}-} |v_-\rangle |-\alpha\rangle \\ &= \frac{1}{6} |\mathrm{g}\rangle (4 |0\rangle + |\alpha\rangle + |-\alpha\rangle) \\ &\quad + \frac{1}{\sqrt{12}} |\mathrm{e}\rangle (|\alpha\rangle - |-\alpha\rangle) \\ &\quad + \frac{1}{\sqrt{18}} |\mathrm{f}\rangle (2 |0\rangle + |\alpha\rangle + |-\alpha\rangle), \end{aligned} \tag{4.9}$$

where $\alpha = \sqrt{3} g_1 (e^{i\delta t} - 1)/2\delta$; when $\delta \to 0$, then $\alpha = -i\sqrt{3} g t/2$. As stated earlier, any term involving the dark state remains unchanged in the time-evolved state. As a result, we find the resonator vacuum state $|0\rangle$ coupled to $|\mathrm{g}\rangle$ and $|\mathrm{f}\rangle$ (does not couple to $|\mathrm{e}\rangle$, since $\langle \mathrm{e}|v_0\rangle = 0$). This results in another non-classical state within the resonator, which is a superposition of the vacuum state and a cat state, obtained when measuring the qutrit in either $|\mathrm{g}\rangle$ or $|\mathrm{f}\rangle$. This state is intriguing in its own right, exhibiting varying Wigner-negative regions and interference patterns. Measuring the qutrit in $|\mathrm{e}\rangle$ yields an odd cat state in the resonator, exactly as in the qubit case.

The presence of the dark state prevents us from deterministically encoding a qubit state in the resonator using cat states. This is because measuring the qutrit in $|\mathrm{g}\rangle$ or $|\mathrm{f}\rangle$ does not leave a cat state in the resonator. To maximize the probability of finding a cat state in the resonator, we seek an alternative recipe. Initializing the qutrit in $|\mathrm{e}\rangle$ removes $|v_0\rangle$ and its stationary vacuum contribution due to its decoupling from the dark state subspace. Therefore, we propose a new recipe for a generating a cat state tailored to the qutrit. Let the system start in an initial state $|\psi_i\rangle = |\mathrm{e}\rangle |0\rangle = |\psi_\mathrm{i}\rangle = (|v_+\rangle - |v_-\rangle) |0\rangle / \sqrt{2}$. Then, the

interaction picture time-evolved state for this initial state is

$$
\begin{aligned}
|\psi(t)\rangle^{(\mathrm{I})} &= \frac{1}{\sqrt{2}}\left(|v_+\rangle\,|\alpha\rangle - |v_-\rangle\,|-\alpha\rangle\right) \\
&= \left(\frac{1}{\sqrt{12}}\,|\mathrm{g}\rangle + \frac{1}{\sqrt{6}}\,|\mathrm{f}\rangle\right)\left(|\alpha\rangle - |-\alpha\rangle\right) + \frac{1}{2}\,|\mathrm{e}\rangle\left(|\alpha\rangle + |-\alpha\rangle\right). \qquad (4.10)
\end{aligned}
$$

We note that a projective measurement on $|\mathrm{g}\rangle$, $|\mathrm{e}\rangle$ and $|\mathrm{f}\rangle$ leaves a cat state in the resonator. While the specified initial state deterministically yields a cat state, the parity remains probabilistic – exactly as in the qubit case. To encode a qubit state, $c_\mathrm{g}\,|\mathrm{g}\rangle + c_\mathrm{e}\,|\mathrm{e}\rangle$, in a cat state as described in Sec. 3.6, prepare the system in an initial state $|\psi_\mathrm{i}\rangle = (c_\mathrm{g}\,|v_+\rangle + c_\mathrm{e}\,|v_-\rangle)\,|0\rangle$. After time-evolving for the desired period and measuring in the bare basis $\{|\mathrm{g}\rangle, |\mathrm{e}\rangle, |\mathrm{f}\rangle\}$, the resonator is left in a state $\propto c_\mathrm{g}\,|\alpha\rangle \pm c_\mathrm{e}\,|-\alpha\rangle$. This serves as a generalized procedure for encoding a qubit state in a resonator using a driven qutrit-resonator system.

The aim of the qutrit extension is to model a weakly anharmonic system, e.g., the transmon. Up to this point, our work has been based on the assumption of the qutrit's perfect harmonicity, which encompasses multiple assumptions. The transition matrix elements of a transmon between the n^{th} and $(n+1)^{\mathrm{st}}$ state are proportional to $\sqrt{n+1}$ [33], so the perfect harmonicity of the coupling strengths is justified. As for the detuning between the transition frequencies, $|\xi|$, the typical values are on the order of $100 - 300$ MHz.

Figures 4.1 and 4.2 display the results of numerical simulations of the complete system Hamiltonian of Eq. (4.1), without any approximations. These simulations are performed in presence of both qutrit and resonator decoherence by means of a Lindblad master equation, as explained in App. A. Figure 4.1(a) shows the occupation probabilities of the qutrit states when the system is initialized in $|\mathrm{g}\rangle\,|0\rangle$. The probability of finding a cat state depends on measuring the qutrit in $|\mathrm{e}\rangle$, which is low for this initial state. The Wigner functions of the resonator state after a projective measurement on different qutrit states are shown in Figs. 4.1 and 4.2. The states shown match the analytical predictions. The anharmonicity used for the simulations is $\xi = -100$ MHz[2]. This anharmonicity is easily achievable by the transmon. The effect of nonzero anharmoncity can be seen in the pertubed interference regions in some of the Wigner functions of Fig. **??**. Additionally, the lobes of the cat states get slightly deformed, but this is also due to the terms neglected in the strong driving RWA.

[2]We performed simulations using anharmonicity values between 50 MHz and 400 MHz. From 50 MHz to $\sim$ 200 MHz, the qualitative predictions of the perfectly harmonic qutrit hold true. See Sec. 4.3 for considerations regarding arbitrary anharmonicity.

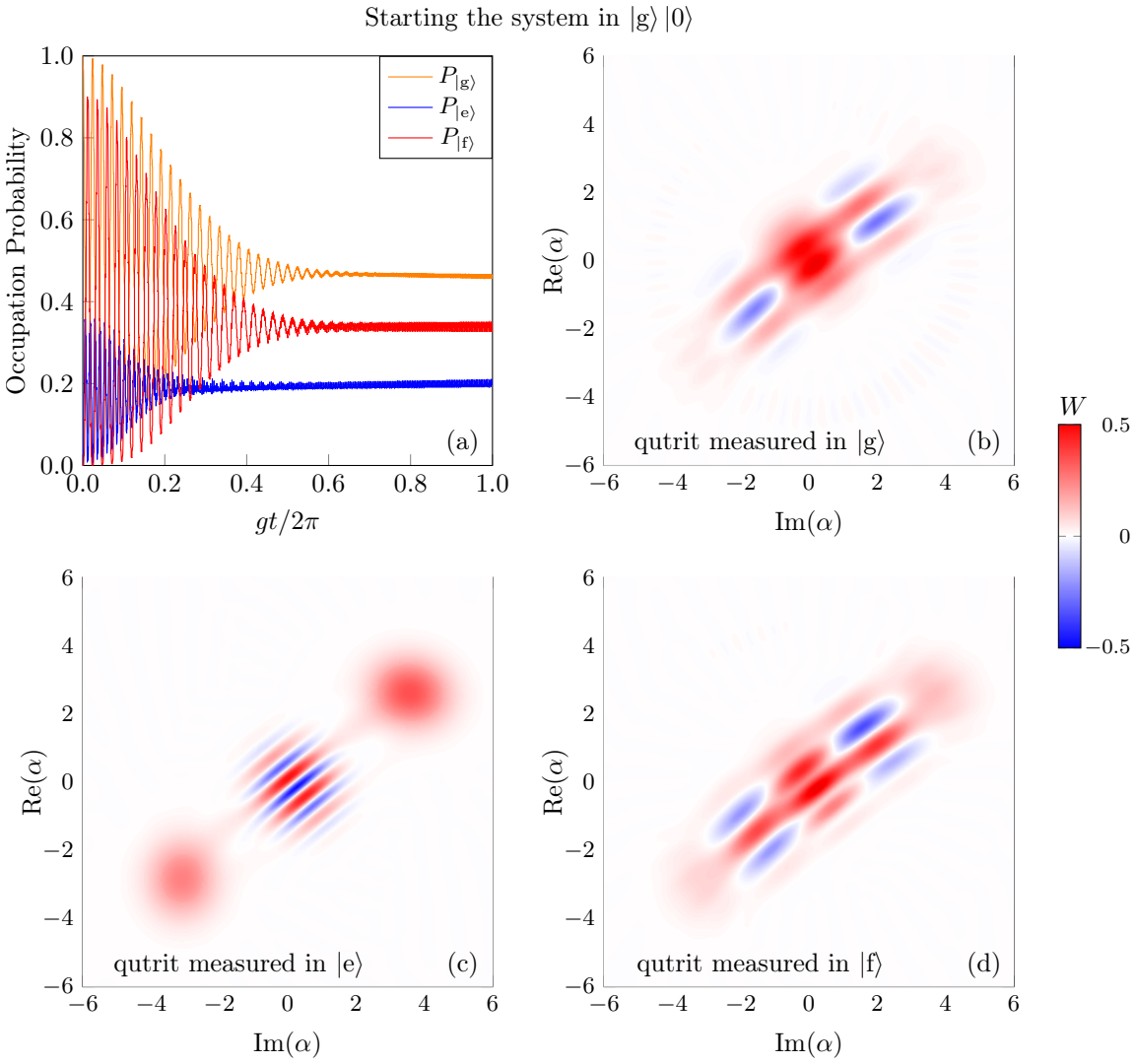

Figure 4.1: Dynamics of a weakly-anharmonic qutrit initialized in the ground state. The parameters used for the simulations are: $\Omega_1 = 2\pi \times 1\,\mathrm{GHz}$. $\Omega_2 = \sqrt{2}\Omega_1$. $g_1 = 2\pi \times 20\,\mathrm{MHz}$. $g_2 = \sqrt{2}g_1$. $\Delta_1 = \delta = 0$. $\omega_q = 2\pi \times 5\,\mathrm{GHz}$. $\xi = -2\pi \times 100\,\mathrm{MHz}$. $\gamma_1 = \kappa = 500\,\mathrm{kHz}$. $\gamma_2 = 2\gamma_1$. $\gamma_\phi = 1\,\mathrm{MHz}$. The Wigner functions are obtained by projectively measuring the qutrit after a time-evolution period of $g_1 t/2\pi = 0.61$.

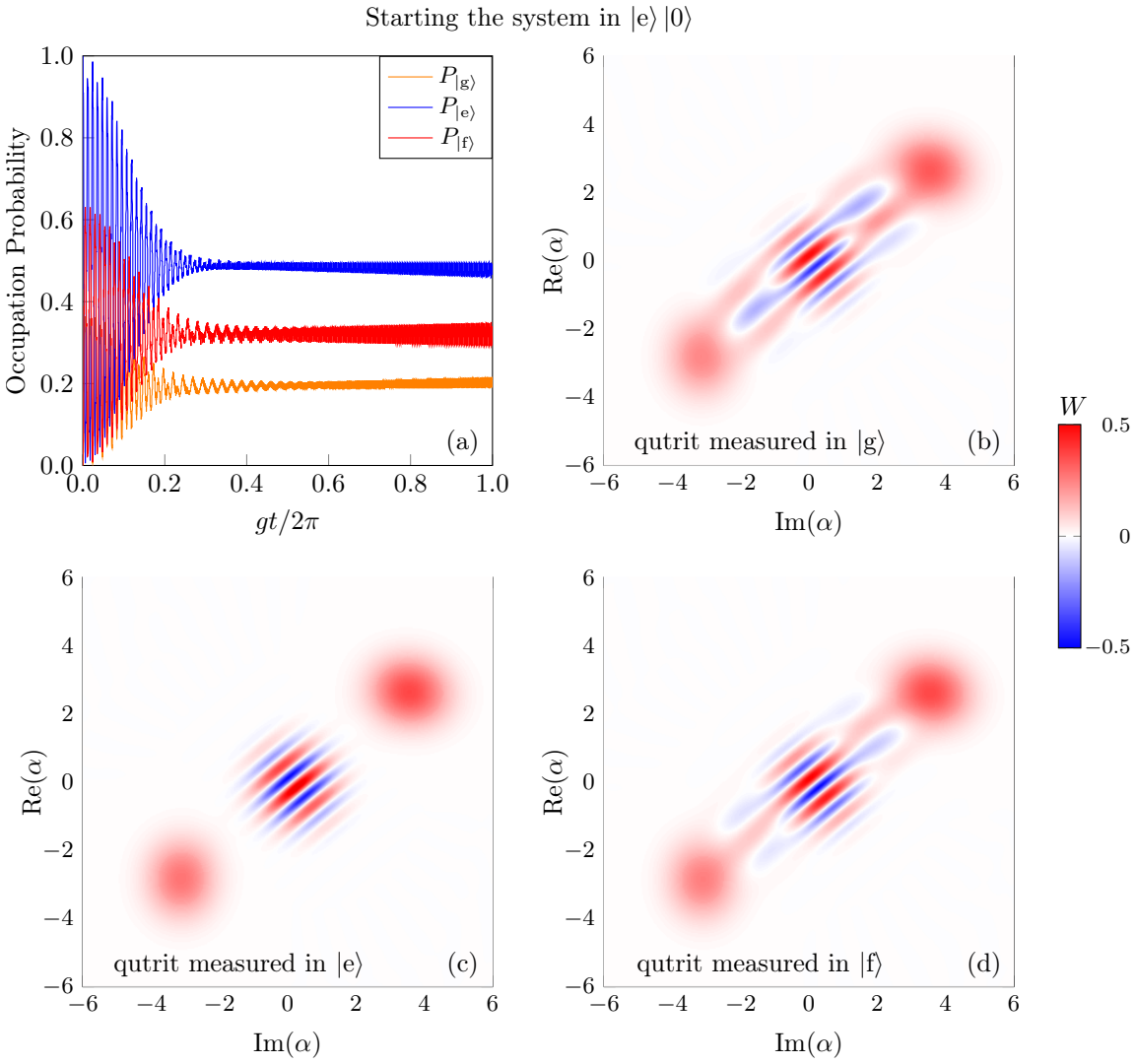

Figure 4.2: Dynamics of a weakly-anharmonic qutrit initialized in the first excited state. The simulation performed is identical to that of Fig. 4.1 with the system initialized in $|e\rangle\,|0\rangle$.

For a weakly anharmonic qutrit, the driven qutrit-resonator protocol presented here generalizes (with some modifications) that of Ch. 3. The perfectly harmonic qutrit model serves as a very good approximation for weakly anharmonic qutrits, as corroborated by

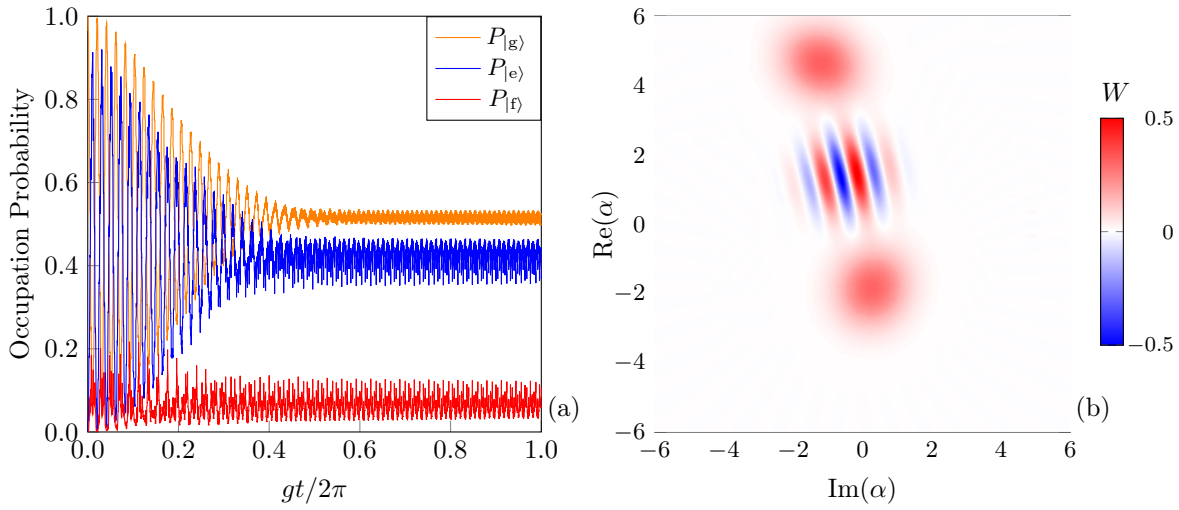

Figure 4.3: Dynamics of a strongly-anharmonic qutrit. The parameters used for the simulations are: $\Omega_1 = 2\pi \times 1\,\mathrm{GHz}$. $\Omega_2 = \sqrt{2}\Omega_1$. $g_1 = 2\pi \times 20\,\mathrm{MHz}$. $g_2 = \sqrt{2}g_1$. $\Delta_1 = \delta = 0$. $\omega_\mathrm{q} = 2\pi \times 5\,\mathrm{GHz}$. $\xi = 2\pi \times 2\,\mathrm{GHz}$. $\gamma_1 = \kappa = 500\,\mathrm{kHz}$. $\gamma_2 = 2\gamma_1$. $\gamma_\phi = 1\,\mathrm{MHz}$. The Wigner functions are obtained by projectively measuring the qutrit in $|\mathrm{e}\rangle$ after a time-evolution period of $g_1 t/2\pi = 0.61$. The results resemble those of a driven qubit-resonator. The cat state is displaced off-center due to the contributions of the $|\mathrm{e}\rangle \leftrightarrow |\mathrm{f}\rangle$ transition.

the numerical simulations.

4.2 Strongly-anharmonic qutrit limit

In this section, we consider the limit of large anharmonicity $|\xi|$ while maintaining the perfectly harmonic coupling strengths.

When $|\xi|$ is very large compared to Ω_1 and g_1, the second transition ($|\mathrm{e}\rangle \leftrightarrow |\mathrm{f}\rangle$) is very far detuned from the first transition ($|\mathrm{g}\rangle \leftrightarrow |\mathrm{e}\rangle$). As a result, the driving barely affects the third state and the resonator is either decoupled from or dispersively coupled to the second transition depending on how far detuned it is. In either case, the effective dynamics are those of a driven qubit-resonator system with slight perturbations to the cat state from small third state leakage population. In Fig. 4.3, we show the results of numerical simulations for such a regime. Figure 4.3(a) shows the occupation probabilities with the $|\mathrm{f}\rangle$ population fluctuating around 0.1 (10%). The arguments presented work for

large $|\xi|$ in the positive and negative limits. From an analytical point of view, we can justify these arguments by explicitly performing an RWA that eliminates terms oscillating with $e^{\pm i\tilde{\chi}t}$ in the Hamiltonian of Eq. (4.2) when $|\xi| \gg \Omega_1, g_1$.

We can now fit this regime of $|\xi| \gg \Omega_1, g_1$ to an experimental implementation context. When the CPB is operated in the transmon regime the analysis of Sec. 4.1 is applicable. While, when the CPB operating in the charge regime at the degeneracy point (as discussed in Sec. 2.4), the anharmonicity between the two transition frequencies fits this very large anharmonicity regime. In this case, the system for the most part is a driven qubit-resonator. This can be extrapolated to different circuit implementations such as flux or fluxonium circuits fitting the anharmonicity to the appropriate regimes[3].

4.3 Extension to an arbitrarily-anharmonic qutrit

In this section, we extend our analytical framework to deal with arbitrarily anharmonic qutrits by carefully selecting an appropriate rotating frame. Additionally, we relax assumptions on coupling strengths and assume arbitrary coupling strengths. However, we maintain the bare minimum assumption, $g_1/g_2 = \Omega_1/\Omega_2$. This is because the mechanism in which the qutrit physically couples to the driving field is the same as it does to the resonator.

We start by transforming driven qutrit-resonator Hamiltonian of Eq. (4.1) into a different rotating frame. This rotating frame is defined by the unitary transformation $\hat{U} = \exp\left[-it\left(\omega_{\mathrm{d}}\left(|\mathrm{e}\rangle\langle\mathrm{e}| - |\mathrm{g}\rangle\langle\mathrm{g}| - |\mathrm{f}\rangle\langle\mathrm{f}|\right) + 2\omega_{\mathrm{d}}\hat{a}^\dagger\hat{a}\right)/2\right]$. In this frame, the system Hamiltonian reads as

$$\begin{aligned}
\hat{H}^{\mathrm{d}} =& \frac{\hbar\Delta_1}{2}\left(|\mathrm{e}\rangle\langle\mathrm{e}| - |\mathrm{g}\rangle\langle\mathrm{g}|\right) + \frac{\hbar\Sigma}{2}|\mathrm{f}\rangle\langle\mathrm{f}| + \hbar\delta\hat{a}^\dagger\hat{a} \\
&+ \frac{\hbar\Omega_1}{2}\left(\hat{\sigma}_{1+} + \hat{\sigma}_{1-} + e^{i2\omega_{\mathrm{d}}t}\hat{\sigma}_{1+} + e^{-i2\omega_{\mathrm{d}}t}\hat{\sigma}_{1-}\right) \\
&+ \frac{\hbar\Omega_2}{2}\left(\hat{\sigma}_{2+} + \hat{\sigma}_{2-} + e^{i2\omega_{\mathrm{d}}t}\hat{\sigma}_{2+} + e^{-i2\omega_{\mathrm{d}}t}\hat{\sigma}_{2-}\right) \\
&+ \hbar\Big[g_1\left(e^{i\omega_{\mathrm{d}}t}\hat{\sigma}_{1+} + e^{-i\omega_{\mathrm{d}}t}\hat{\sigma}_{1-}\right) + g_2\left(e^{i\omega_{\mathrm{d}}t}\hat{\sigma}_{2+} + e^{-i\omega_{\mathrm{d}}t}\hat{\sigma}_{2-}\right)\Big] \\
&\times\left(e^{i\omega_{\mathrm{d}}t}\hat{a}^\dagger + e^{-i\omega_{\mathrm{d}}t}\hat{a}\right),
\end{aligned} \tag{4.11}$$

[3] In fact, this can be extrapolated to other implementations when you scale the parameters accordingly; the analysis presented works with qubits and qutrits in general.

where $\Sigma = \widetilde{\omega}_{\mathrm{f}} + \omega_{\mathrm{d}}$. The intuition behind this particular frame is that it sets both transitions on equal footing. The off-diagonal terms have the same form in their time-dependence for both transitions. This Hamiltonian can be simplified by a set of RWA conditions that read

$$\omega_{\mathrm{eg}} - \omega_{\mathrm{r}} \ll \omega_{\mathrm{eg}} + \omega_{\mathrm{r}} \text{ and } g_1 \ll \min(\omega_{\mathrm{eg}}, \omega_{\mathrm{r}}), \tag{4.12a}$$
$$g_1 \ll 2\omega_{\mathrm{d}}, \tag{4.12b}$$
$$\Omega_1 \ll 4\omega_{\mathrm{d}}, \tag{4.12c}$$
$$\omega_{\mathrm{fe}} - \omega_{\mathrm{r}} \ll \omega_{\mathrm{fe}} + \omega_{\mathrm{r}} \text{ and } g_2 \ll \min(\omega_{\mathrm{fe}}, \omega_{\mathrm{r}}), \tag{4.12d}$$
$$g_2 \ll 2\omega_{\mathrm{d}}, \text{ and} \tag{4.12e}$$
$$\Omega_2 \ll 4\omega_{\mathrm{d}}. \tag{4.12f}$$

These conditions generalize those of Eq. (4.3) for arbitrary coupling strengths. Then, taking all the conditions stated above to hold true allows us to perform an RWA and obtain the Hamiltonian

$$\begin{aligned}\hat{H}^{\mathrm{d}}_{\mathrm{RWA}} =& \frac{\hbar\Delta_1}{2}\left(|\mathrm{e}\rangle\langle\mathrm{e}| - |\mathrm{g}\rangle\langle\mathrm{g}|\right) + \frac{\hbar\Sigma}{2}|\mathrm{f}\rangle\langle\mathrm{f}| + \hbar\delta\hat{a}^\dagger\hat{a} \\ &+ \frac{\hbar\Omega_1}{2}\left(\hat{\sigma}_{1+} + \hat{\sigma}_{1-}\right) + \frac{\hbar\Omega_2}{2}\left(\hat{\sigma}_{2+} + \hat{\sigma}_{2-}\right) \\ &+ \hbar\left(g_1\hat{\sigma}_{1+} + g_2\hat{\sigma}_{2+}\right)\hat{a} + \hbar\left(g_1\hat{\sigma}_{1-} + g_2\hat{\sigma}_{2-}\right)\hat{a}^\dagger.\end{aligned} \tag{4.13}$$

For simplicity, we only deal with the case where $\Delta_1 = 0$. We now diagonalize the qutrit part of the free Hamiltonian, $\hbar\Sigma|\mathrm{f}\rangle\langle\mathrm{f}|/2 + \hbar\Omega_1(\hat{\sigma}_{1+} + \hat{\sigma}_{1-})/2 + \hbar\Omega_2(\hat{\sigma}_{2+} + \hat{\sigma}_{2-})/2$, to find the eigenvalues and eigenstates [57]:

$$\lambda_1 = -\frac{1}{3}a + \frac{2}{3}p\cos\left(\frac{\theta}{3}\right), \tag{4.14}$$
$$\lambda_2 = -\frac{1}{3}a - \frac{2}{3}p\cos\left(\frac{\theta}{3} + \frac{\pi}{3}\right), \tag{4.15}$$
$$\lambda_3 = -\frac{1}{3}a - \frac{2}{3}p\cos\left(\frac{\theta}{3} - \frac{\pi}{3}\right), \tag{4.16}$$

and

$$|v_k\rangle = \frac{1}{\mathcal{N}_k}\left[\left(\Omega_1\left(\lambda_k - \frac{\Sigma}{2}\right)\right)|\mathrm{g}\rangle + \left(2\lambda_k\left(\lambda_k - \frac{\Sigma}{2}\right)\right)|\mathrm{e}\rangle + \Omega_2|\mathrm{f}\rangle\right], \tag{4.17}$$

where

$$a = -\frac{\Sigma}{2}, \tag{4.18a}$$

$$b = -\frac{1}{4}\left(\Omega_1^2 + \Omega_2^2\right), \tag{4.18b}$$

$$c = \frac{1}{8}\Sigma\Omega_2^2, \tag{4.18c}$$

$$p = \sqrt{a^2 - 3b}, \tag{4.18d}$$

$$\cos\theta = -\frac{27c + 2a^3 - 9ab}{2p^3}, \tag{4.18e}$$

and

$$\mathcal{N}_k = \sqrt{\lambda_k^2|\Omega_2|^2 + (4\lambda_k^2 + |\Omega_1|^2)\left(\lambda_k - \frac{\Sigma}{2}\right)^2} \quad (k = 1, 2, 3). \tag{4.18f}$$

Next, we proceed as done in previous sections by transforming to the interaction picture. For that purpose, we define $\hat{H}_0 = \hbar\Sigma\,|\mathrm{f}\rangle\langle\mathrm{f}|\,/2 + \hbar\delta\hat{a}^\dagger\hat{a} + \hbar\Omega_1(\hat{\sigma}_{1+} + \hat{\sigma}_{1-})/2 + \hbar\Omega_2(\hat{\sigma}_{2+} + \hat{\sigma}_{2-})/2$ and $\hat{H}_\mathrm{I} = \hbar(g_1\hat{\sigma}_{1+} + g_2\hat{\sigma}_{2+})\hat{a} + \hbar(g_1\hat{\sigma}_{1-} + g_2\hat{\sigma}_{2-})\hat{a}^\dagger$. Then, the interaction picture Hamiltonian reads as

$$\begin{aligned}\hat{H}^{(\mathrm{I})} =& \hbar\sum_{k=1}^{3}\left[\frac{2\lambda_k\left(\lambda_k - \frac{\Sigma}{2}\right)}{\mathcal{N}_k^2}\left(g_1\Omega_1\left(\lambda_k - \frac{\Sigma}{2}\right) + g_2\Omega_2\right)|v_k\rangle\langle v_k|\right.\\ &\left. + \sum_{l\neq k}\frac{\left(\lambda_l - \frac{\Sigma}{2}\right)}{\mathcal{N}_k\mathcal{N}_l}\left(2g_1\Omega_1\lambda_k\left(\lambda_k - \frac{\Sigma}{2}\right) + g_2\Omega_2\right)|v_k\rangle\langle v_l|\, e^{i\Delta\lambda_{kl}t}\right]\\ &\times\left(\hat{a}^\dagger e^{+i\delta t} + \hat{a}e^{-i\delta t}\right),\end{aligned} \tag{4.19}$$

where $\Delta\lambda_{kl} = \lambda_k - \lambda_l$. In this Hamiltonian, there time-independent (diagonal) terms and time-dependent (off-diagonal) terms. The separation of timescales cannot be assumed *a priori*. To achieve a similar Hamiltonian as in the previous sections, we must find the *strong driving-anharmoncity*[4] regime where

$$g_1, g_2, |\delta| \ll |\Delta\lambda_{kl}|. \tag{4.20}$$

[4]The parameters $\Delta\lambda_{kl}$ are functions of the driving strengths Ω_1 and Ω_2, as well as Σ, which can be directly reformulated in terms of ξ.

We note that this has to be satisfied with the RWA conditions of Eq. (4.12). If this regime is achieved, we can neglect the off-diagonal terms modulated by $\Delta\lambda_{kl}$ and obtain the effective Hamiltonian

$$\hat{H}_{\text{eff}}^{(\text{I})} = \hbar \sum_{k=1}^{3} \widetilde{g}_k \left|v_k\right\rangle\!\left\langle v_k\right| \left(\hat{a}^\dagger e^{+i\delta t} + \hat{a} e^{-i\delta t}\right), \tag{4.21}$$

where $\widetilde{g}_k = 2\lambda_k(\lambda_k - \Sigma/2)(g_1\Omega_1(\lambda_k - \Sigma/2) + g_2\Omega_2)/\mathcal{N}_k^2$. This Hamiltonian generates resonator displacements conditioned the dressed qutrit basis $\{\left|v_1\right\rangle, \left|v_2\right\rangle, \left|v_3\right\rangle\}$. Initializing the system in $\left|\psi_{\text{i}}\right\rangle = \sum_{k=1}^{3} c_k \left|v_k\right\rangle \left|0\right\rangle$ with $\sum_{k=1}^{3} \left|c_k\right|^2 = 1$, then time-evolving under the effective Hamiltonian yields

$$\left|\psi(t)\right\rangle^{(\text{I})} = \sum_{k=1}^{3} c_k \left|v_k\right\rangle \left|\alpha_k\right\rangle, \tag{4.22}$$

where $\alpha_k = -\widetilde{g}_k(e^{i\delta t} - 1)/2\delta$; when $\delta \to 0$, then $\alpha_k = -i\widetilde{g}_k t/2$. Similar to the previous sections, we can create interesting nonclassical states composed of a superposition of coherent states by rewriting the states in the bare basis and measuring the qutrit. This leaves the resonator in a nonclassical state dependent on which qutrit state was measured.

The framework presented in this section has been quite general and abstracted away from a particular circuit implementation. The purpose of this section is to present a general framework for an arbitrarily anharmonic driven qutrit-resonator that does not conform to either of the two extremes introduced in the previous two sections. Thus, we outlined a step-by-step procedure to obtain an effective Hamiltonian similar to the previously derived results. Additionally, the approach presented here is useful for tailoring parameters to a particular device (describing a driven qutrit-resonator system). One can use the derived analytical eigenvalues and eigenstates along with all the given constraints to numerically optimize for the generation of a cat state or a particular (collinear[5]) superposition of coherent states of interest for a set of particular device parameters.

[5] All the displacements generated are on the same axis.

Chapter 5

Conclusions and Outlook

In this thesis, we layed out a practical theory for generating cat states using a resonant continuous drive on a qubit coupled to a resonator. For that purpose, we formulated bounds on the strong driving regime. We leveraged the Bloch-Siegert shift to allow for a detuned-driving to generate cat states. We showed how to encode a qubit state into a resonator with a probablistic phase depending on the measurement outcome. urthermore, we extended the scheme to encompass a driven qutrit-resonator system with varying anharmonicity. These considerations are an important step considering potential implementation challenges on a transmon or charge qubit. Lastly, we showed that our method outperforms two commonly used methods even when accounting for decoherence effects.

What is the future for this work? Currently, one of my colleagues in my research group is working on implementing the theory proposed here. Beyond implementing the theory, this work can be built on in two directions. The first direction is to incorporate it within the broader context of cat state generation for cat codes. The problems to be addressed are: 1) resolving the issue of the probabilistic phase, exploring the potential for deterministic solutions or somehow accommodating it with parity-fluid protocols, and 2) developing a method that, in conjunction with the work presented here, enables the generation of multi-component cat states, particularly those with three or four components. The second direction aims to generalize the driven qubit/qutrit-resonator system to encompass higher-order interactions, such as a two-photon (or more generally, n-photon) interaction as proposed in circuit QED [17] and trapped ions [48]. An interaction of the form $\hat{\sigma}_x(\hat{a}^{\dagger 2} + \hat{a}^2)$ (or of higher order) in the presence of a drive could facilitate the creation of exotic states that are traditionally challenging to synthesize but may offer significant computational advantages. In fact, due to time constraints, we had to omit some material related to this analysis.

References

[1] Konrad Banaszek and Krzysztof Wódkiewicz. Testing quantum nonlocality in phase space. *Phys. Rev. Lett.*, 82:2009–2013, Mar 1999.

[2] Félix Beaudoin, Jay M. Gambetta, and A. Blais. Dissipation and ultrastrong coupling in circuit qed. *Phys. Rev. A*, 84:043832, Oct 2011.

[3] M V Berry. Transitionless quantum driving. *Journal of Physics A: Mathematical and Theoretical*, 42(36):365303, aug 2009.

[4] Alexandre Blais, Arne L. Grimsmo, S. M. Girvin, and Andreas Wallraff. Circuit quantum electrodynamics. *Rev. Mod. Phys.*, 93:025005, May 2021.

[5] F. Bloch and A. Siegert. Magnetic resonance for nonrotating fields. *Phys. Rev.*, 57:522–527, Mar 1940.

[6] J. Bourassa, F. Beaudoin, Jay M. Gambetta, and A. Blais. Josephson-junction-embedded transmission-line resonators: From kerr medium to in-line transmon. *Phys. Rev. A*, 86:013814, Jul 2012.

[7] J. Bourassa, F. Beaudoin, Jay M. Gambetta, and A. Blais. Josephson-junction-embedded transmission-line resonators: From kerr medium to in-line transmon. *Phys. Rev. A*, 86:013814, Jul 2012.

[8] D. Braak. Integrability of the rabi model. *Phys. Rev. Lett.*, 107:100401, Aug 2011.

[9] Heinz-Peter Breuer and F. Petruccione. *The Theory of Open Quantum Systems*. Oxford University Press, 2010.

[10] J. H Béjanin. *Advances in Superconducting Circuit Quantum Electrodynamics*. PhD thesis. University of Waterloo, 2022.

[11] Howard Carmichael. *An Open Systems Approach to Quantum Optics: Lectures presented at the Universite Libre de Bruxelles, October 28 - November 4, 1991*. Springer-Verlag, 1993.

[12] Carlton M. Caves. Quantum-mechanical noise in an interferometer. *Phys. Rev. D*, 23:1693–1708, Apr 1981.

[13] A Cottet. *Implementation of a quantum bit in a superconducting circuit*. PhD thesis. University of Paris, 2002.

[14] Frank DiFilippo, Vasant Natarajan, Kevin R. Boyce, and David E. Pritchard. Classical amplitude squeezing for precision measurements. *Phys. Rev. Lett.*, 68:2859–2862, May 1992.

[15] Paul A. M. Dirac. The quantum theory of the emission and absorption of radiation. *Proceedings of the Royal Society of London. Series A, Containing Papers of a Mathematical and Physical Character*, 114(767):243–265, 1927.

[16] A. Einstein, B. Podolsky, and N. Rosen. Can quantum-mechanical description of physical reality be considered complete? *Phys. Rev.*, 47:777–780, May 1935.

[17] S. Felicetti, D. Z. Rossatto, E. Rico, E. Solano, and P. Forn-Díaz. Two-photon quantum rabi model with superconducting circuits. *Phys. Rev. A*, 97:013851, Jan 2018.

[18] V. Fock. Konfigurationsraum und zweite quantelung. *Zeitschrift für Physik*, 75(9):622–647, Sep 1932.

[19] Thomas Gerrits, Scott Glancy, Tracy S. Clement, Brice Calkins, Adriana E. Lita, Aaron J. Miller, Alan L. Migdall, Sae Woo Nam, Richard P. Mirin, and Emanuel Knill. Generation of optical coherent-state superpositions by number-resolved photon subtraction from the squeezed vacuum. *Phys. Rev. A*, 82:031802, Sep 2010.

[20] S. M. Girvin. Schrodinger cat states in circuit qed, 2017.

[21] Arne L. Grimsmo, Joshua Combes, and Ben Q. Baragiola. Quantum computing with rotation-symmetric bosonic codes. *Phys. Rev. X*, 10:011058, Mar 2020.

[22] Gilbert Grynberg, Alain Aspect, and Claude Fabre. *Introduction to Quantum Optics: From the semi-classical approach to quantized light*. Cambridge University Press, 2011.

[23] Serge Haroche and Jean-Michel Raimond. *Exploring the Quantum: Atoms, Cavities, and Photons*. Oxford University Press, 08 2006.

[24] Max Hofheinz, H. Wang, M. Ansmann, Radoslaw C. Bialczak, Erik Lucero, M. Neeley, A. D. O'Connell, D. Sank, J. Wenner, John M. Martinis, and A. N. Cleland. Synthesizing arbitrary quantum states in a superconducting resonator. *Nature*, 459(7246):546–549, May 2009.

[25] K. Huang, H. Le Jeannic, J. Ruaudel, V. B. Verma, M. D. Shaw, F. Marsili, S. W. Nam, E Wu, H. Zeng, Y.-C. Jeong, R. Filip, O. Morin, and J. Laurat. Optical synthesis of large-amplitude squeezed coherent-state superpositions with minimal resources. *Phys. Rev. Lett.*, 115:023602, Jul 2015.

[26] R.L. Hudson. When is the wigner quasi-probability density non-negative? *Reports on Mathematical Physics*, 6(2):249–252, 1974.

[27] E.T. Jaynes and F.W. Cummings. Comparison of quantum and semiclassical radiation theories with application to the beam maser. *Proceedings of the IEEE*, 51(1):89–109, 1963.

[28] J.R. Johansson, P.D. Nation, and Franco Nori. Qutip: An open-source python framework for the dynamics of open quantum systems. *Computer Physics Communications*, 183(8):1760–1772, 2012.

[29] J.R. Johansson, P.D. Nation, and Franco Nori. Qutip 2: A python framework for the dynamics of open quantum systems. *Computer Physics Communications*, 184(4):1234–1240, 2013.

[30] Atharv Joshi, Kyungjoo Noh, and Yvonne Y Gao. Quantum information processing with bosonic qubits in circuit qed. *Quantum Science and Technology*, 6(3):033001, apr 2021.

[31] Anatole Kenfack and Karol Życzkowski. Negativity of the wigner function as an indicator of non-classicality. *Journal of Optics B: Quantum and Semiclassical Optics*, 6(10):396, aug 2004.

[32] Andrei B. Klimov and Sergei M. Chumakov. *A group-theoretical approach to Quantum Optics: Models of Atom-field interactions*. Wiley, 2009.

[33] Jens Koch, Terri M. Yu, Jay Gambetta, A. A. Houck, D. I. Schuster, J. Majer, Alexandre Blais, M. H. Devoret, S. M. Girvin, and R. J. Schoelkopf. Charge-insensitive qubit design derived from the cooper pair box. *Phys. Rev. A*, 76:042319, Oct 2007.

[34] Jonas Larson and Themistoklis Mavrogordatos. *The Jaynes–Cummings Model and Its Descendants*. 2053-2563. IOP Publishing, 2021.

[35] Z. Leghtas, S. Touzard, I. M. Pop, A. Kou, B. Vlastakis, A. Petrenko, K. M. Sliwa, A. Narla, S. Shankar, M. J. Hatridge, M. Reagor, L. Frunzio, R. J. Schoelkopf, M. Mirrahimi, and M. H. Devoret. Confining the state of light to a quantum manifold by engineered two-photon loss. *Science*, 347(6224):853–857, 2015.

[36] Z. Leghtas, S. Touzard, I. M. Pop, A. Kou, B. Vlastakis, A. Petrenko, K. M. Sliwa, A. Narla, S. Shankar, M. J. Hatridge, M. Reagor, L. Frunzio, R. J. Schoelkopf, M. Mirrahimi, and M. H. Devoret. Confining the state of light to a quantum manifold by engineered two-photon loss. *Science*, 347(6224):853–857, 2015.

[37] Zaki Leghtas, Gerhard Kirchmair, Brian Vlastakis, Michel H. Devoret, Robert J. Schoelkopf, and Mazyar Mirrahimi. Deterministic protocol for mapping a qubit to coherent state superpositions in a cavity. *Phys. Rev. A*, 87:042315, Apr 2013.

[38] Ning Lu. Effects of dissipation on photon statistics and the lifetime of a pure number state. *Phys. Rev. A*, 40:1707–1708, Aug 1989.

[39] M Mariantoni. *New Trends in Superconducting Circuit Quantum Electrodynamics: Two Amplifiers, Two Resonators, and Two Photons*. PhD thesis. Technical University of Munich, 2009.

[40] Matteo Mariantoni, Frank Deppe, A. Marx, R. Gross, F. K. Wilhelm, and E. Solano. Two-resonator circuit quantum electrodynamics: A superconducting quantum switch. *Phys. Rev. B*, 78:104508, Sep 2008.

[41] Eduardo Martín-Martínez. Quantum mechanics in phase space: An introduction, 2023.

[42] Mazyar Mirrahimi, Zaki Leghtas, Victor V Albert, Steven Touzard, Robert J Schoelkopf, Liang Jiang, and Michel H Devoret. Dynamically protected cat-qubits: A new paradigm for universal quantum computation. *New Journal of Physics*, 16(4):045014, 2014.

[43] Vasant Natarajan, Frank DiFilippo, and David E. Pritchard. Classical squeezing of an oscillator for subthermal noise operation. *Phys. Rev. Lett.*, 74:2855–2858, Apr 1995.

[44] J. S. Neergaard-Nielsen, B. Melholt Nielsen, C. Hettich, K. Mølmer, and E. S. Polzik. Generation of a superposition of odd photon number states for quantum information networks. *Phys. Rev. Lett.*, 97:083604, Aug 2006.

[45] Alexei Ourjoumtsev, Rosa Tualle-Brouri, Julien Laurat, and Philippe Grangier. Generating optical schrödinger kittens for quantum information processing. *Science*, 312(5770):83–86, 2006.

[46] Michael J. Peterer, Samuel J. Bader, Xiaoyue Jin, Fei Yan, Archana Kamal, Theodore J. Gudmundsen, Peter J. Leek, Terry P. Orlando, William D. Oliver, and Simon Gustavsson. Coherence and decay of higher energy levels of a superconducting transmon qubit. *Phys. Rev. Lett.*, 114:010501, Jan 2015.

[47] I. Pietikäinen, S. Danilin, K. S. Kumar, A. Vepsäläinen, D. S. Golubev, J. Tuorila, and G. S. Paraoanu. Observation of the bloch-siegert shift in a driven quantum-to-classical transition. *Phys. Rev. B*, 96:020501, Jul 2017.

[48] Ricardo Puebla, Myung-Joong Hwang, Jorge Casanova, and Martin B. Plenio. Protected ultrastrong coupling regime of the two-photon quantum rabi model with trapped ions. *Phys. Rev. A*, 95:063844, Jun 2017.

[49] Shruti Puri, Samuel Boutin, and Alexandre Blais. Engineering the quantum states of light in a kerr-nonlinear resonator by two-photon driving. *npj Quantum Information*, 3(1), 2017.

[50] I. I. Rabi. On the process of space quantization. *Phys. Rev.*, 49:324–328, Feb 1936.

[51] Daniel Z. Rossatto, Celso J. Villas-Bôas, Mikel Sanz, and Enrique Solano. Spectral classification of coupling regimes in the quantum rabi model. *Phys. Rev. A*, 96:013849, Jul 2017.

[52] D. Rugar and P. Grütter. Mechanical parametric amplification and thermomechanical noise squeezing. *Phys. Rev. Lett.*, 67:699–702, Aug 1991.

[53] J. J. Sakurai and Jim Napolitano. *Modern Quantum Mechanics*. Cambridge University Press, 2 edition, 2017.

[54] Wolfgang P. Schleich. *Quantum Optics in Phase Space*. John Wiley Sons, Ltd, 2001.

[55] E. Schrödinger. Die gegenwärtige situation in der quantenmechanik. *Die Naturwissenschaften*, 23(48):807–812, 1935.

[56] Jon H. Shirley. Solution of the schrödinger equation with a hamiltonian periodic in time. *Phys. Rev.*, 138:B979–B987, May 1965.

[57] Bruce W. Shore. *The Theory of Coherent Atomic Excitation*. Wiley, 1990.

[58] E. Solano, G. S. Agarwal, and H. Walther. *Phys. Rev. Lett.*, 90:027903, Jan 2003.

[59] Francisco Soto and Pierre Claverie. When is the Wigner function of multidimensional systems nonnegative? *Journal of Mathematical Physics*, 24(1):97–100, 01 1983.

[60] Hiroki Takahashi, Kentaro Wakui, Shigenari Suzuki, Masahiro Takeoka, Kazuhiro Hayasaka, Akira Furusawa, and Masahide Sasaki. Generation of large-amplitude coherent-state superposition via ancilla-assisted photon subtraction. *Phys. Rev. Lett.*, 101:233605, Dec 2008.

[61] R. J. Thompson, G. Rempe, and H. J. Kimble. Observation of normal-mode splitting for an atom in an optical cavity. *Phys. Rev. Lett.*, 68:1132–1135, Feb 1992.

[62] Kentaro Wakui, Hiroki Takahashi, Akira Furusawa, and Masahide Sasaki. Photon subtracted squeezed states generated with periodically poled ktiopo4. *Opt. Express*, 15(6):3568–3574, Mar 2007.

[63] A. Wallraff, D. I. Schuster, A. Blais, L. Frunzio, R.-. S. Huang, J. Majer, S. Kumar, S. M. Girvin, and R. J. Schoelkopf. Strong coupling of a single photon to a superconducting qubit using circuit quantum electrodynamics. *Nature*, 431(7005):162–167, Sep 2004.

[64] Christian Weedbrook, Stefano Pirandola, Raúl García-Patrón, Nicolas J. Cerf, Timothy C. Ralph, Jeffrey H. Shapiro, and Seth Lloyd. Gaussian quantum information. *Rev. Mod. Phys.*, 84:621–669, May 2012.

[65] E. Wigner. On the quantum correction for thermodynamic equilibrium. *Phys. Rev.*, 40:749–759, Jun 1932.

[66] Waltraut Wustmann and Vitaly Shumeiko. Parametric resonance in tunable superconducting cavities. *Phys. Rev. B*, 87:184501, May 2013.

[67] Yiying Yan, Zhiguo Lü, and Hang Zheng. Bloch-siegert shift of the rabi model. *Phys. Rev. A*, 91:053834, May 2015.

[68] B. Yurke and D. Stoler. Generating quantum mechanical superpositions of macroscopically distinguishable states via amplitude dispersion. *Phys. Rev. Lett.*, 57:13–16, Jul 1986.

[69] David Zueco, Georg M. Reuther, Sigmund Kohler, and Peter Hänggi. Qubit-oscillator dynamics in the dispersive regime: Analytical theory beyond the rotating-wave approximation. *Phys. Rev. A*, 80:033846, Sep 2009.

[70] Wojciech Hubert Zurek. Decoherence, einselection, and the quantum origins of the classical. *Rev. Mod. Phys.*, 75:715–775, May 2003.

APPENDICES

Appendix A

Open system

In Sec. 2.1, we introduced the Lindblad master equation for describing Markovian non-unitary evolution in a zero-temperature environment. Here, we specify the form of the Lindblad jump operators, $\hat{L}_k$, along with their rates, γ_k, for both qubit- and qutrit-resonator systems.

For the qubit-resonator system, the master equation reads as

$$\frac{d}{dt}\hat{\rho} = -\frac{i}{\hbar}[\hat{H}, \hat{\rho}] + \gamma_1 \mathcal{D}(\hat{\sigma}_-)\hat{\rho} + \frac{\gamma_\phi}{2}\mathcal{D}(\hat{\sigma}_z)\hat{\rho} + \kappa\mathcal{D}(\hat{a})\hat{\rho}, \tag{A.1}$$

where $\hat{\rho}$ is the full system density matrix, is the dissipator for a given operator $\hat{O}$, γ_1 and γ_ϕ are the qubit energy relaxation and dephasing rate, and κ is the resonator photon loss rate. While for the qutrit-resonator system, the master equation reads as

$$\begin{aligned}\frac{d}{dt}\hat{\rho} = &-\frac{i}{\hbar}[\hat{H}, \hat{\rho}] + \gamma_1 \mathcal{D}(\hat{\sigma}_{1-})\hat{\rho} + \gamma_2 \mathcal{D}(\hat{\sigma}_{2-})\hat{\rho} \\ &+ \frac{\gamma_\phi}{2}\mathcal{D}(\hat{\sigma}_z + 2\,|\mathrm{f}\rangle\langle\mathrm{f}|)\hat{\rho} + \kappa\mathcal{D}(\hat{a})\hat{\rho}.\end{aligned} \tag{A.2}$$

For the purpose of simulating a qutrit resembling a CPB, we assume $\gamma_2 \simeq 2\gamma_1$ and that the dephasing operator is $\hat{\sigma}_z + 2\,|\mathrm{f}\rangle\langle\mathrm{f}|$. Explicitly, this is related to the fact that in a harmonic oscillator, the n^{th} Fock state has a relaxation rate $\gamma_n = n\gamma_1$, n-times the relaxation rate of the first excited Fock state [38]. Additionally, experiments testing the coherence times of a transmons higher levels (even past $|\mathrm{f}\rangle$) have confirmed this Fock-state-like scaling of decay times [46]. These assumptions are fairly reasonable for the CPB in both transmon and charge regimes. All the numerical simulations of the master equation are performed with QuTiP [28, 29].